Roll coating in the presence of a stationary constraint.

ROLL COATING IN THE PRESENCE OF A STATIONARY CONSTRAINT

A Thesis Presented

By

THERESE M. BAUMAN

Submitted to the Graduate School of the
University of Massachusetts in partial fulfillment
of the requirements for the degree of

MASTER OF SCIENCE

September 1980

Polymer Science and Engineering

ROLL COATING IN THE PRESENCE
OF A STATIONARY CONSTRAINT

A Thesis Presented

By

THERESE M. BAUMAN

Approved as to style and content by:

Robert L. Laurence, Chairperson of Committee

Richard Farris, Member

Julio M. Ottino, Member

W.J. MacKnight, Department Head
Polymer Science and Engineering

TABLE OF CONTENTS

ACKNOWLEDGEMENT

I am deeply indebted to my parents and family for their much needed support and concern about my well being.

I wish to thank Dr. Laurence for all of his time, patience, and knowledge which enabled me to complete this research. I would also like to thank Dr. Middleman for his support and advice which were much appreciated.

I am grateful for all the advice of Tong and Pradeep and for their interest in the progress of my research.

Finally, a special thanks to all my friends for their help in making the last two years a fun filled adventure.

This research was funded by the Department of Polymer Science and Engineering at the University of Massachusetts and a grant from the Eastman-Kodak Company.

LIST OF FIGURES

Figures

Figures

LIST OF TABLES

CHAPTER I

INTRODUCTION

I-1 Background

A coating process involves the deposition of a thin, uniform film of fluid onto a moving or stationary sheet, often referred to as a web. Examples of coating processes are encountered in many industries, e.g. the photographic, printing and paper pulp industries. A number of methods have been developed in response to the many different coating purposes. Some systems used in industry are the roll coater, kiss coater, reverse roll coater and blade coater. Schematic diagrams of these systems are shown in Figure I-1.

A common hydrodynamic instability often observed in roll coating systems is known as the ribbing phenomenon. At critical conditions, the flow in the region between the roller and web becomes unstable. This instability results in the production of a film with regularly spaced waves or ribs aligned in the direction of motion of the web. An illustration of the ribbing instability for the system of a roller in the presence of a stationary constraint is shown in Figure I-2. This instability limits conditions under which roll coating systems can be effectively operated and still produce a uniform coating. In order to determine the effective range of stable operating conditions, one must understand the nature and mechanism of this instability. This has motivated the study of roll coating operations.

In the analysis of the roll coating process a mathematical model is formulated based on certain simplifications. Figure I-3 shows

Figure I-1. Schematic diagrams of typical roll coating systems.

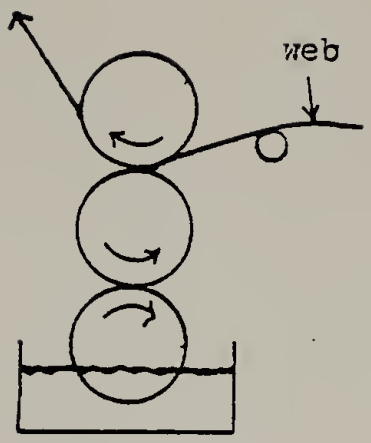

Roll Coater

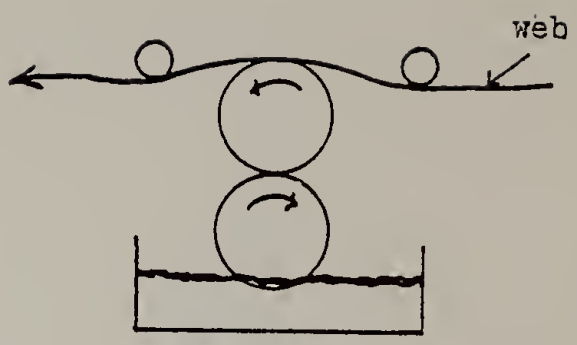

Kiss Coater

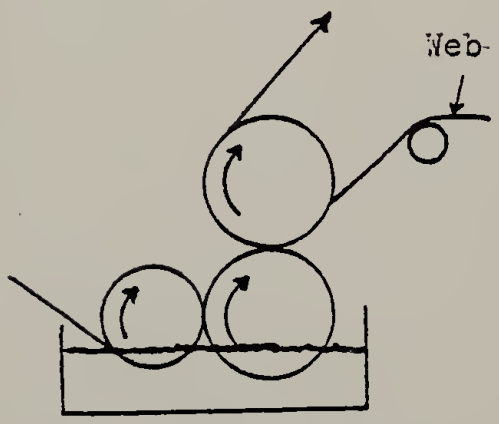

Reverse Roll Coater

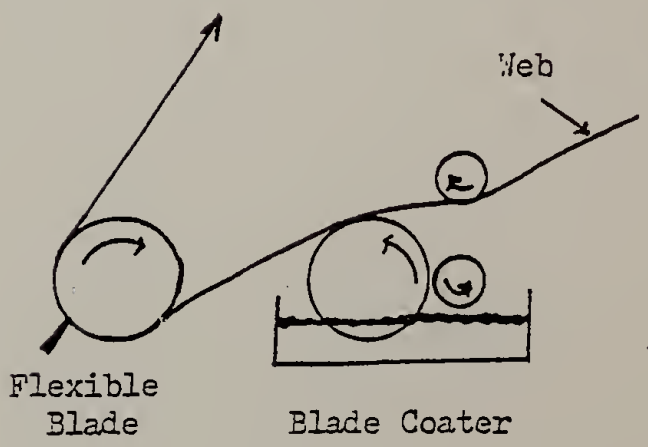

Flexible Blade

Blade Coater

Figure I-1

Figure I-2. An illustration of the ribbing phenomenon for the system of a roller and stationary constraint.

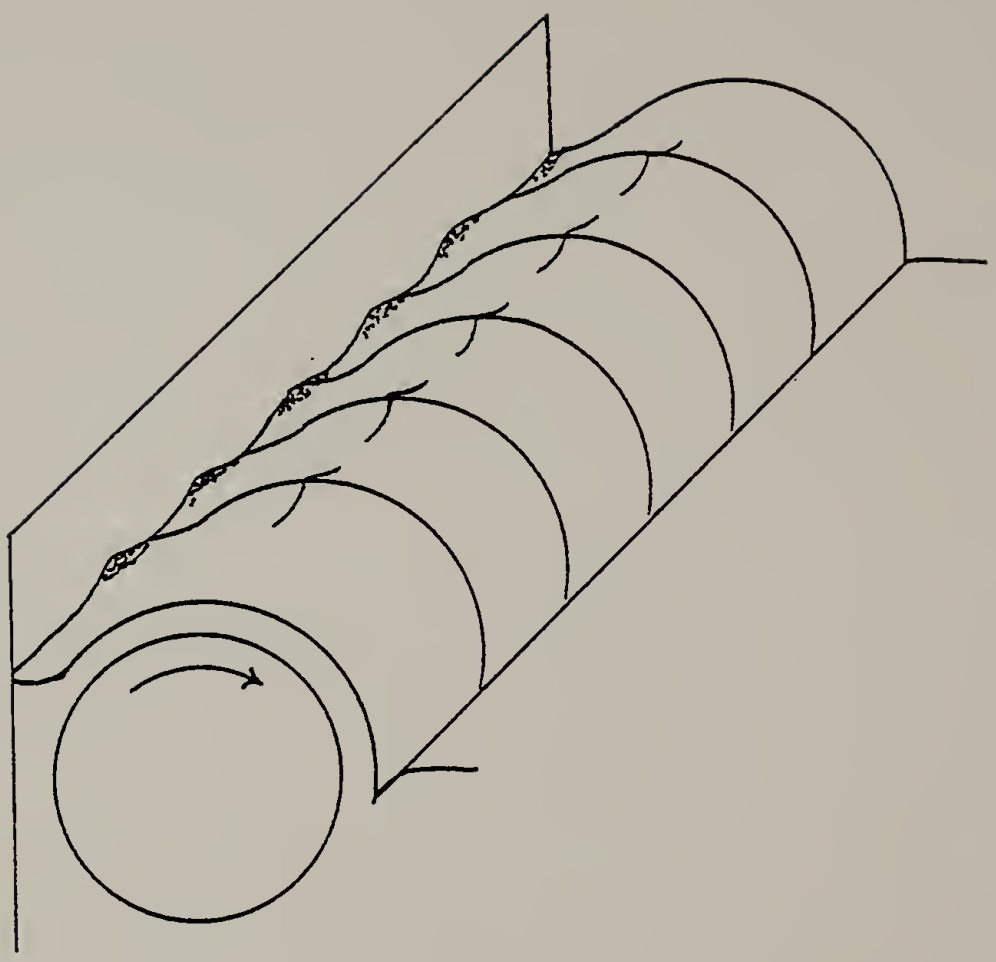

Figure I-2

Figure I-3. Geometry of a roll coating system

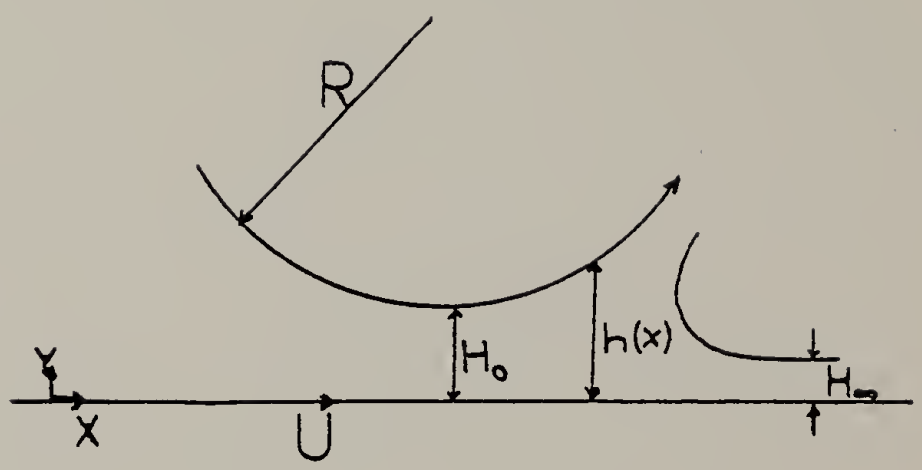

Figure I-3

the geometry of the system of interest for analysis. It is customary to apply the lubrication approximations to this type of coating flow. These approximations simplify and convert the equations of motion into a single partial differential equation to which an analytical solution might be obtained. The following four assumptions of the lubrication theory apply to a system where two arbitrarily shaped but nearly parallel boundaries are separated by a Newtonian incompressible fluid. First, it is assumed that steady isothermal laminar flow exists between the boundaries. Secondly, the inertia and acceleration terms in the equation of motion are assumed to be negligible as compared to the viscous forces. Thirdly, the geometry of the system is such that the length of the sheet is much larger than any value of the distance separating the roller and the sheet. Consequently, the velocity gradient in the direction of the primary flow is assumed to be much smaller than the gradient across the film thickness. Finally, it is assumed that the hydrostatic pressure varies only in the primary flow direction. From these assumption, the dynamic equation can be simplified to the form

$$0 = -\partial p/\partial x + \mu \partial^2 u_x/\partial y^2 \qquad \text{(I-1)}$$

Equation 1 integrated twice yields

$$u(x,y) = (y^2/2\mu)(\partial p/\partial x) + C_1 y + C_2 \qquad \text{(I-2)}$$

The application of the boundary conditions

$$u_x = 0 \text{ at } y = 0 \qquad \text{(I-3)}$$

$$u_x = U \text{ at } y = h(x) \qquad \text{(I-4)}$$

leads to

$$u_x = (1/2\mu)(\partial p/\partial x)\,[y^2 - yh(x)] + Uy/h(x) \qquad \text{(I-5)}$$

This equation is then reduced to

$$\partial p/\partial x = 6\mu\, U/h^2(x)\,[1 + 2H_\infty/h(x)] \qquad \text{(I-6)}$$

by using the law of mass convservation which requires

$$\int_0^{h(x)} u\,dy = Uh_\infty \qquad \text{(I-7)}$$

The next step in the analysis then is to solve equation I-6 through the application of additional boundary conditions at the entry and free surface.

This presents a problem since the position of the cavity is unknown. It is at this point in the analysis where uncertainty exists and this promotes differences in the work by various authors.

I.2 Review of Previous Work

The ribbing phenomenon was first observed and reported by Mill and South (1937), and subsequently by Sone and Fukushima (1960), who conducted a study using a number of viscous materials on a roll mill. The mill consisted of two rollers of equal size, 17.5 cm in length and 7.6 cm in diameter. This experimental study showed that the distance between the ribs (the wavelength) was related to the viscosity of the material. As the viscosity decreased, the rib spacing also decreased. The results, using butter as the experimental fluid, are shown in Figure I-4. Similar results were also found for condensed milk, honey, syrup, grease and silicone oil.

Figure I-4. Relation between the peak distance, D, and the viscosity, η, of butter during rolling

	a*(mm)	η(Poise)
1	0.55	68
2	1.65	68
3	4.05	68

*a is the gap thickness between the rollers.

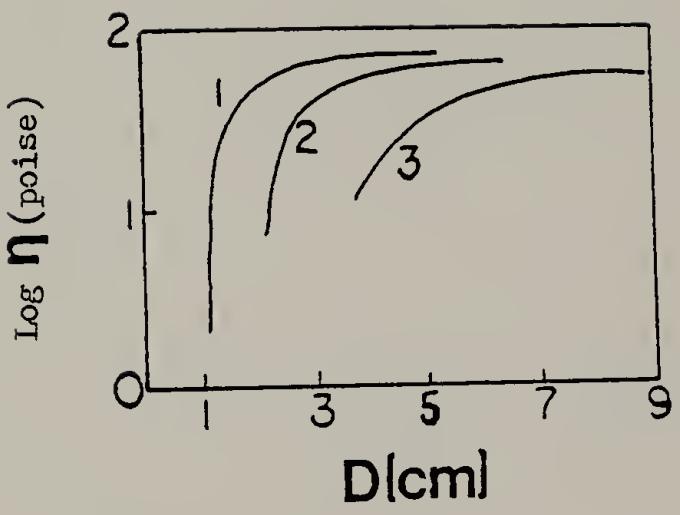

Figure I-4

Pearson (1960) did an analysis of the instability of viscous flow under a roller or spreader. The mathematical model, based on Figure I-5, defines two regions: 1) the region in which the lubrication approximation applies, $x < b$ and 2) the region where air separates the fluid into two layers, $x > b$. The lubrication approximation is no longer valid in the neighborhood of the menicus, $x=b$, and the pressure field must be described by two boundary conditions. The first is the pressure boundary condition which states that the pressure in region 1 at the boundary equals the sum of the pressure in region 2 plus the effect of surface tension forces acting on the boundary. The pressure in region 2 is assumed to be negligible in comparison to the other forces acting at the boundary. Thus, the appropriate relation is

$$p(b)\, h(b) = -2\sigma \tag{I-8}$$

The second is the mass flux boundary condition which states that the amount of fluid entering and leaving each region is equal. That is

$$m_1(b) = t_1^*(b)/h(b) \tag{I-9}$$

$$m_2(b) = t_2^*(b)/h(b) \tag{I-10}$$

From this general analysis, Pearson determined that for Newtonian fluids the stability of the system is dependent on its geometry and a capillary number, defined as

$$Ca = \mu U/\sigma \tag{I-11}$$

where μ is the viscosity, U is the speed of the roller and σ is the

Figure I-5. Flow through a narrow region between two arbitrarily moving surfaces.

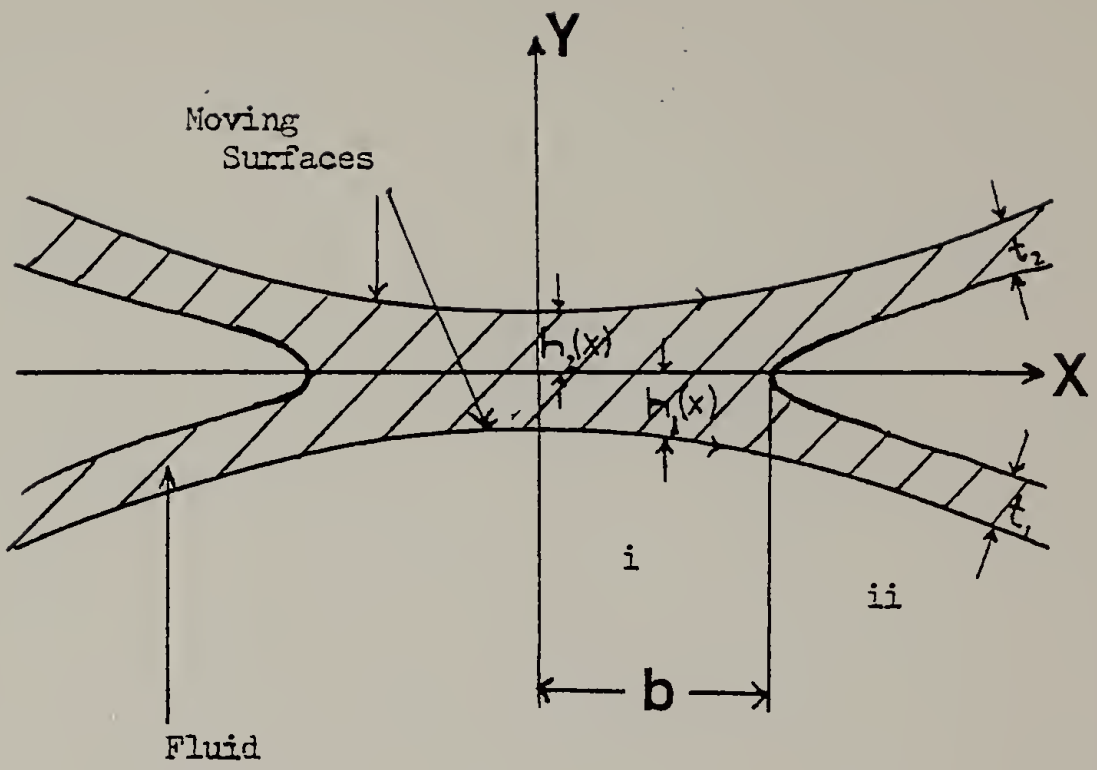

Figure I-5

surface tension. The general analysis was applied to the particular case of the wide angle wedge spreader (Figure I-6). Although Pearson did not determine quantitatively the condition for the transition from stable flow to ribbing, he did determine that the spacing between the ribs was a function of Ca and geometry. This result is shown in Figure I-7 as a plot of N, the number of ribs per inch, versus τ where

$$\tau = 2\sigma\alpha/\mu U_0 \tag{I-12}$$

$$h(x) = H_0\alpha|x| \tag{I-13}$$

Reasonable agreement between theory and experimental data was found at $\tau > 0.1$. However, with decreasing τ, the agreement deteriorated.

Pitts and Greiller (1961) studied the two roller system in which a thin film is produced between two counterrotating rollers of equal radii. They sought to derive a criterion for Newtonian fluids which specified the conditions for the onset of ribbing. A cross section of the separation region is shown in Figure I-8. The x direction pertains to the direction of flow and the z direction is that of the neutral axis. It is assumed that the perturbation arises from some small physical distrubance. The perturbation either grows or decays depending on the pressure at points 1 and 2. If the pressure is greater at point 1 than at point 2, the fluid will move in the direction of the perturbation causing it to grow. From a simple force balance, the pressure at points 1 and 2 are

$$P_1 = -\sigma/r \tag{I-14}$$

Figure I-6. Flow through a wide angle wedge spreader.

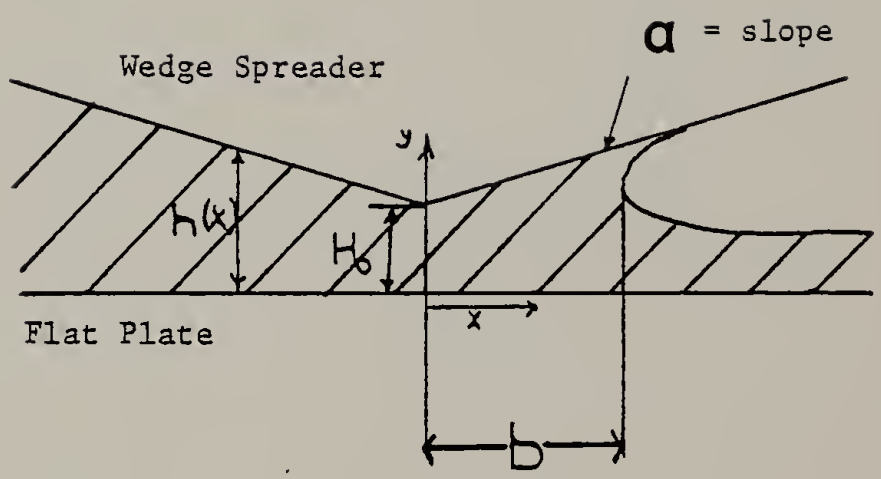

Figure I-6

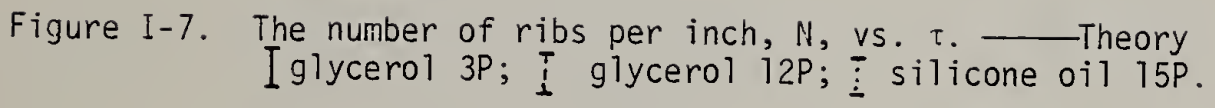

Figure I-7. The number of ribs per inch, N, vs. τ. ———Theory
I glycerol 3P; I glycerol 12P; I silicone oil 15P.

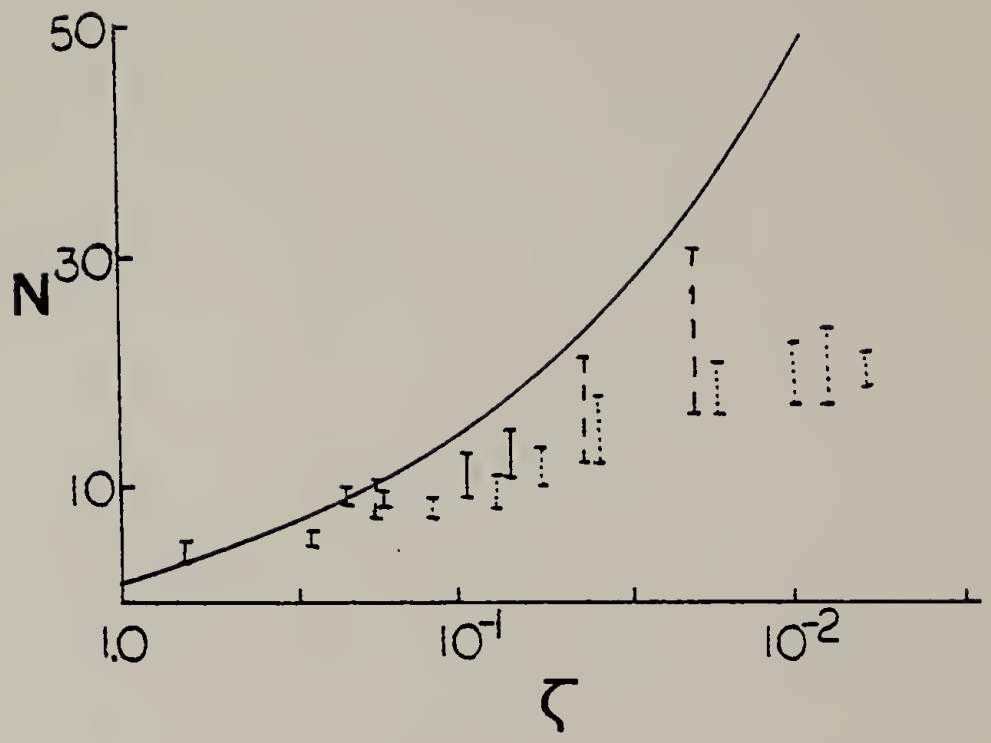

Figure I-7

Figure I-8. A cross section of the separation region. The perturbation of the separation line is assumed to be due to a small physical disturbance.

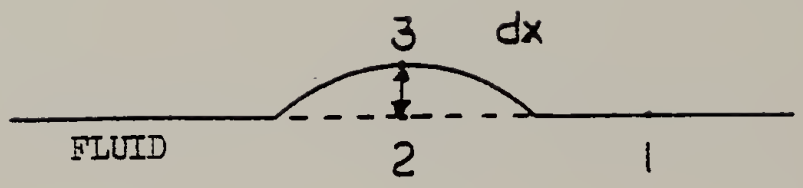

Figure I-8

$$P_2 = \frac{-\sigma}{r} + \frac{d}{dx}\left(\frac{-\sigma}{r}\right)dx + \left.\frac{dp}{dx}\right|_x (dx) \qquad \text{(I-15)}$$

The difference between these two pressures is then

$$\Delta P = \left[-\sigma/r^2 \frac{dr}{dx} + \left.\frac{dp}{dx}\right|_{x_1}\right]dx \qquad \text{(I-16)}$$

Pitts and Greiller proposed that since a positive ΔP would increase the perturbation, a negative ΔP should decrease it. Thus, they propose the criterion for stability to be

$$\frac{\sigma}{r^2}\frac{dr}{dx} > \frac{dp}{dx} \qquad \text{(I-17)}$$

Quantitatively, they derive the following condition

$$Ca_1^* = \left(\frac{\mu U^*}{\sigma}\right)(R/H_0) = 28 \qquad \text{(I-18)}$$

where R is the radius and $2H_0$ is the minimum distance separating the two rollers. However, experimentally Ca_1^* was found to be 62 ± 15. Pitts and Greiller attributed the discrepancy to the difficulty in determining precisely the speed at which the instability appeared.

Mill and South (1966) also did an experimental study of the two roller system. The apparatus consisted of a pair of rollers, mounted one above the other. The apparatus was designed so that the upper roller was interchangeable. This enabled one to perform experiments using different sized rollers which in effect varied the gap thickness. From the experimental data, it was found that the onset of ribbing satisfied the relation

$$(Ca)^* \left(\frac{R}{H_o}\right)^{3/4} = 10.3 \qquad \text{(I-19)}$$

where R is the radius of the interchangeable roller. This result

was unexpected since $(H_0/R)^{3/4}$ was found to be a parameter governing the ribbing onset rather than (H_0/R) as predicted by theory. Mill and South also presented experimental results which showed that the wavelength decreased rapidly with increasing Ca and reached a limiting value dependent solely on the geometrical parameters R and H_0.

Coyne and Elrod (1970) developed a theoretical model for the physical situation shown in Figure I-9. In this case, the fluid flows between two parallel plane surfaces, one stationary and one moving. As the fluid separates from the stationary surface, it is drawn out by the opposing moving surface. In their derivation of a model, Coyne and Elrod took a different approach than that of Pearson and Pitts and Greiller. The model is developed in two parts.

In the first part, they derived an approximate solution of the two dimensional Navier Stokes equations without applying the usual lubrication approximations. The major assumption in this derivation was that the x component of the fluid velocity was a quadratic function of y. It was also assumed that the fluid was Newtonian and had a constant density, viscosity and surface tension. The resulting theory showed the velocity distribution to be related to three parameters

$$\text{a Capillary number } N = (3Ca)^{1/3} \tag{I-20}$$

$$\text{a Reynolds number } Re = \rho g H_\infty/\mu \tag{I-21}$$

$$\text{a Gravity number } G = \rho g H_\infty/3\mu U \tag{I-22}$$

Further results showed the parameters c/H_∞ and R_0/c to be related to N as shown in Figure I-10. R_0 is defined as the radius of curvature

Figure I-9. Physical situation analyzed by Coyne and Elrod (1970).

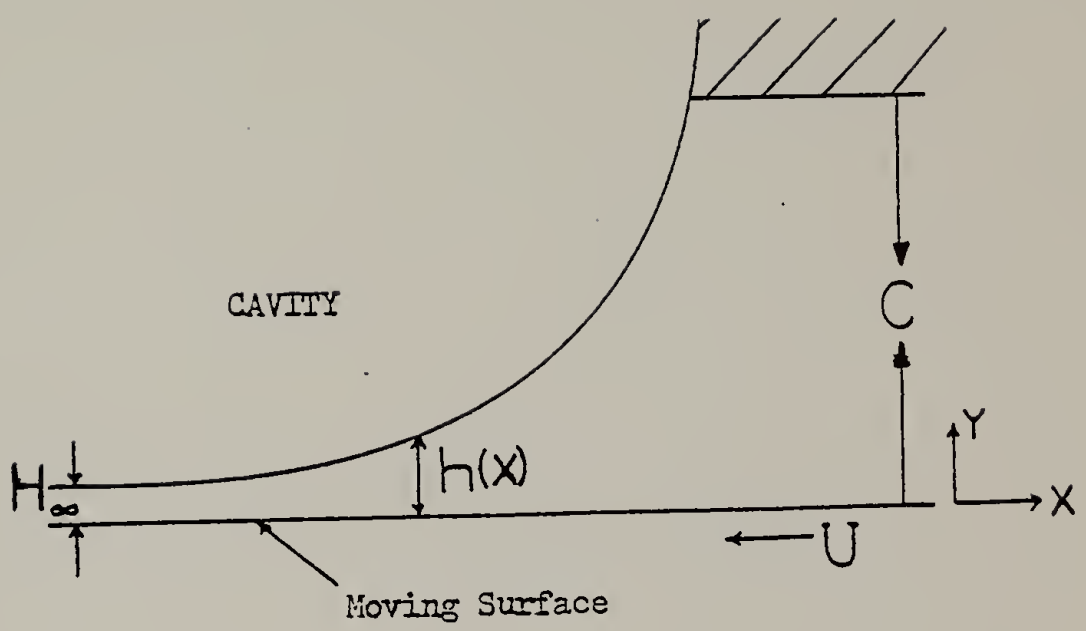

Figure I-9

Figure I-10. Theoretical results of the relation $Ca_2=(3Ca)^{1/3}$ and the two parameters c/h_∞ and R_0/c.

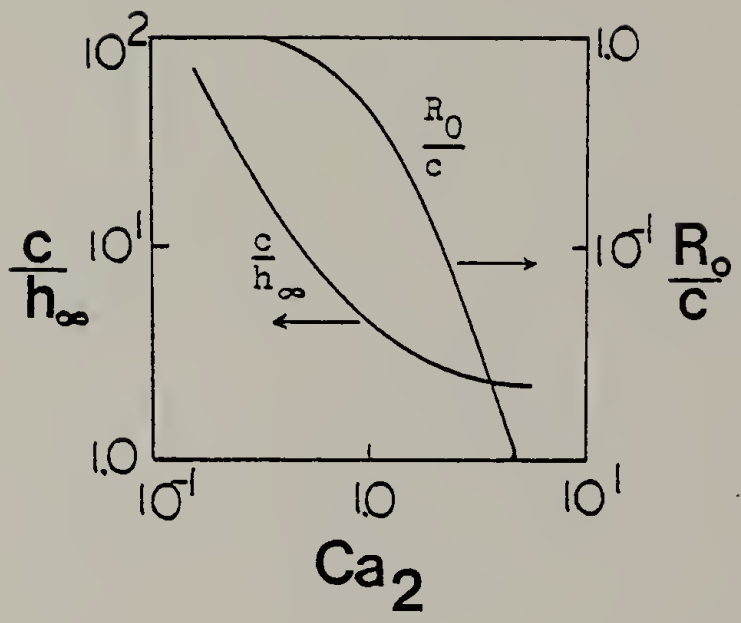
10^2
1.0
10^1
10^{-1}
1.0
10^{-1}
1.0
10^1
$\frac{c}{h_\infty}$
$\frac{R_0}{c}$
$\frac{c}{h_\infty}$
$\frac{R_0}{c}$
Ca_2

Figure I-10

of the free film boundary at the separation point.

In part II, these results were applied in the formulation of two boundary conditions needed to solve equation (I-6) which was derived from the Reynolds equation. The first of the two conditions comes from continuity and results in the following condition

$$(dp/dx)_0 = 6\mu U/H_0^2 \ (1 - 2H_\infty/H_0) \qquad \text{(I-23)}$$

Equation I-23 is the exact solution of the pressure gradient at film separation provided the angle at which the film separates from the stationary surface, the wetting angle, is 90° (Figure I-11). In this case $H_0 = c$ and this enables c/H_∞ to be determined directly from Figure I-10. For a wetting angle less than 90° it was assumed that an approximation for H_0 could be found from

$$H_0/H_\infty = c/H_\infty \ (1 + R_0/c \cos \phi) \qquad \text{(I-24)}$$

The secondary boundary condition comes from pressure continuity and results in

$$P_0 = -\sigma/R_0 + \Delta p \qquad \text{(I-25)}$$

where Δp is the pressure across the transition region which is negligible when $H_0 > c$. Essentially these two conditions determined the pressure at the film edge and the location of the film edge. Coyne and Elrod then applied these boundary conditions to the case of the infinitely wide slider bearing. Experiments were conducted and good agreement was found between the experimental and theoretical results. Thus, Coyne and Elrod's boundary conditions appear to be appropriate in the proposed theory.

Figure I-11. Wetting of the stationary surface.

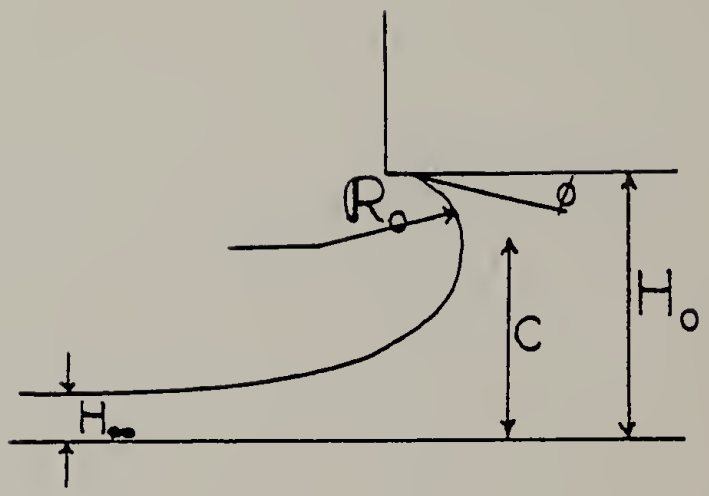

Figure I-11

Eckert and Novotny (1972) had reported findings of the ribbing phenomenon for viscoelastic fluids flowing through a rectangular channel. This phenomenon is not necessarily the same as what is being discussed in this report since the two surfaces are stationary. The experimental fluids were aqueous solutions of polyethylene oxide and the apparatus consisted of a long rectangular channel constructed from aluminum. It was observed that at a capillary number less than 2.5 the exit stream of fluid was smooth. At a Ca between 2.5 and 3.5 the fluid stream, still in contact with the lower plate, was ribbed and the wavelength was observed to be nearly constant. At Ca greater than 3.5 the fluid exited out and away from the lower plate without the presence of ribs.

Further study of the ribbing phenomenon was done by Savage (1976). He reviewed the different boundary conditions that have been used to determine the position of the cavity in a cylinder plane geometry. A diagram showing this and the flow in the cavity region is shown in Figures I-12 and I-13, respectively. The Swift-Stieber condition (1932) stated that the pressure was zero at the cavity position. Thus

$$(\partial P/\partial x)_{x=c} = 0 \qquad \text{(I-26)}$$

This cannot be applied in the type of systems under consideration for two reasons: 1) it does not predict the presence of an eddy upstream of the cavity which was observed experimentally by van den Bergh (1974) and 2) it does not account for any interruption, such

Figure I-12. Cavitation in a cylinder plane geometry.

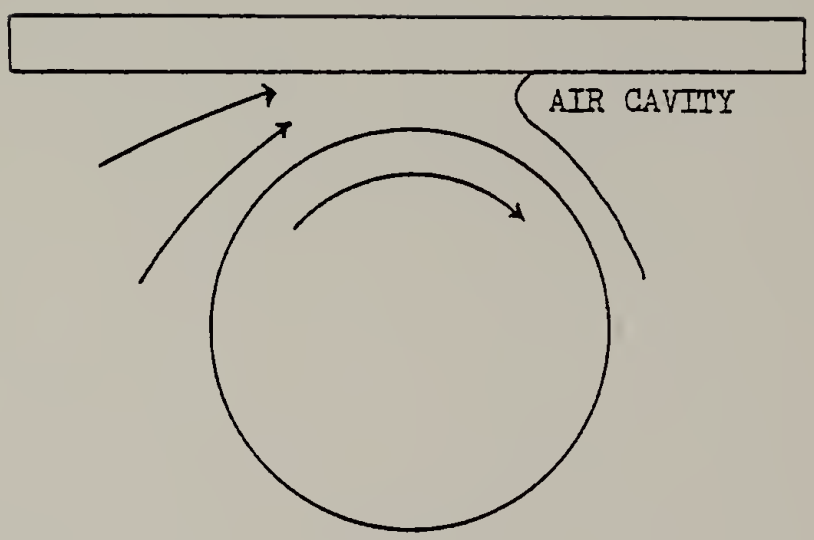

Figure I-12

Figure I-13. Flow in a cavity region.

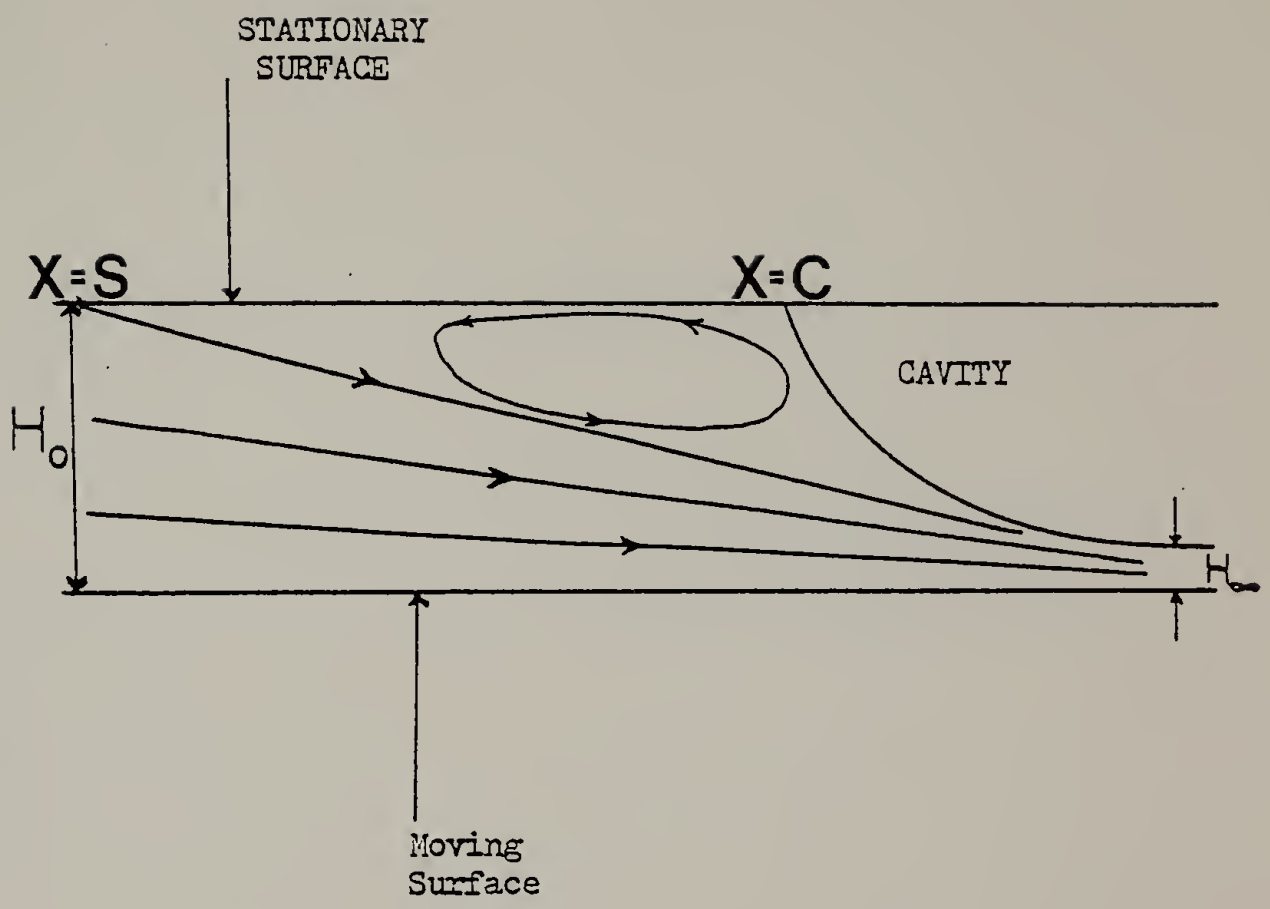

Figure I-13

as ribbing, in the steady flow of fluid preceeding the cavity. In the Hopkins (1957) separation condition, the initial position of the cavity was assumed to be at the point where the fluid separated from the stationary surface, i.e. where the velocity and tangential stress were both zero. The following condition resulted

$$(\partial P/\partial x)_{x=c} = 2\mu U/h^2(c) \qquad \text{(I-27)}$$

Thus it was implied that the point of separation and cavitation, x=c and x=s were coincident. This, however, like the Swift-Steiber condition, did not account for the presence of an eddy. The Coyne-Elrod (1970) condition as stated earlier accounted for surface tension effects and introduced the Ca into the solution. Savage did a linearized perturbation analysis similar to Pearson's and employed the Coyne-Elrod boundary condition which described the position of the cavity. The theoretical solution was applied to the cylinder-plane geometry and the results were compared to experimental findings. The dimensionless wavenumber, $Rn/2\pi$ where n is the number of waves per unit length, was related to the geometric parameter, $(R/H_0)^{1/2}$ for a specified Ca. The transition from stable flow to perturbed flow occurred at a critical value of $(R/H_0)^{1/2}$ for fixed Ca. In the analytical solution, a bifurcation occurred at the critical point and produced an upper and lower branch. Savage determined both experimentally and numerically that the upper branch, corresponding to the larger wavelength, could be found in actuality. This agreement between theory and experiment was found because the theory overestimated the value of n as $(R/H_0)^{1/2}$ increased.

Greener and Middleman (1979) completed theoretical and experimental work for both Newtonian and viscoelastic fluids using the two roller system. The stability criterion derived by Pitts and Greiller was applied to a Newtonian fluid, a purely viscous power law fluid and a viscoelastic fluid. Newtonian fluids were used in the experiments and the results were compared to previous work. It was found that the Ca offered adequate characterization of the onset of ribbing in agreement with the theory proposed by Pitts and Greiller. However, a discrepancy between the quantitative value for the ribbing onset had been observed. The experimental value of Ca_1^* was 93 ± 20 according to Greener and Middleman whereas Pitts and Greiller reported Ca_1^* to be 62 ± 15. Greener attributed the discrepancy to be due to the difficult in detection of the critical speed. Savage's (1976) theory for the cylinder plane geometry was modified by Greener to apply to the two roll system so that a comparison between experiment and theory could be made. The theoretical and experimental results for the two roller system are presented in Figure I-14. The curves are in qualitative agreement in that they all lie in a common neighborhood. Greener suggested that this discrepancy was supportive of the possibility of Savage's criterion being a necessary but not sufficient condition to predict the onset of ribbing. Greener also collected wavelength data which compared fairly well to Mill and South's data. The latter suggested that the dimensionless wavelength, $W/2H_0$ where W is the number of ribs per inch, was independent of Ca. However, Savage's theory indicated

Figure I-14. The critical capillary number, Ca^*, vs. H_0/R. Theoretical results of Savage (1977) and Pitts and Greiller (1961). Experimental data of Greener (1979).

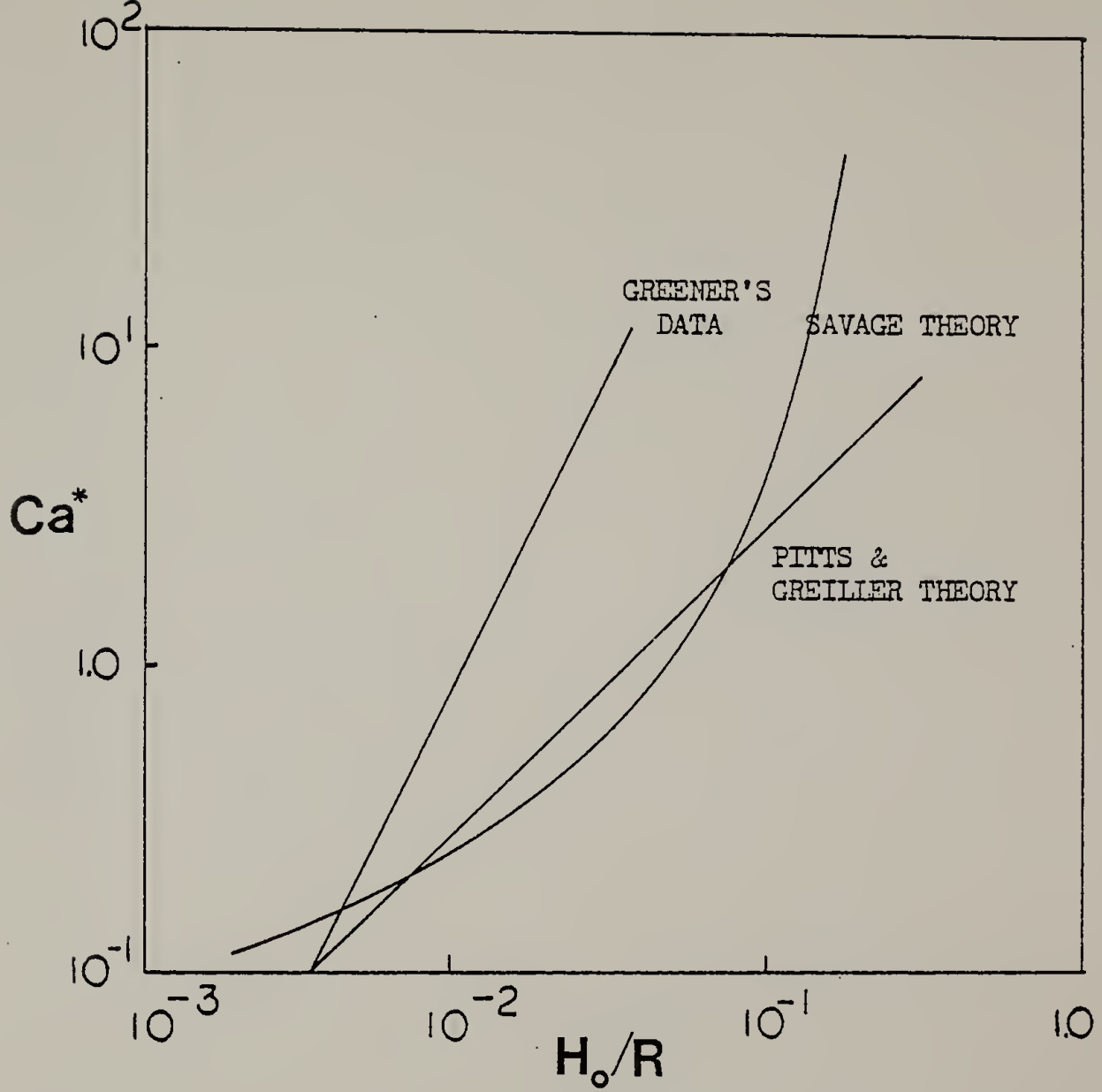
10^2
10^1
1.0
10^{-1}
Ca*
GREENER'S DATA
SAVAGE THEORY
PITTS & GREILLER THEORY
10^{-3}
10^{-2}
10^{-1}
1.0
H_o/R

Figure I-14

that there was some kind of dependence. The effect of viscoelasticity was studied using 0.15 - 0.75% by weight polyacrylamide solutions. According to Greener, the transition from stable to unstable flow was clearly observed with these solutions. Experimental results suggested that the controlling factors for instability were gravity, a stabilizing factor, and viscoelasticity, a destabilizing factor. The recoverable shear was used to account for elastic effects in correlating the data. Surface tension was found experimentally to be of minor importance in the stability criterion for these viscoelastic fluids. Theoretically, surface tension is predicted to stabilize the flow. Greener's theoretical achievements consisted of extending the stability criterion to a second order fluid. The first step in the analysis was to modify equation I-16 so that the z component of the total stress was incorporated; thus,

$$\frac{\sigma}{r^2}\frac{dr}{dx} > \frac{-d\,T_{zz}}{dx}\Big|_{x_1} \qquad \text{(I-28)}$$

where $-T_{zz} = p - \tau_{zz}$.

In the evaluation of the pressure gradient in equation I-28, Greener applied the Giesekus-Tanner-Pipkin equation (Bird et al. 1977a). This equation resulted from the Giesekus-Tanner (1966) theorem which stated that for creeping and planar flows a second order fluid and a corresponding Newtonian fluid have the same velocity field as long as the velocity boundary conditions are the same for both cases. As a result, the stability criterion is as follows,

$$\frac{dP^\circ}{dx}\Big|_{x_1} < \frac{\sigma}{r^2}\frac{dr}{dx} + \frac{\infty 2}{\alpha_1}\left(\frac{du}{dx}\frac{dP^\circ}{dx}\right)\Big|_{x_1} + \rho g \qquad \text{(I-29)}$$

where P° is the pressure for a corresponding Newtonian fluid and α is the constant viscosity of the second order fluid. Upon non-dimensionalization of equation I-29 and evaluation of the surface tension term, the resulting stability criterion is

$$2 < (Ca_1)^{-1/2}[14.1(3\lambda - 1)]^{1/2} + 9F\lambda^2 - S_R(\beta\lambda - 2)^{1/2}/3\lambda \qquad \text{(I-30)}$$

where λ is the dimensionless coating thickness and β is a function representing the position of the roll surface. A graphical representation of the stability limits is shown in Figure I-15 as a plot of S_R^* versus F^* with Ca^* as a parameter. For each Ca^* there exists two regions; below the curve, which is the region of stable conditions, and above, which is unstable conditions. After completion of this analysis Greener stated that the resulting criterion was not expected to be in quantitative agreement with experiments and pointed out the failure of this theory. First, the criterion was expected to be a necessary condition but not sufficient for ribbing onset. Secondly, the experimental viscoelastic fluids do not generally behave as second order fluids except at very low deformation rates. Finally, the role of surface tension is not definitely known. Theoretically, surface tension is predicted to stabilize the flow. Experimentally, it was found to be of minor importance in the stability criterion for the viscoelastic fluids tested.

The coating system consisting of a roller in the presence of a stationary constraint was considered by Sullivan and Middleman (1979).

Figure I-15. The critical recoverable shear, S_R^*, vs. the critical number, F^*, with the modified critical capillary number, Ca_1^*, as a parameter.

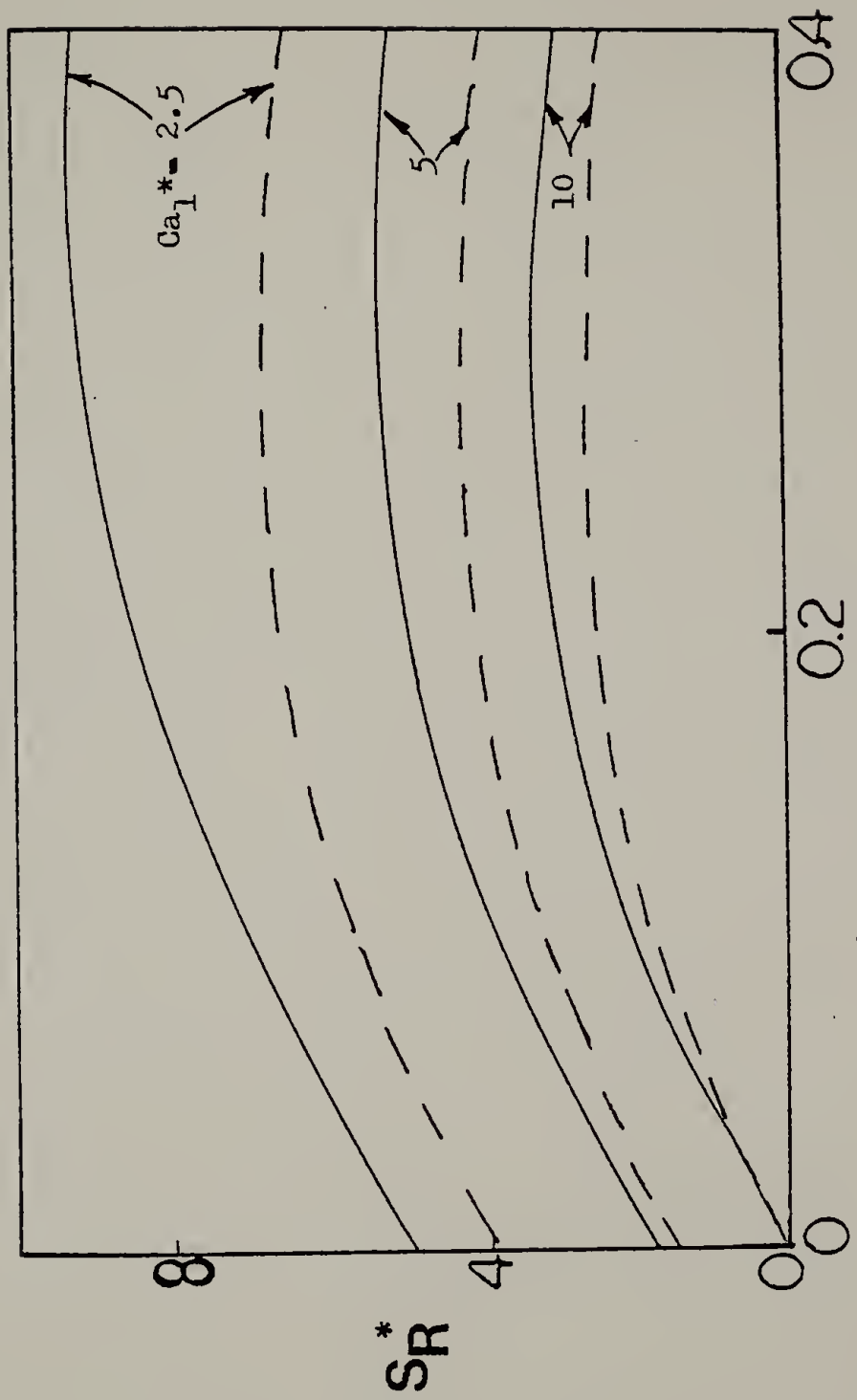

Figure I-15

A mathematical model for flow of a Newtonian fluid was presented using the lubrication approximation. The theory predicted the coating thickness, $\lambda=H_\infty/H_0$, to be related to gravity through a parameter, F,

$$F = Re/Fr = \rho g H_0^2/\mu U \qquad (I\text{-}31)$$

The coating thickness was expected to decrease as F increased. Figure I-16 shows the range of λ to be between 0.5 and an asymptotic value of 0.605. The proposed theory was compared to experimental results (Figure I-16) and good agreement was found in the small F value region, $F<1.0$.

Sullivan and Middleman (1979) also studied the ribbing phenomenon using the same system. The data of Ca_1^* as a function of H_0/R presented by Savage were extended to larger gap thicknesses, $0.02\leq H_0/R\leq 0.08$, for Newtonian fluids. The value for the onset of ribbing was found to be $Ca_1^*=25$. It was thought that the discrepancy could have possibly been due to the fact that the two sets of data corresponded to two different regions of H_0/R.

The work done by Sullivan and Middleman was extended experimentally to viscoelastic fluids by Turner (1979). The results suggested that the presence of elasticity significantly affected the onset of ribbing and the nature of the instability.

I.3 Current Research

The lack of understanding in predicting the ribbing onset in roll coating operations has become evident from the review of

Figure I-16. Results of Greener's theoretical model and experimental data for the dimensionless coating thickness, λ, vs. the gravity number, F. —— Theory; ○ glycerin; △ glycerin/water; □ motor oil; ◇ mineral oil; ▽ glycerin/water/surfactant.

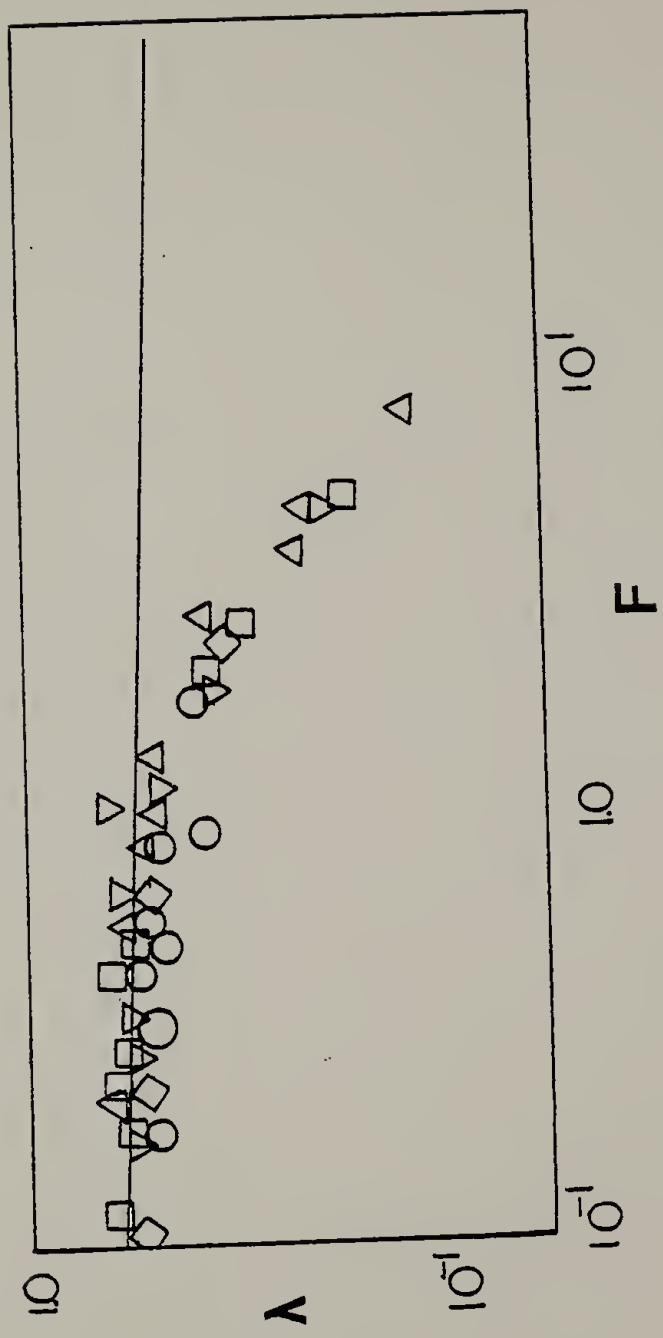

Figure I-16

previous work. The inability to explain the experimental results verifies the need for further work to be done in this area. Further studies are not only necessary for Newtonian fluids but also for viscoelastic fluids since they are commonly used in industrial processes.

The fundamental purpose of this study is to investigate the ribbing phenomenon for roll coating operations. The particular system of interest is that of a roller in the presence of a stationary constraint. A detailed description of the apparatus and the experiments performed is given in Chapter II. Both Newtonian and viscoelastic fluids were experimentally tested and the results discussed in Chapter III. Chapter IV deals with experiments conducted with variants of the general roll and plate system described in Chapter II. In Chapter V a discussion of the results for both Newtonian and viscoelastic fluids is presented. Finally, conclusions regarding the experimental work are drawn and recommendations given as to what future experiments might help to gain a more complete understanding of the ribbing phenomenon.

CHAPTER II

EXPERIMENTS

II.1 Scope

An experimental study was conducted to investigate the stability of roll coating in the presence of a stationary constraint. A general view of the experimental apparatus is shown in Figure II-1. A schematic diagram of a top view is also pictured in Figure II-2. The apparatus was designed in this fashion for a number of reasons. First, it simulated systems typically used in industrial coating operations. Second, its very simple design enabled experiments to be performed very easily. Third, it was economically feasible to run a large number of experiments since the fluid was always recirculated. Finally, it enabled studies to be done on free boundary flows and converging-diverging flow systems.

In this study, experiments entailed determining the conditions for the onset of instability, the film thickness under stable conditions, the wavelength of the ribbing pattern and the contact angle formed at the fluid plate interface. The experiments were conducted with several fluids, both Newtonian and viscoelastic in nature.

II.2 Apparatus

The experimental apparatus comprised a transparent acrylic box which contained a steel roller supported by a pair of sealed ball bearings and a stationary constraint. Experiments were done using

Figure II-1. General view of the experimental apparatus.

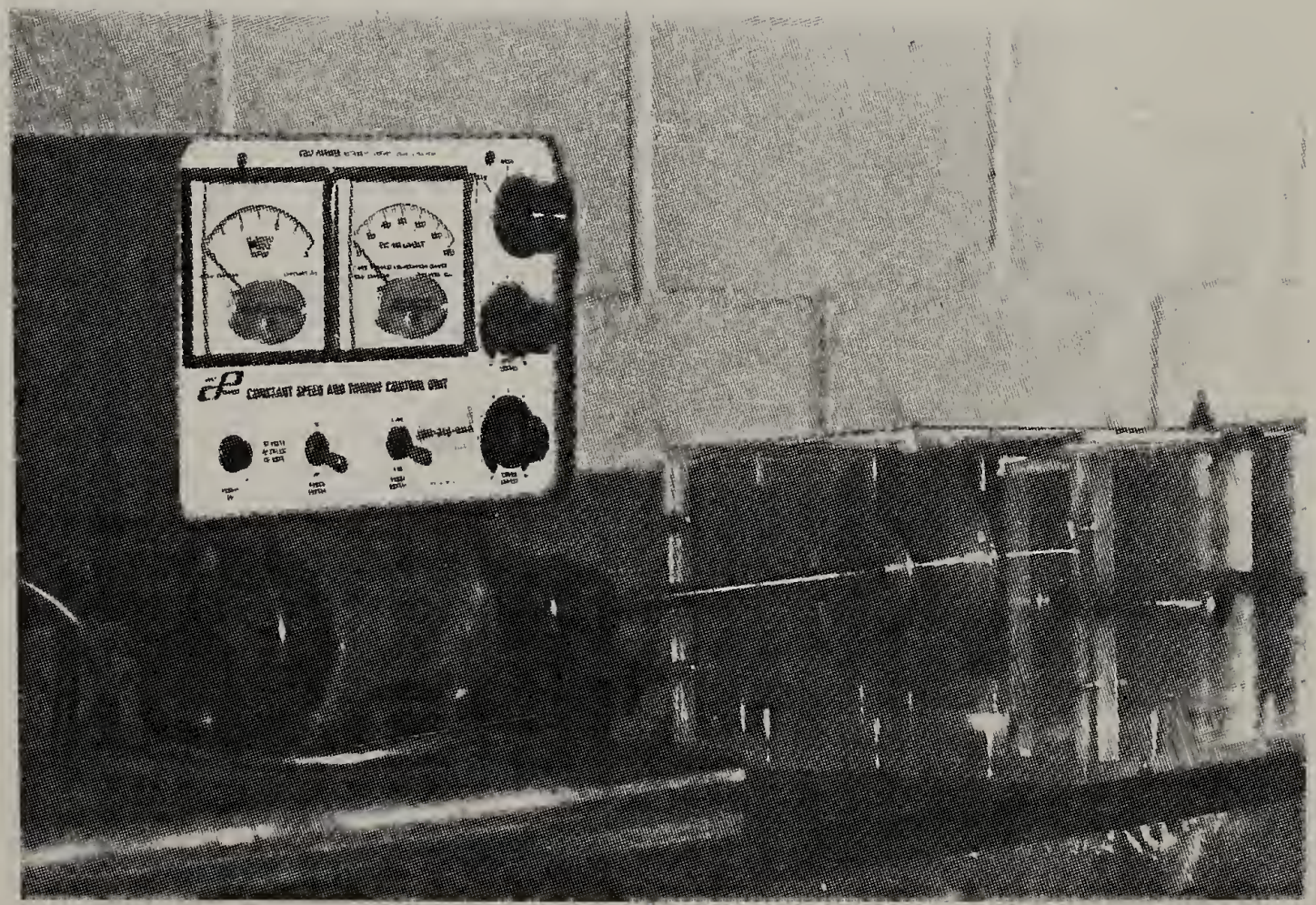

Figure II-1

Figure II-2. Schematic diagram of the experimental apparatus. Top view: 1. Reservoir, 2. Roller, 3. Plate, 4. Adjusting screws, 5. Sealed ball bearings, 6. Shaft, 7. Speed motor.

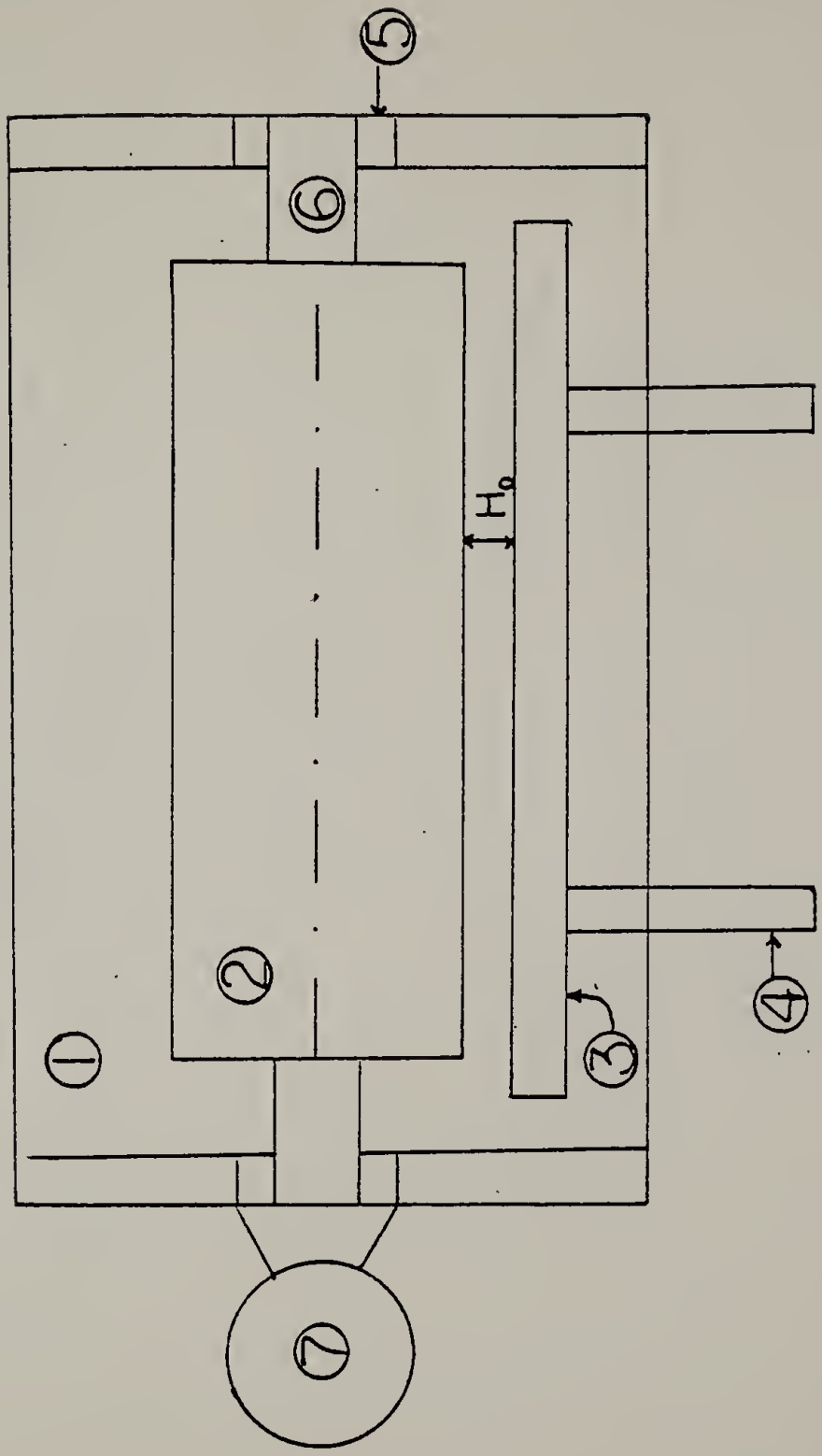

Figure II-2

two different size systems, one containing a two inch diameter roller and the other a four inch diameter roller. The dimensions of both systems are listed in Table II-1.

The rollers were fabricated from steel pipes and machined with a lathe to the proper diameter with an accuracy of ±0.0005 inches in concentricity. The roller was connected to a motor by an eleven inch long shaft. A Cole-Parmer Constant Speed and Torque Control Unit was used to control the speed of the motor.

The stationary constraint consisted of a rigid plexiglass plate positioned parallel to the axis of the roller. The plate was attached to the main system in such a way that the gap thickness (defined as the distance between the plate and roller) was ajustable. This was accomplished through the use of a pair of 3.5 inch long screws. One end of each screw was mounted a half inch from the side of the plate. The other end screwed into the wall and extended to the outside of the box. Motion of the screws moved the plate horizontally with respect to the roller axis and thus enabled the gap thickness to be set to any desired value.

A schematic diagram of the system used to make coating thickness measurements is shown in Figure II-3. It consisted of a micrometer attached to a needle which moved vertically with a change in the micrometer setting. The needle was positioned over the top of the roll near the center and a traveling microscope was used to determine when the needle contacted the surface of the roller or film.

Table II-1

DIMENSIONS OF EXPERIMENTAL APPARATA

	System 1	System 2
Roller:		
Diameter	10.0 cm	4.93 cm
Length	12.7 cm	12.7 cm
Box:		
Length	20.0 cm	15.2 cm
Width	15.1 cm	15.1 cm
Depth	12.5 cm	7.5 cm
Plate:		
Length	13.7 cm	14.3 cm
Width	12.5 cm	7.5 cm
Thickness	1.3 cm	1.0 cm

Figure II-3. Schematic diagram of apparatus used to measure coating thickness. Side view: 1. Reservoir, 2. Roller, 3. Plate, 4. Shaft, 5. Speed motor, 6. Micrometer, 7. Needle.

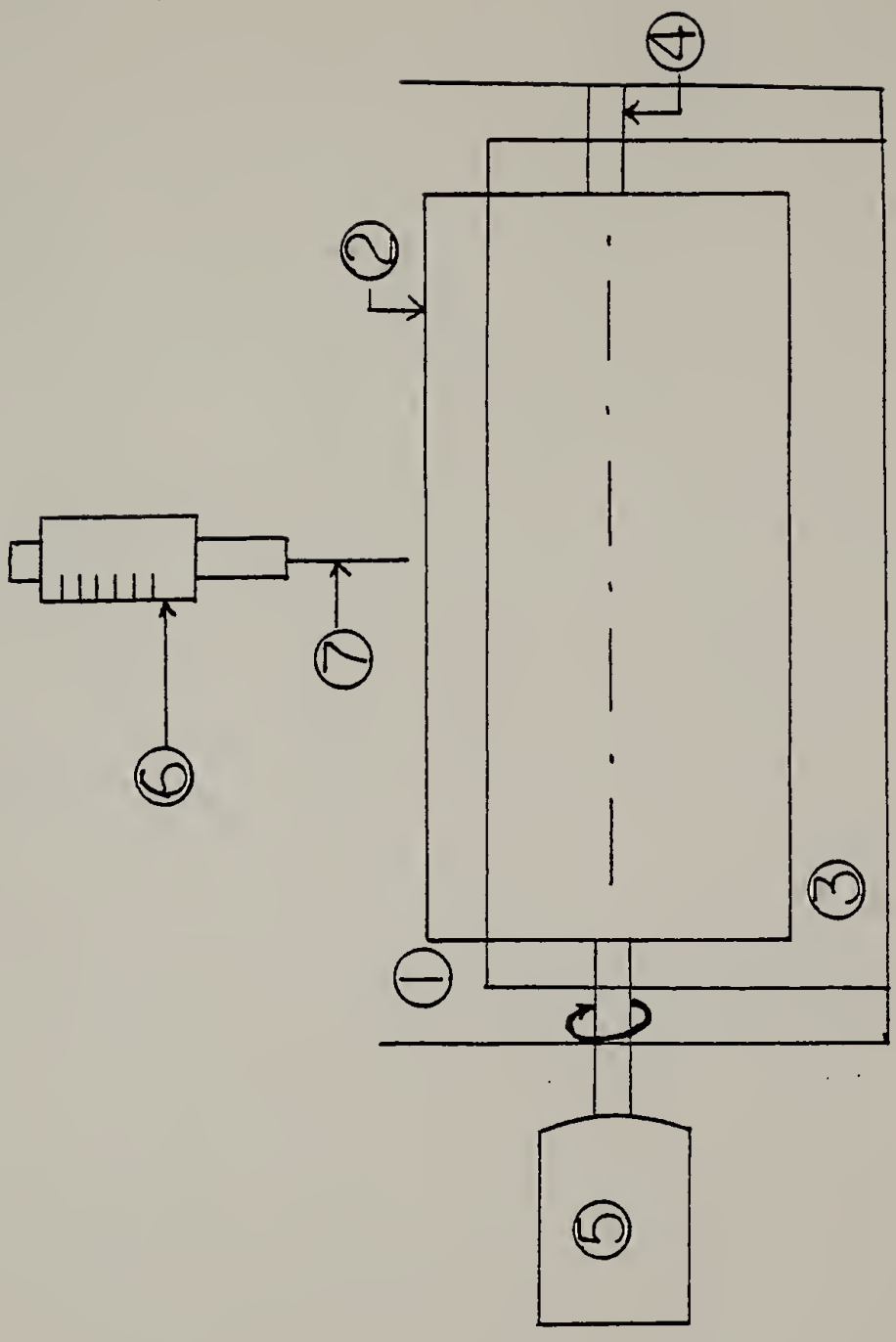

Figure II-3

II.3 Procedure

For each experiment the box was filled with fluid to the midpoint of the axis of the roller. The desired gap thickness, H_0, was fixed under static conditions by adjustment of the position of the plate. Feeler gauges of various widths were used to set a number of different gap thicknesses. The feeler gauge was placed between the roller and plate and the plate was positioned so that the feeler gauge could be slid in and out of the gap without causing any motion to the roller. To insure that the gap was uniform with respect to the roller, the feeler gauge was inserted approximately one inch from both ends of the plate. The experimental gap thickness ranged between 3 and 100 mils and was dependent on the size of the system and the fluid being tested. The accuracy to which the gap thickness could be set was ±0.5 mils.

After setting the desired gap thickness, the roller was set into motion by a constant speed motor. The speed of the roller was gradually increased until the onset of ribbing became apparent. The onset was detected visually by observing the formation of a wavy film on top of the roller and/or the formation of waves at the fluid-plate interface. Both techniques were used because for some fluids and gap thicknesses, the visual onset of ribbing was sharper at the interface than at the roller surface. The procedure was repeated three times for each gap thickness and fluid. The average of the three speeds was calculated and recorded as the critical speed for the onset of ribbing.

The coating thickness was measured at various speeds below critical speed. With aid of a travelling microscope, the micrometer was adjusted until the needle contacted the clean surface of the static roll. The value of the micrometer setting was recorded and the needle was raised. After the desired speed of the roller was fixed, the needle was driven by the micrometer until it contacted the surface of the coating formed at the top of the roller. The micrometer reading was again recorded and the difference between the two readings was the film thickness, H_0. Measurements were repeated three times and the results averaged to insure the collection of reliable data. Using this technique, the coating thickness was measurable to an accuracy within ±2 mils.

The wavelength of the ribs were determined at various speeds and gap thicknesses photographically. A 35 mm SLR Nikon F2 camera and Kodak Tri X black and white film was used to photograph the ribbing pattern observed at the fluid plate interface. From the photograph, the number of ribs across the roll, exclusive of the ends, were counted and the corresponding distances measured. From these data the wavelengths were calculated.

Contact angles at speeds below ribbing onset and at various gap thicknesses were also determined photographically. The contact angle was defined as that angle formed by the plate surface and the line drawn tangent to the separation point of the fluid from the plate. A schematic diagram of a typical contact angle is shown in Figure II-4. The projection of the negatives was sketched onto a

Figure II-4. Schematic diagram of the contact angle, θ.

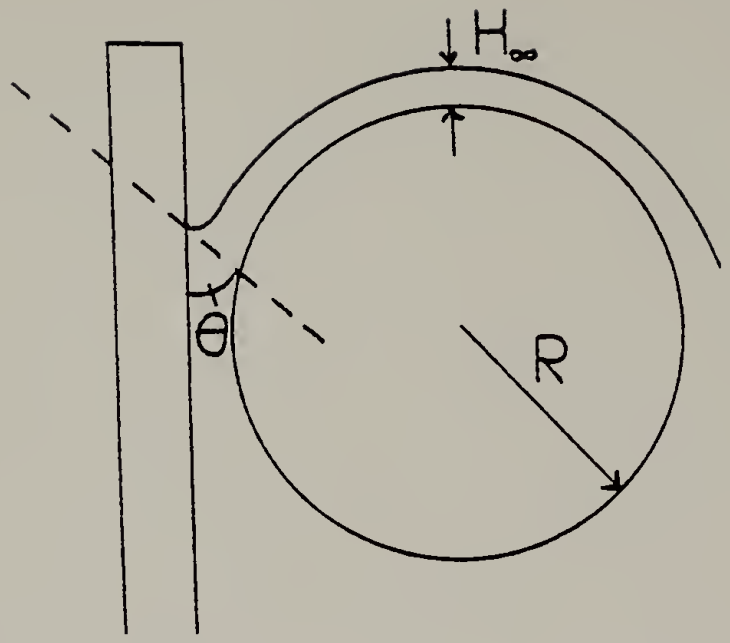

Figure II-4

sheet of paper from which the contact angles were measured using a protactor.

II.4 Fluids

The experimental fluids were either Newtonian or viscoelastic in nature.

The Newtonian fluids consisted of pure glycerin, 90/10 glycerin-water, mineral oil, Ivory Liquid and oleic acid.

The viscoelastic fluids consisted of a 90/10 glycerin-water base with increasing concentrations of polyacrylamide (10, 20, 50, 100, 300 ppm polyacrylamide), an approximate 25/75 glycerin water base with one percent polyacrylamide, and a one and a half percent polyacrylamide aqueous base solution. The polyacrylamide used was Polyhall M-295.

The viscoelastic fluids were prepared by adding the polyacrylamide in small quantitites to a specific amount of cooled distilled water. This was done with rapid and constant stirring to aid in dissolving the polymer and to help prevent the formation of large polymer aggregates. This mixture was then added to glycerin or water depending on the solution being prepared and stirred using an S shaped impeller. Stirring was maintained until all the polymer had dissolved. The fluids were then set aside for a minimum time of three days to allow them to reach equilibrium.

The viscosities of the Newtonian fluids were measured in an Epprecht-Rheomat 15 coaxial cylinder viscometer and are listed in

Table II-2. The viscosity data were taken at a temperature corresponding to the average temperature at which the experiments were conducted.

The viscometric and viscoelastic properties of the polyacrylamide solutions were measured at room temperature using a Rheometrics Mechanical Spectrometer. A cone and cylinder mode was used rather than the standard cone and plate mode to reduce any change in fluid concentration that might have occurred through water evaporation. The viscometric properties for these solutions, the viscosity and primary normal stress coefficient as a function of shear rate, are shown in Figures II-5 and II-6. The viscoelastic properties, η' and η''/ω as a function of frequency, are shown in Figures II-7 and II-8. The corresponding viscosities and viscoelastic data for the polyacrylamide solutions are listed in appendix A.

The static surface tension of each experimental fluid was measured using the pendant drop technique as described by Gaines (1972). With reference to Figure II-9, the equation used by this method to calculate the surface tension is

$$\sigma = \rho g (d_e)^2 / H \qquad \text{(II-1)}$$

where ρ is the fluid density, g is the acceleration of gravity, de is the largest diameter of the drop, and H is a correction factor dependent on the shape of the drop. 1/H is known to be a function of S where S is the ratio of ds to de, ds being the drop

Table II-2

VISCOMETRIC DATA FOR THE EXPERIMENTAL NEWTONIAN FLUIDS

Temperature: 25°C

Fluid	η(Poise)	σ(dynes/cm)
Glycerin	10.7	64
90/10 Glycerin water	2.49	63
Mineral Oil	1.71	35
Oleic Acid	0.319	32
Ivory Liquid	1.69	25

Figure II-5. The viscosity, η, vs. the shear rate, $\dot{\gamma}$, for viscoelastic fluids.

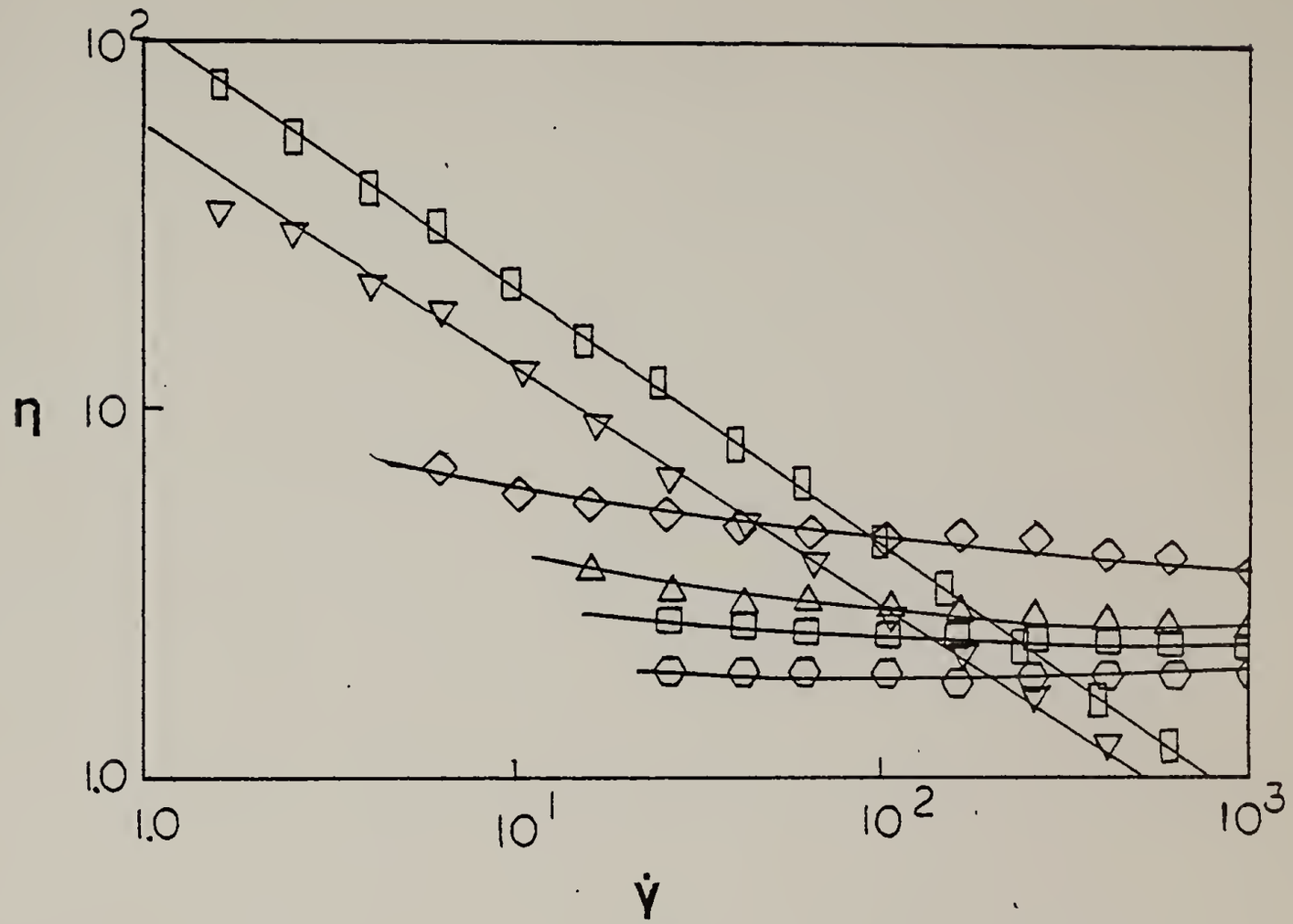

Figure II-5

Figure II-6. The primary normal stress coefficient, ψ_{12}, vs. the shear rate, $\dot{\gamma}$, for viscoelastic fluids.

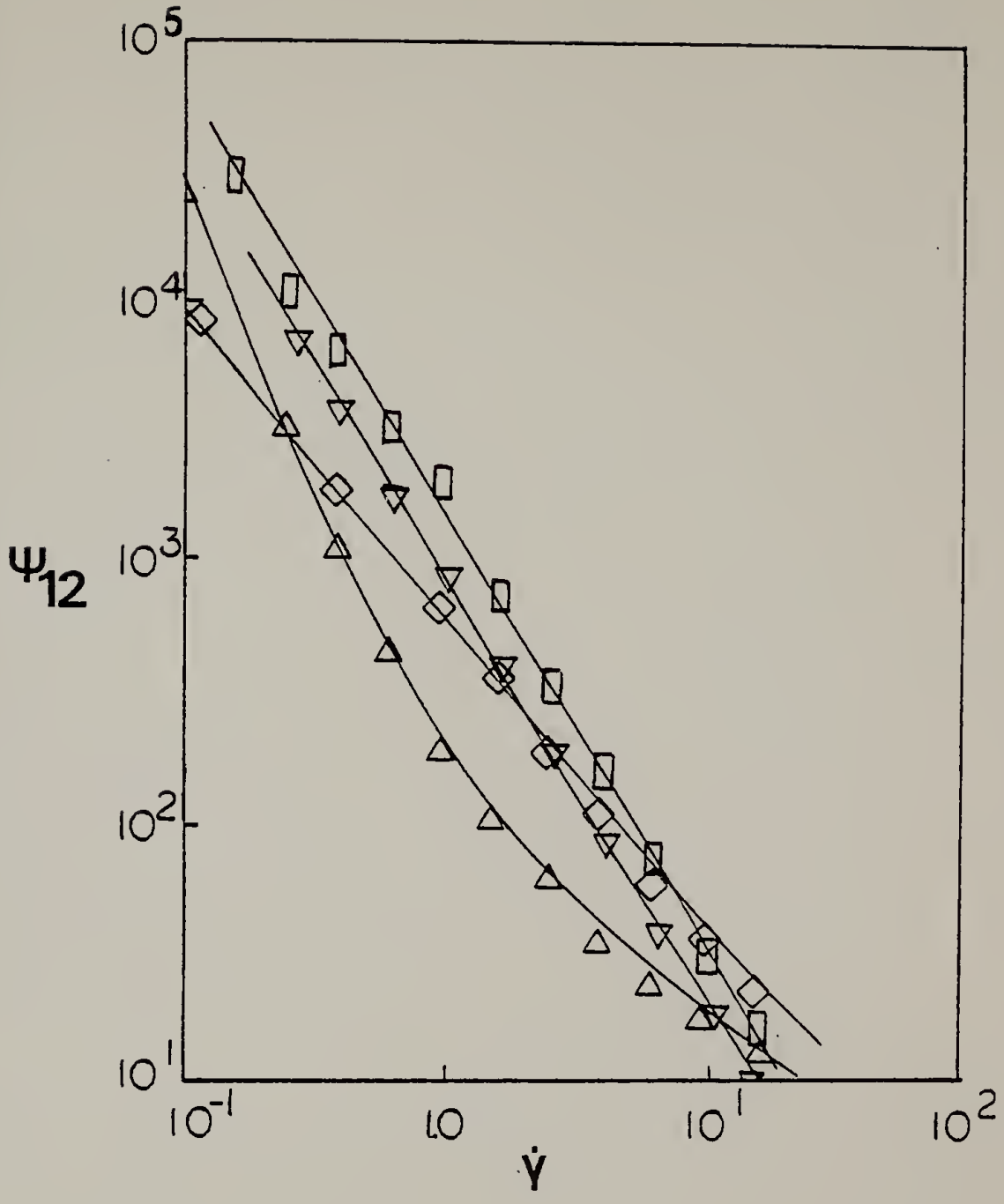

Figure II-6

Figure II-7. The dynamic viscosity, η', vs. the frequency, ω, for viscoelastic fluids.

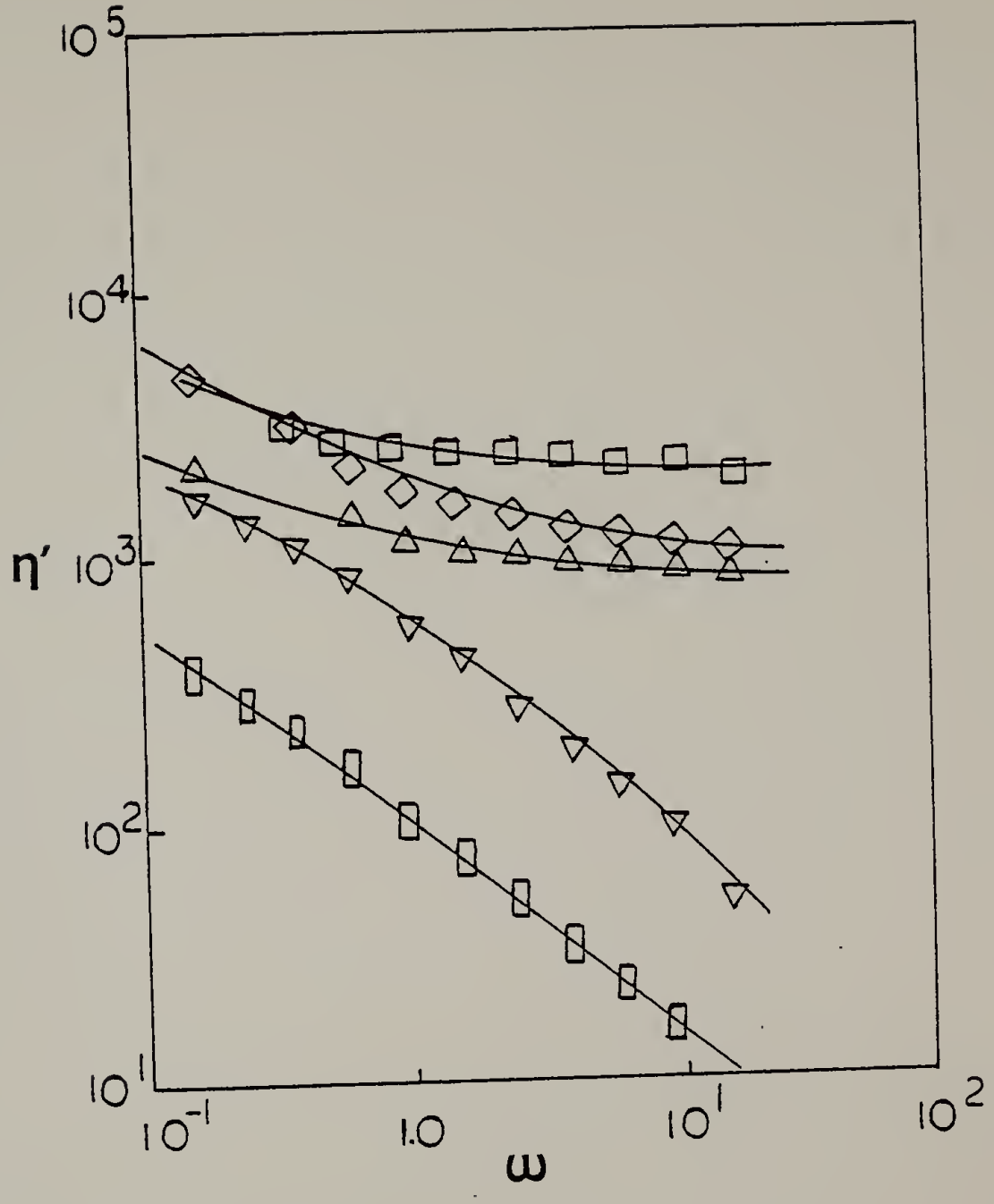

Figure II-7

Figure II-8. The complex viscosity function, η''/ω, vs. the frequency, ω, for viscoelastic fluids.

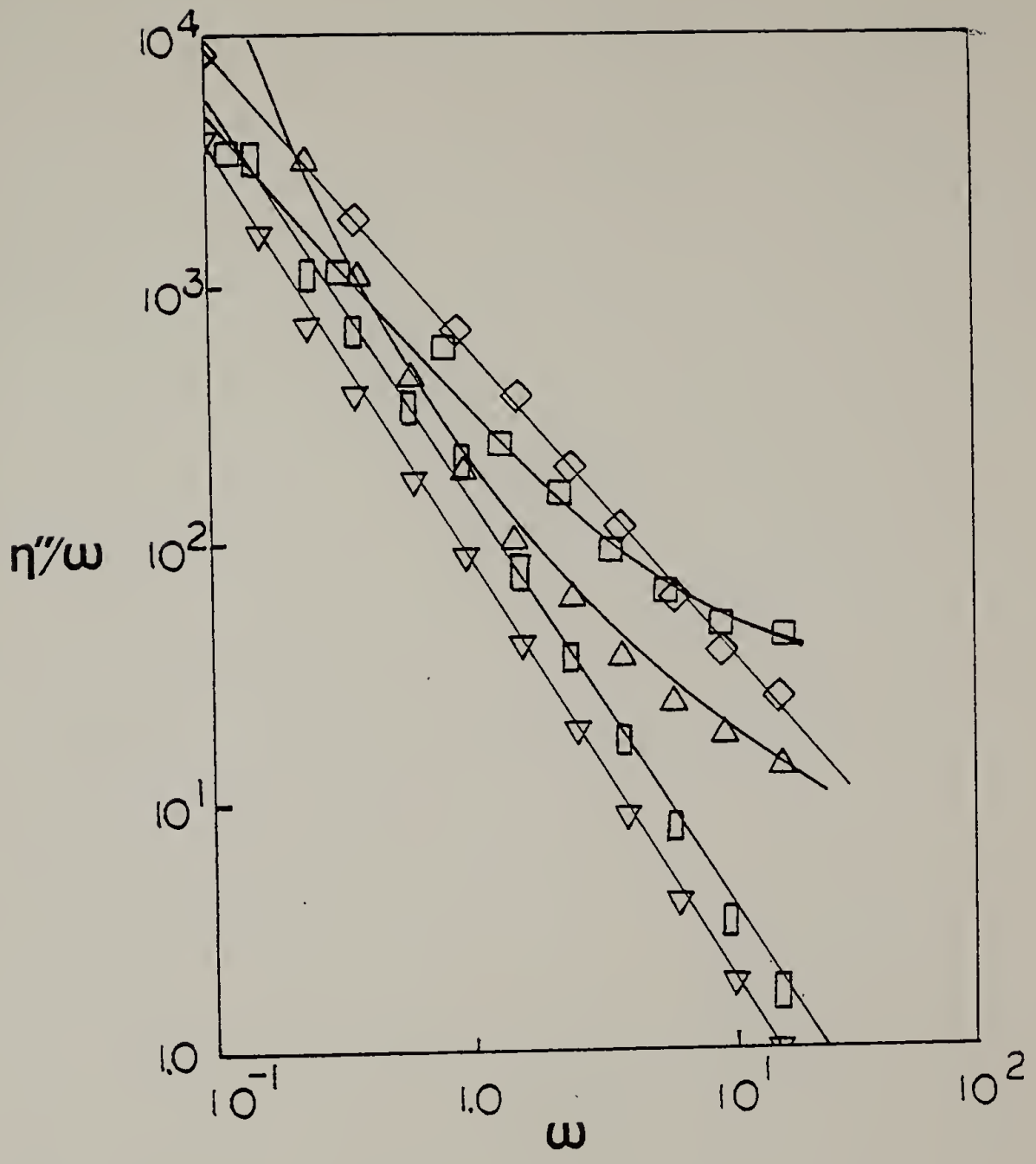

Figure II-8

Figure II-9. Shape of the pendant drop used to measure surface tension, σ.

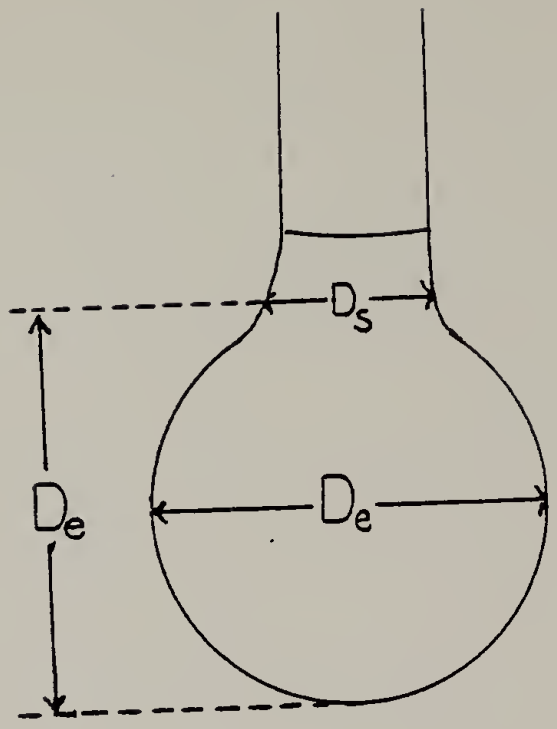

Figure II-9

diameter measured at a height de from the bottom of the drop. Values of 1/H as a function of S have been tabulated by Fordham (1948) and are listed in tables. This allows one to simply determine H once S is known. S was determined for each experimental fluid photographically using a 35 mm SLR Nikon F2 Photomic camera. Photographs were taken of a static drop of fluid suspended from a capillary attached to a syringe. The surface tension was calculated for five different drops of various sizes for each fluid. The averaged value of the five surface tensions are listed in Table II-2 for the Newtonian fluids and Table II-3 for the viscoelastic fluids. Using this technique, the surface tension of water was determined reliably within ±2 dynes/cm.

Table II-3

SURFACE TENSION DATA FOR EXPERIMENTAL VISCOELASTIC FLUIDS

Temperature: 25°C

Fluids	σ(dynes/cm)
10 ppm PAA	63
20 ppm PAA	60
50 ppm PAA	64
100 ppm PAA	59
300 ppm PAA	64
1% PAA	73
1.5% PAA	73

CHAPTER III

RESULTS

III.1 Newtonian Results

III 1.1 Conditions for Ribbing. The onset of ribbing was determined for a number of Newtonian fluids using the technique as described in Chapter II. The data for these experiments are listed in Appendix B. It has been previously predicted by Savage (1977), that ribbing occurs at a critical value of the capillary number Ca^*, and is dependent solely on a geometrical parameter defined as H_0/R. Accordingly, the critical capillary number of the corresponding data is plotted as a function of H_0/R for both a one inch and two inch radius roller. This is shown in Figure III-1. A correlation is found between Ca^* and H_0/R but the data do not conform for the two different size rollers. This is evident in comparison of the stability criteria for the two systems. Ca_1^* was found to be 25 for the smaller roller and 59 for the larger one. Consequently, there appears to be a roller size dependence in the correlation of the Ca^* with H_0/R thus contradicting the theory proposed by Savage.

Further analysis of the data shows that Ca^* was a function of the gap thickness, H_0, and did not appear to be dependent on the roller size. These results are shown in Figure III-2.

III 1.2 Wavelength Data. Wavelength measurements using a two inch radius roller were taken from photographs for three Newtonian fluids:

Figure III-1. The critical capillary number Ca*, vs. H_0/R for Newtonian fluids using a 1" and 2" radius roller. (Key in Table B-10.)

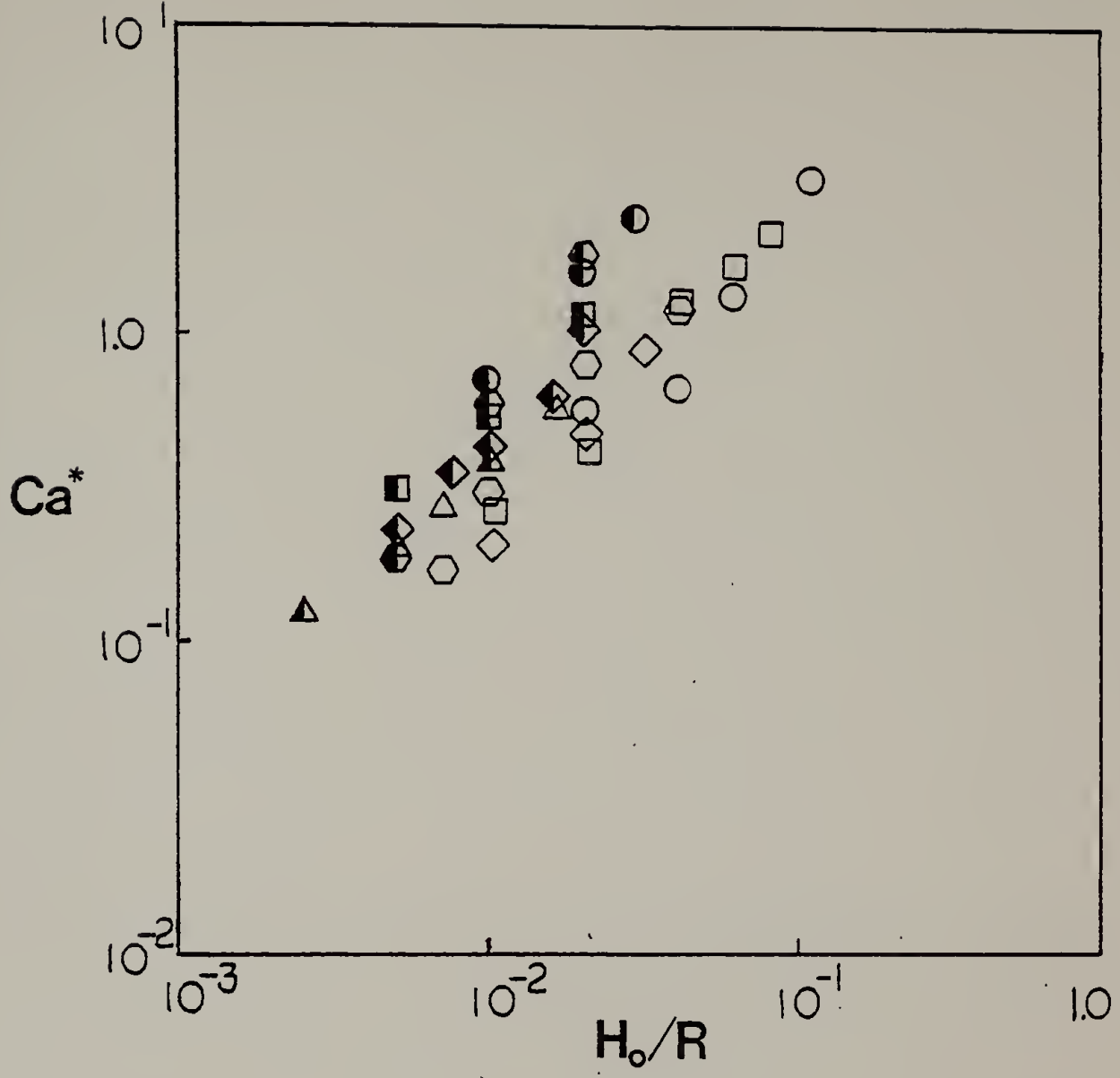

Figure III-1

Figure III-2. The critical capillary number, Ca^*, vs. the gap thickness, H_0, for Newtonian fluids using a 1" and 2" radius roller. (Key in Table B-10.)

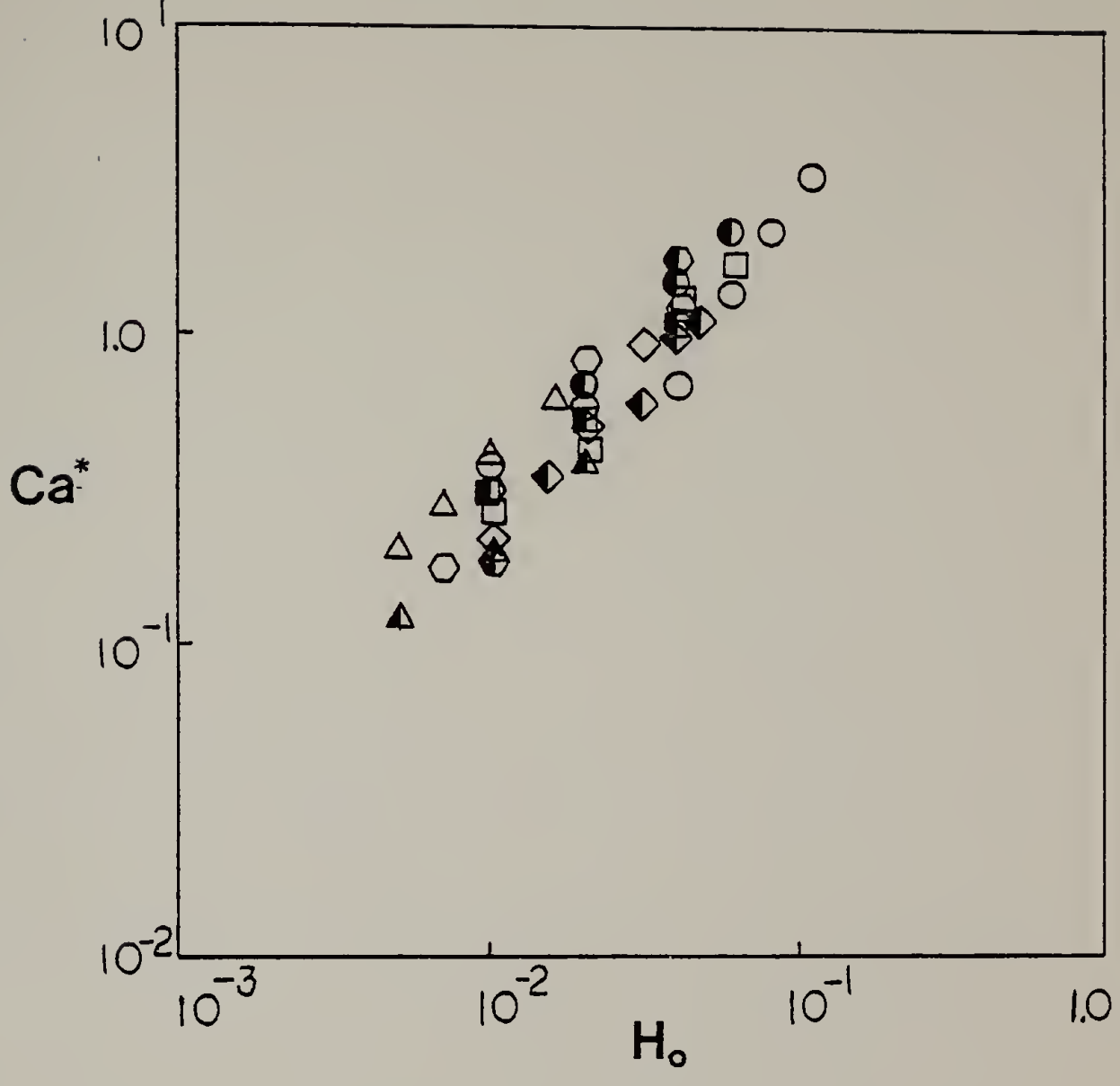

Figure III-2

90/10 glycerin water, mineral oil and oleic acid. Some photographs from which these measurements were made are shown in Figure III-3. From the data listed in Appendix B, the normalized wavelength, W/H_0, was calculated and plotted against the reduced speed, U/U^*, (Figures III-4 and III-5). The graph shows that as the speed increases, the normalized wavelength becomes smaller and reaches an asymptotic value independent of the gap thickness.

Some wavelength data were also collected for the one inch radius roller. The Newtonian fluids used for these measurements were glycerin and 90/10 glycerin water. Despite the paucity of the data, the trend observed is similar to that in the case of the larger roller. The wavelength decreases as the speed and gap thickness both increase. In comparing the two sets of data, it is found that the effect of roller size becomes more apparent when the normalized wavenumber is plotted as a function of Ca. Comparison of Figures III-6 and III-7 shows that the variation of wavelength with speed is unaffected by roller size. Once the instability has set in, there is no longer a roller size dependence.

III 1.3 Coating Thickness Data. As stated earlier in Chapter I.2, Sullivan and Middleman (1979) proposed a theory based on the lubrication approximation which suggested that a dimensionless coating thickness, λ, defined as H_∞/H_0, should depend only on the gravity parameter, F, where

$$F = \rho g H_0^2/\mu U \qquad \text{(III-1)}$$

Figure III-3. Photographs of the ribbing phenomenon for Newtonian fluids.
a. Mineral oil, R=2", H_0=0.02", Ω=20 r.p.m.
b. Mineral oil, R=2", H_0=0.02", Ω=30 r.p.m.

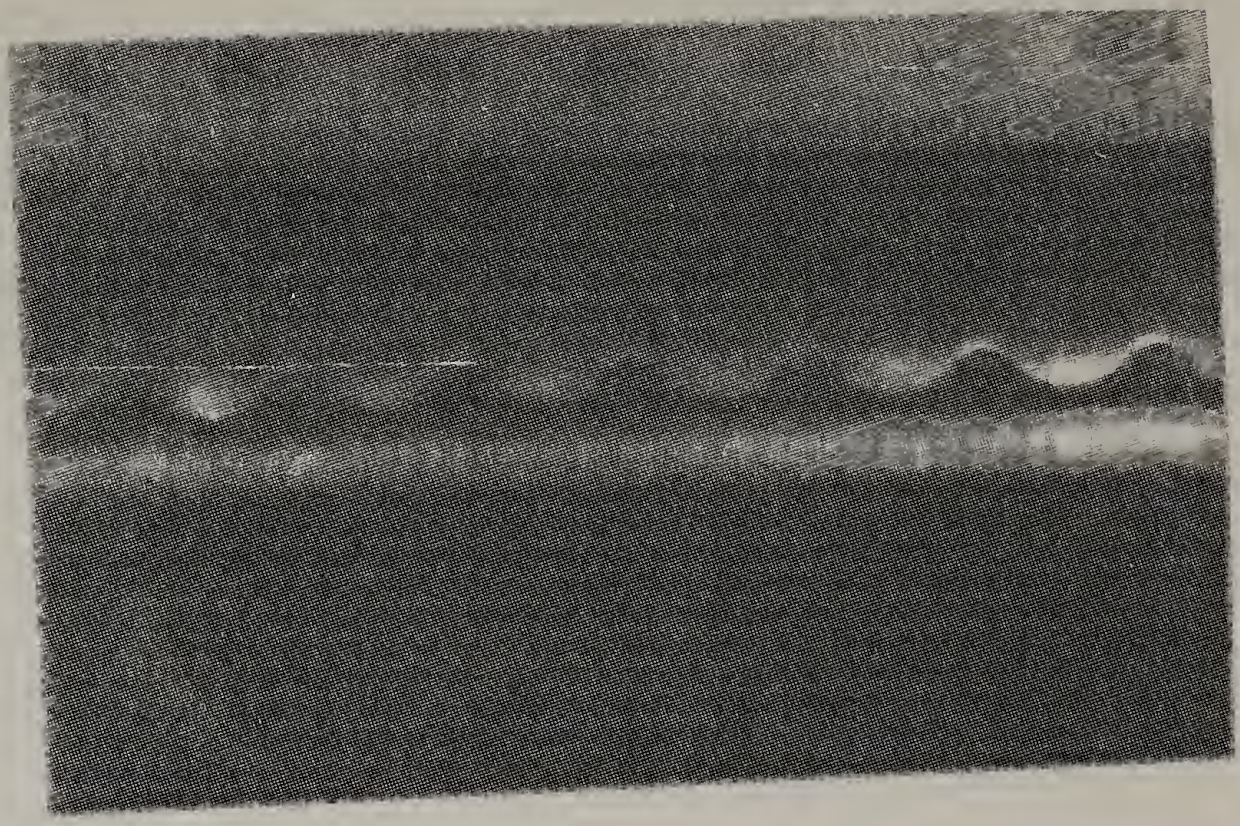

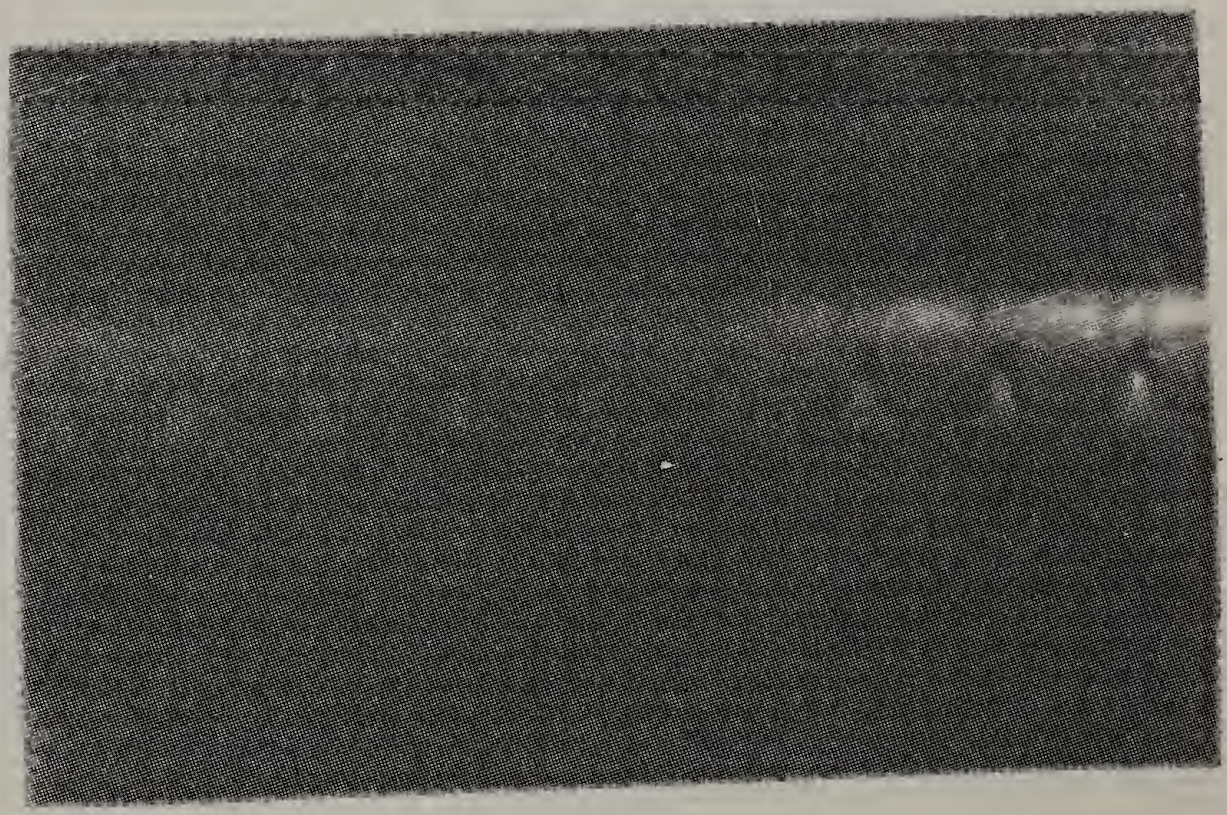

Figure III-3

Figure III-4. Normalized wavelength, W/H_0, vs. the reduced speed, U/U^*, for Newtonian fluids. Roller size: R=1". (Key in Table B-10.)

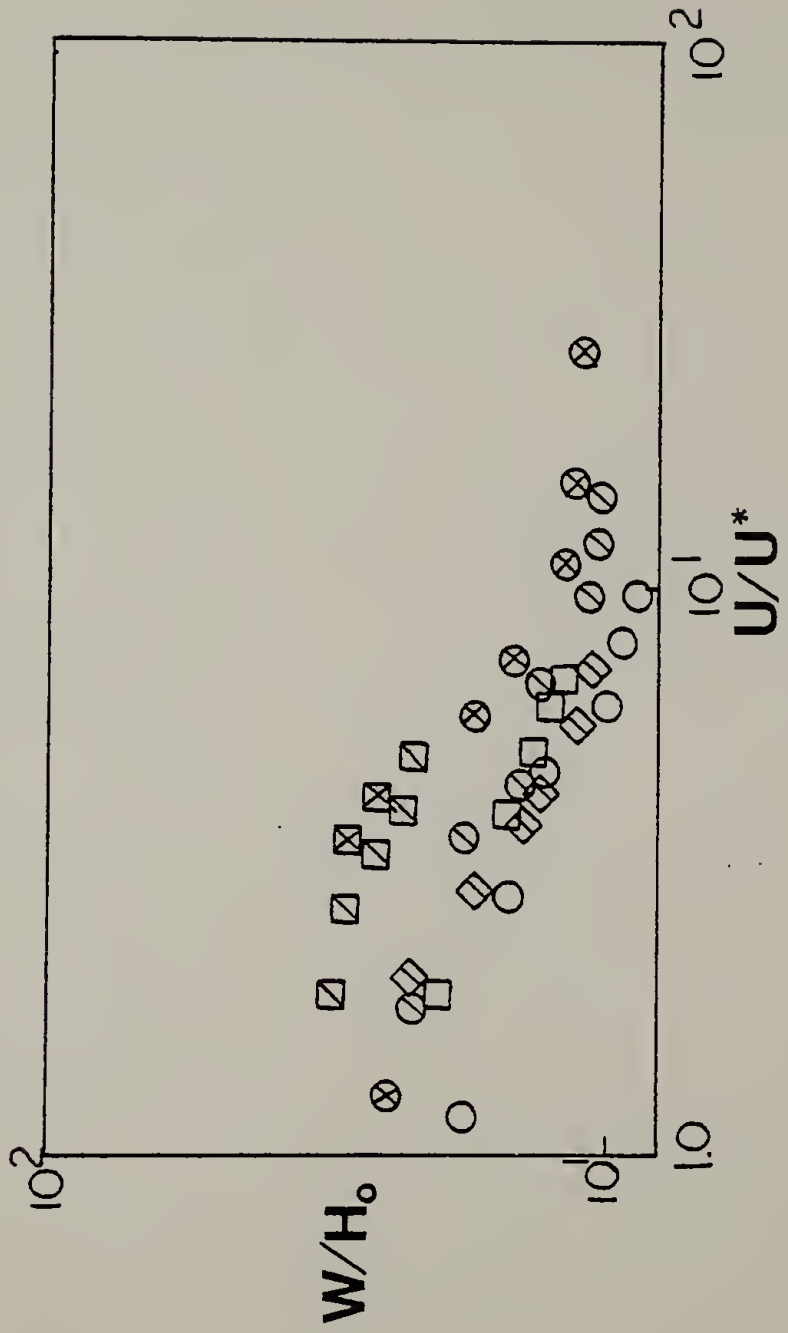

Figure III-4

Figure III-5. Normalized wavelength, W/H_0, vs. the reduced speed U/U^* for Newtonian fluids. Roller size: R=2". (Key in Table B-10.)

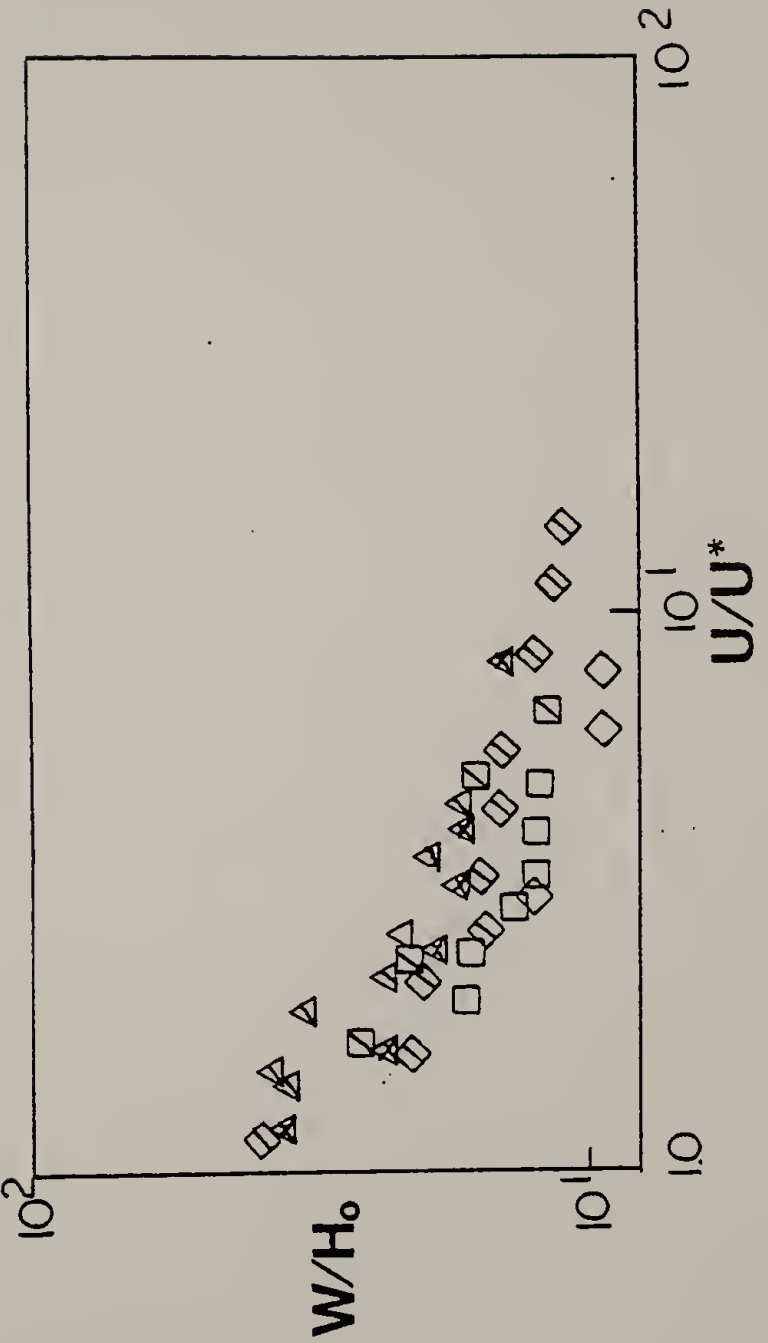

Figure III-5

Figure III-6. Normalized wavelength, W/H_0, vs. the capillary number, Ca, for Newtonian fluids. Roller size: R=1". (Key in Table B-10.)

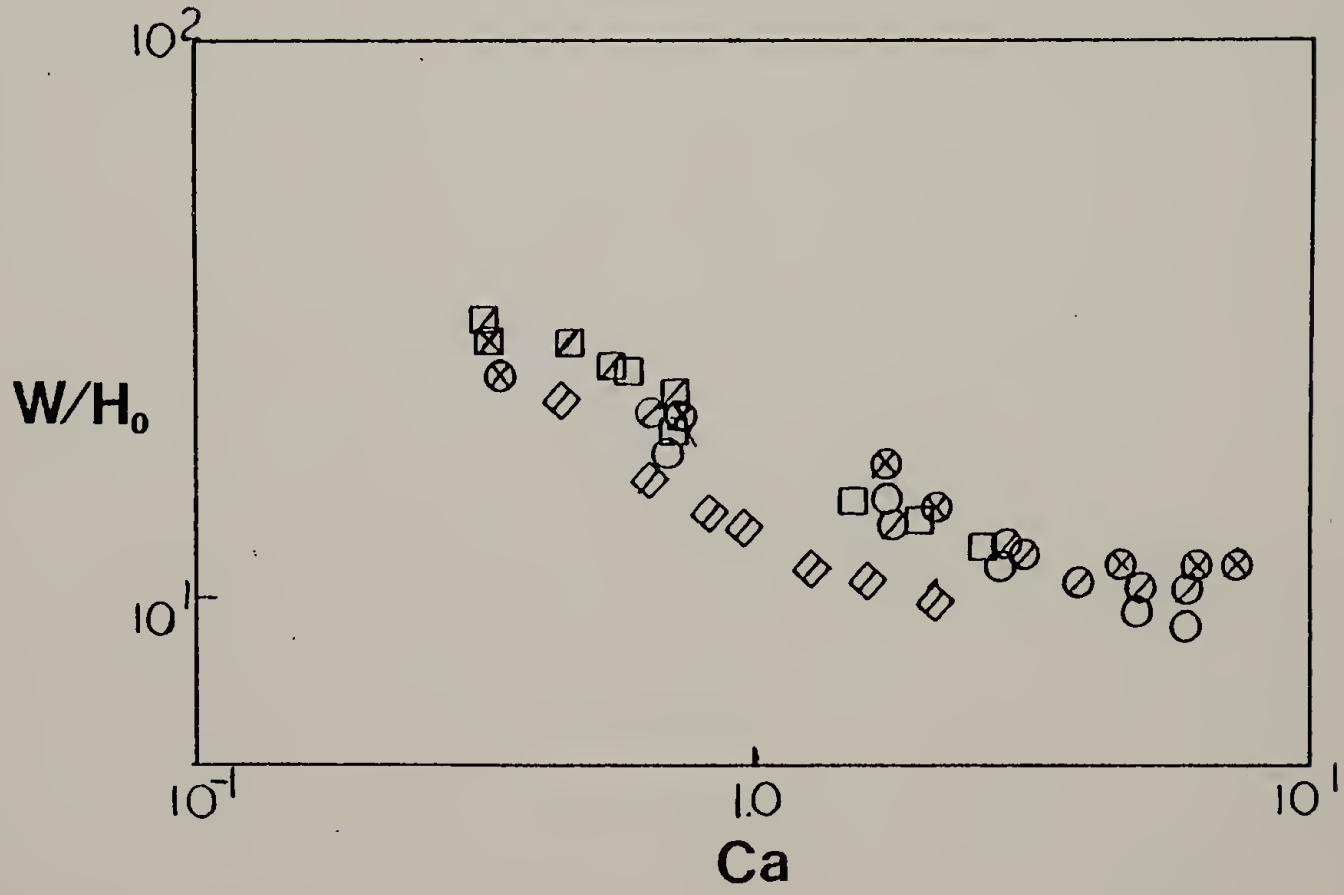

Figure III-6

Figure III-7. Normalized wavelength, W/H_0, vs. the capillary number, Ca, for Newtonian fluids. Roller size: R=2". (Key in Table B-10.)

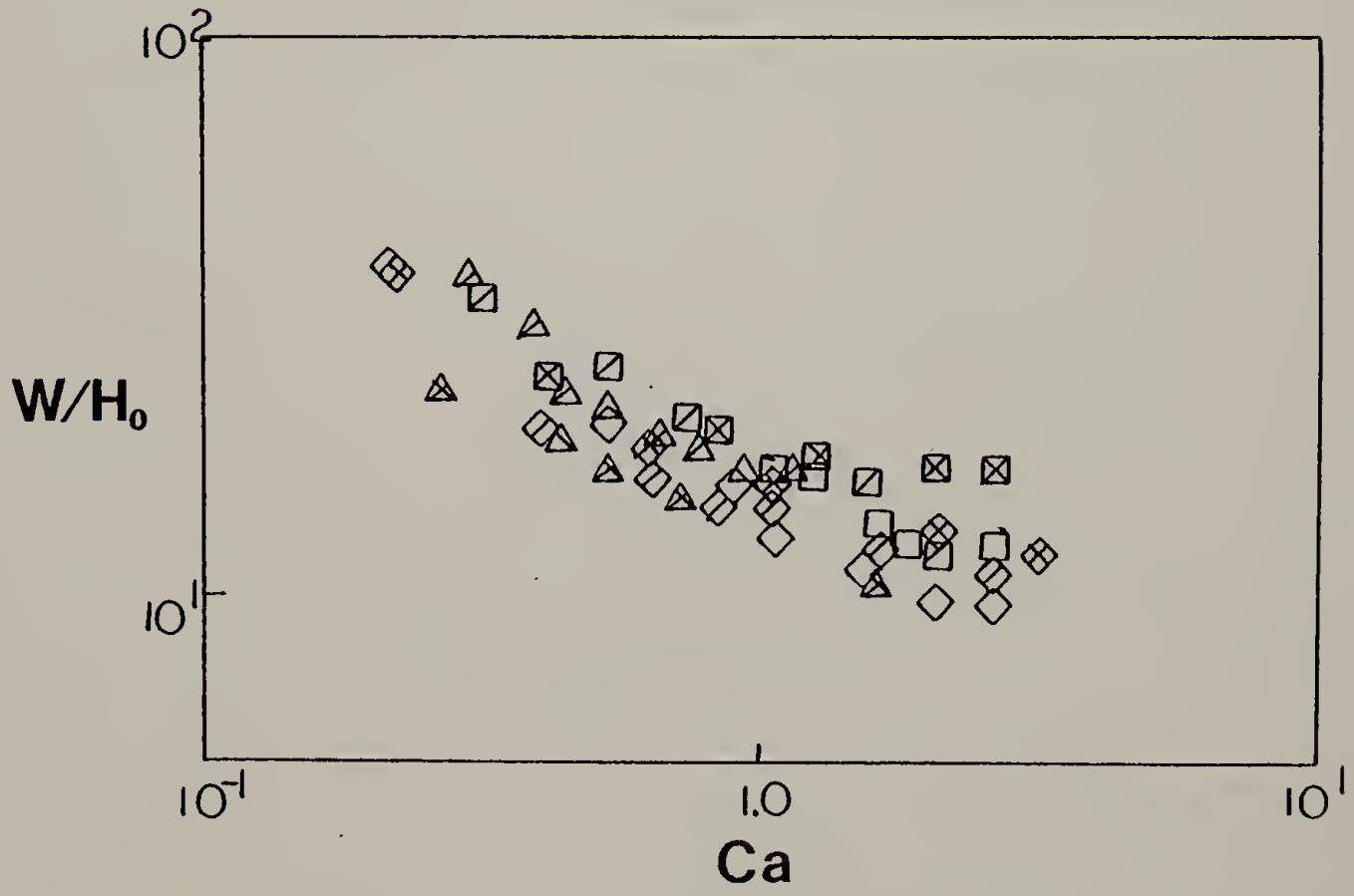

Figure III-7

As a result, λ is found theoretically to be in the range $0.5<\lambda<0.605$.

Coating thickness data were collected for three Newtonian fluids and are reported in appendix B-5. Comparison of these data with theory shows good agreement at low F values, that is at high speeds. Deviation from theory begins at $F>0.6$ and becomes greater as F increases. This comparison is shown in Figure III-8. Sullivan and Middleman (1979) also found deviation at high F values and attributed it to an effect of surface tension which was unaccounted for in this particular theory. As a result, Sullivan and Middleman modified the theory to include surface tension. Their revised theory was based on the idea that at low speed, surface tension forces could dominate the behavior of the fluid in the separation region. The point where the fluid separates from the plate was determined by a simple force balance, the result being

$$\xi_1 = S/(1 + \tfrac{1}{2}\xi_1^2) \qquad \text{(III-2)}$$

where

$$S = 2\sigma/\rho g H_0 (RH_0)^{1/2} \qquad \text{(III-3)}$$

and ξ_1 is a dimensionless variable defined as

$$\xi_1 = X_1/(RH_0)^{1/2} \qquad \text{(III-4)}$$

This value of ξ_1 is introduced into the theory and the resulting values of λ as a function of F are shown in Figure III-8. Compared to experimental results, $\lambda<0.5$ was accounted for. However, the modified theory still did not predict sufficiently values of λ at high gravity numbers.

Figure III-8. The dimensionless coating thickness, λ, vs. the gravity parameter, F, for Newtonian fluids compared to Sullivan and Middleman's (1979) theory. —— Theory. (Key in Table B-10.)

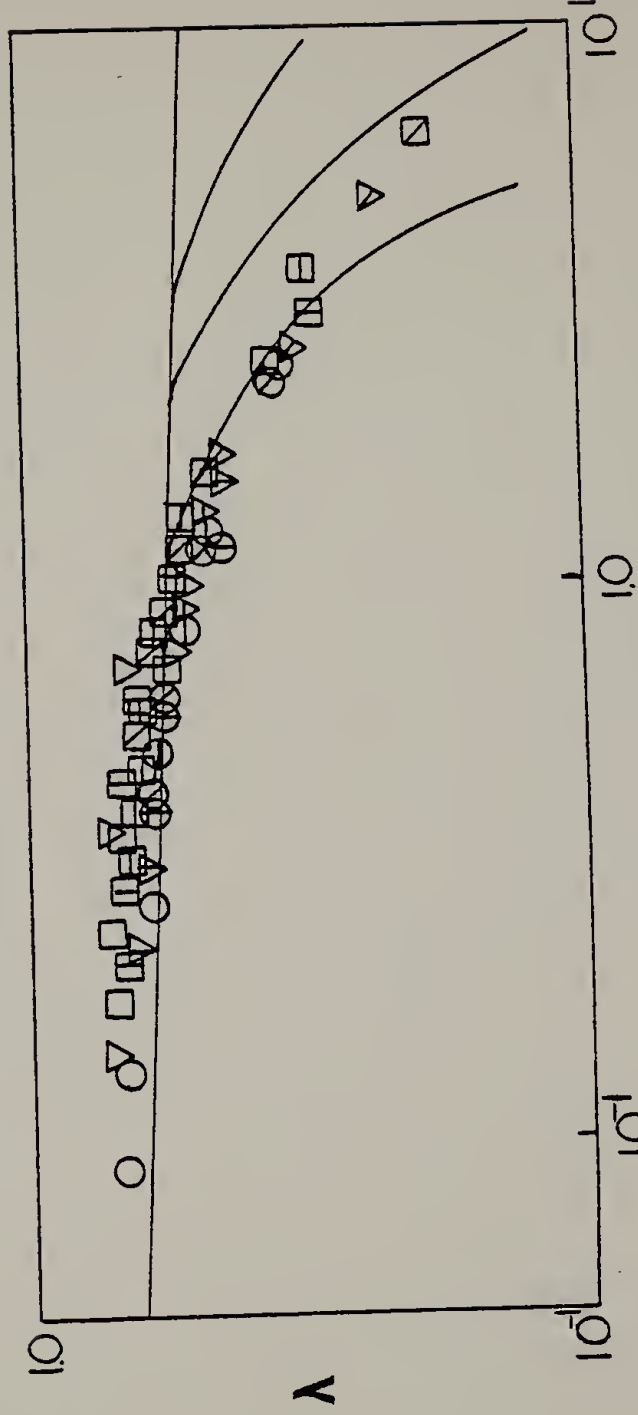

Figure III-8

Coyne and Elrod's theory which accounted for the effect of surface tension predicted λ to be a function solely of Ca. This however, was not found experimentally to be the case (Figure III-9). There appears also to be a dependency on gap thickness, i.e. at Ca$\leq$1.0, film thickness decreases with increasing gap thickness.

III 1.4 Contact Angle Data. The problem in deriving a model which correctly predicts the critical conditions for ribbing lies in the difficulty of formulating the correct boundary conditions applicable at the separation point. In previous theories it has been assumed that the contact angle, θ, or wetting angle formed by the fluid on the surface of the plate as pictures in Figure II-4, is constant. The actual value of the angle is not really known. In the theory proposed by Coyne and Elrod (1970), it is assumed that the wetting angle is 90°. However, Taylor (1963) presents experimental results which agree with this theory if a wetting angle is assumed to be 60°.

Experimental data of contact angles were collected in order to give some indication of the typical values occurring under certain conditions, e.g. speed, gap thickness, roller size. Some photographs from which data were taken are shown in Figure III-10. The overall results for a 90/10 glycerin-water solution using two different size rollers are recorded in Table III-1. From the data, there appears to be a roller size dependency on the contact angle. It was found that for the same H_0/R the contact angle for the larger system was greater than that for the small system.

Figure III-9. The dimensionless coating thickness, λ, vs. the capillary number, Ca, for Newtonian fluids compared to Coyne and Elrod's (1970) theory. ——Theory. (Key in Table B-10.)

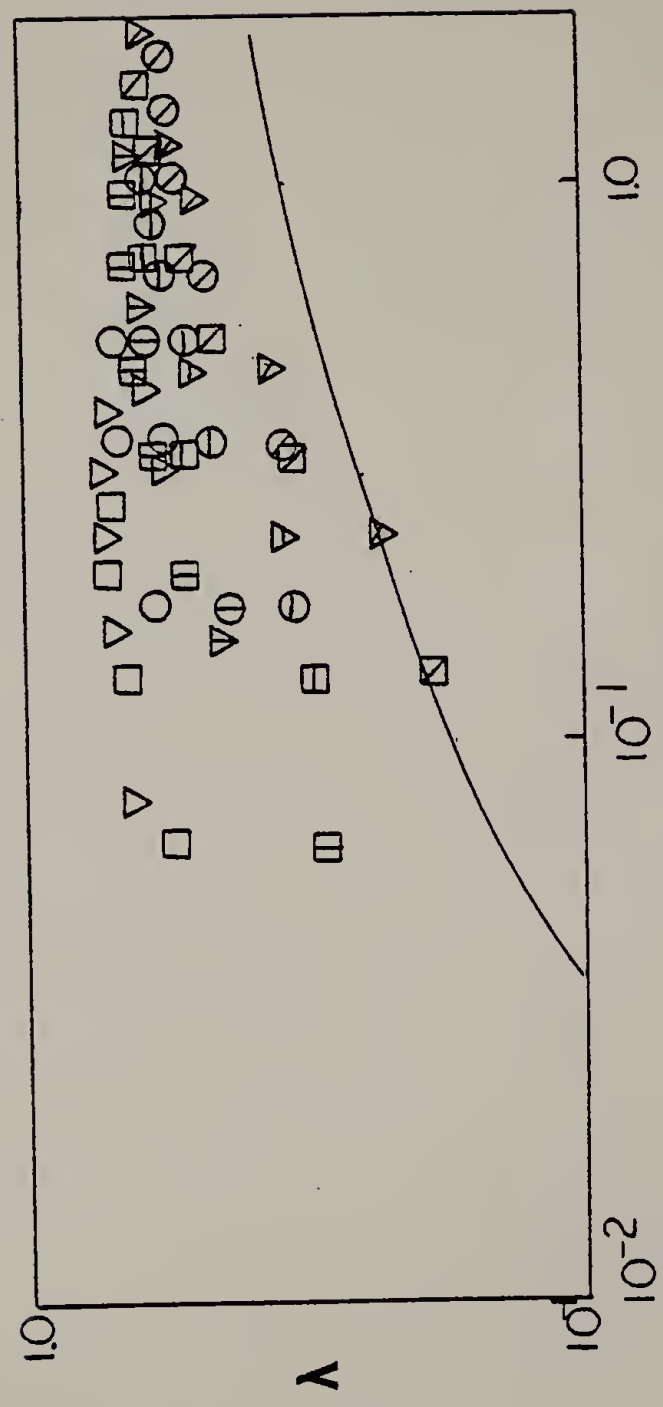

Figure III-9

Figure III-10. Photographs of the contact angle formed by Newtonian fluids on the surface of the plate.
a. 90/10 glycerin water, R=2", H_0=0.03", Ω=25 r.p.m.
b. 90/10 glycerin water, R=2", H_0=0.03", Ω=25 r.p.m.

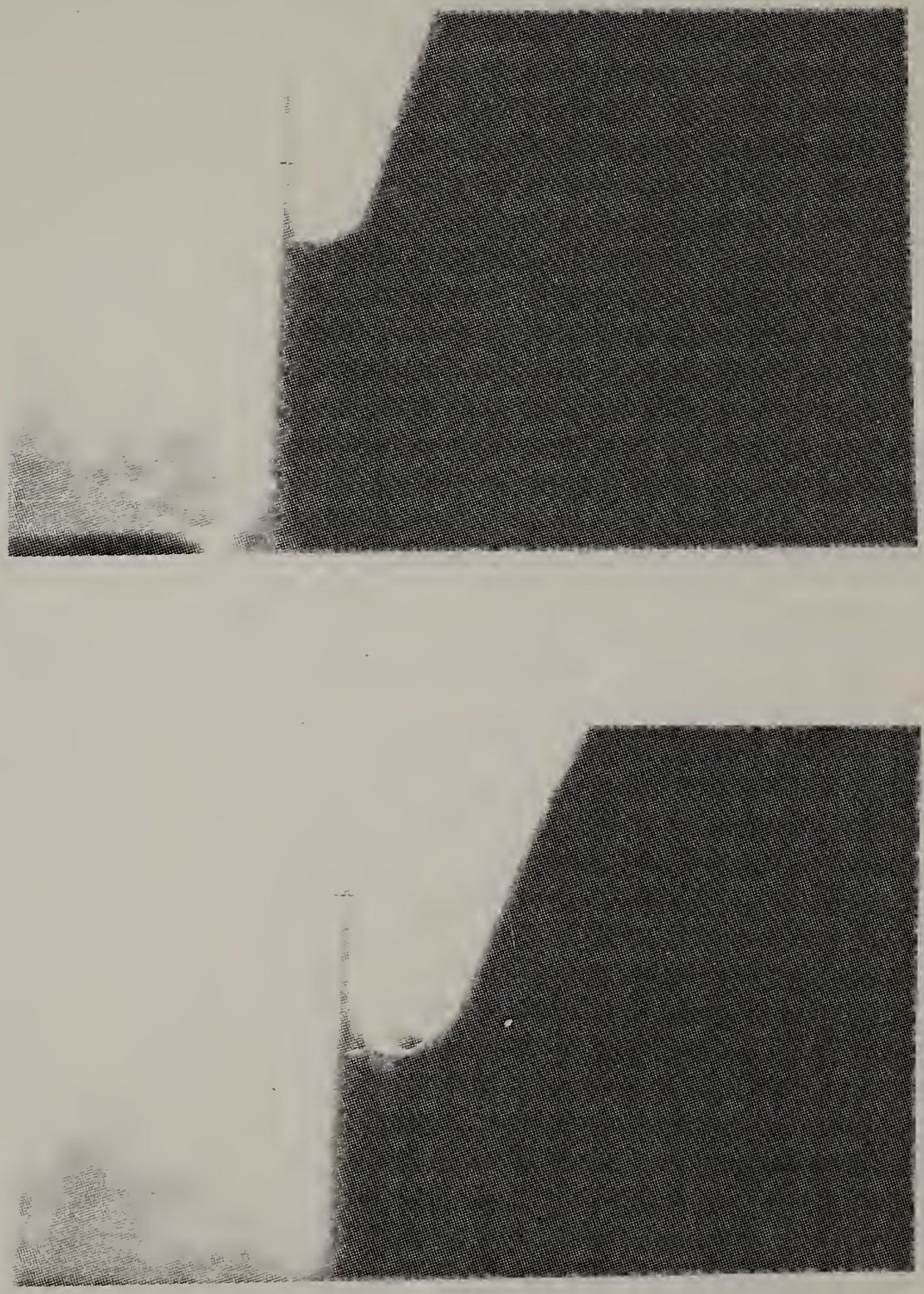

Figure III-10

Table III-1

CONTACT ANGLE DATA FOR A 90/10 GLYCERIN WATER SOLUTION

Plexiglass^R Plate

Roller Size: R=1"			Roller Size: R=2"		
H_0(in)	H_0/R	θ(degrees)	H_0(in)	H_0/R	θ(degrees)
0.02	0.02	81	0.02	0.01	75
0.03	0.03	70	0.03	0.015	79
0.04	0.04	90	0.04	0.02	89
0.06	0.06	72	0.06	0.03	71

Parafilm^R Plate

Roller Size: R=1			Roller Size: R=2"		
H_0(in)	H_0/R	θ(degrees)	H_0(in)	H_0/R	θ(degrees)
0.02	0.02	106	0.02	0.01	108
0.03	0.03	119	0.03	0.015	100
0.04	0.04	104	0.04	0.02	100
0.06	0.06	87	0.06	0.03	76

In addition, it was found that the material of the plate affected the contact angle. A piece of Parafilm^R was attached to the plate and the contact angle for this surface was determined and recorded in Table III-1. A roller size dependence was also observed. However, in this case the opposite trend existed, i.e. θ for the larger system was less than that for the small system for the same H_0/R. Comparison of the data for the two different plate surfaces under the same experimental conditions shows that the contact angle for the Parafilm^R surface is larger than that for the Plexiglass^R plate.

III.2 Viscoelastic Results

III 2.1 Conditions for Ribbing. The effect of elasticity on stability is of importance since many of the fluids used in today's industrial coating operations are viscoelastic. Thus the ribbing phenomenon was also investigated for a number of viscoelastic fluids.

The results of the critical speed data are reported in Appendix B, and displayed graphically in Figure III-11.

As in the Newtonian results, the critical capillary number, Ca^*, depends only upon H_0 and is independent of roller size, R.

III. 2.2 Wavelength Data. Wavelength data were also collected for some viscoelastic fluids and the results are listed in Appendix B. Some photographs from which measurements were made are shown in Figure III-12. Two different sized systems were used, a one inch and two inch radius roller, and the final results are represented

Figure III-11. The critical capillary number Ca^*, vs. the gap thickness, H_0, for viscoelastic fluids using a 1" and 2" radius roller. (Key in Table B-11.)

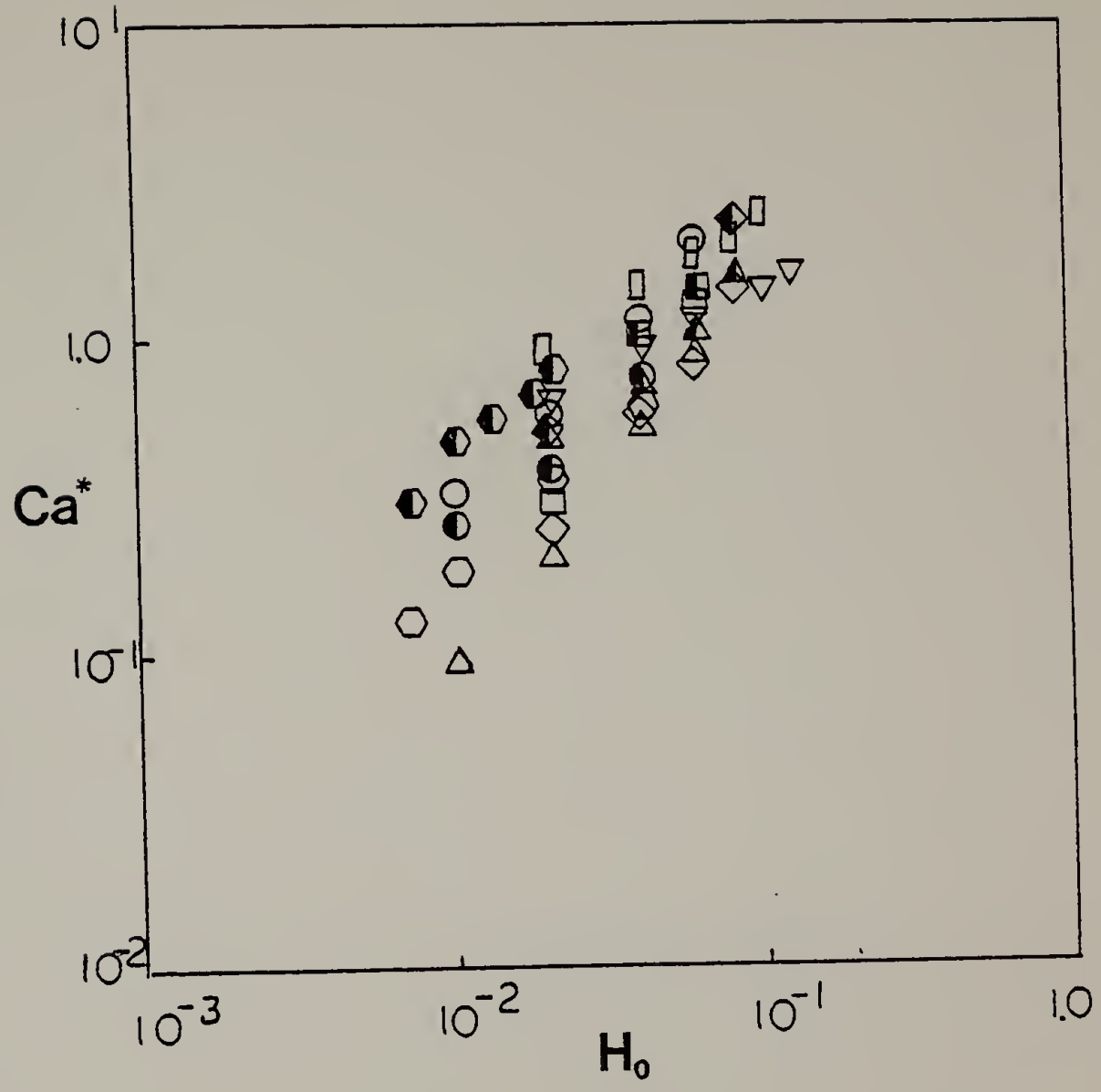

Figure III-11

Figure III-12. Photographs of the ribbing phenomenon for viscoelastic fluids.
a. 300 ppm PAA solution, R=2", H_0=0.01", Ω=50 r.p.m.
b. 300 ppm PAA solution, R=2", H_0=0.016", Ω=20 r.p.m.

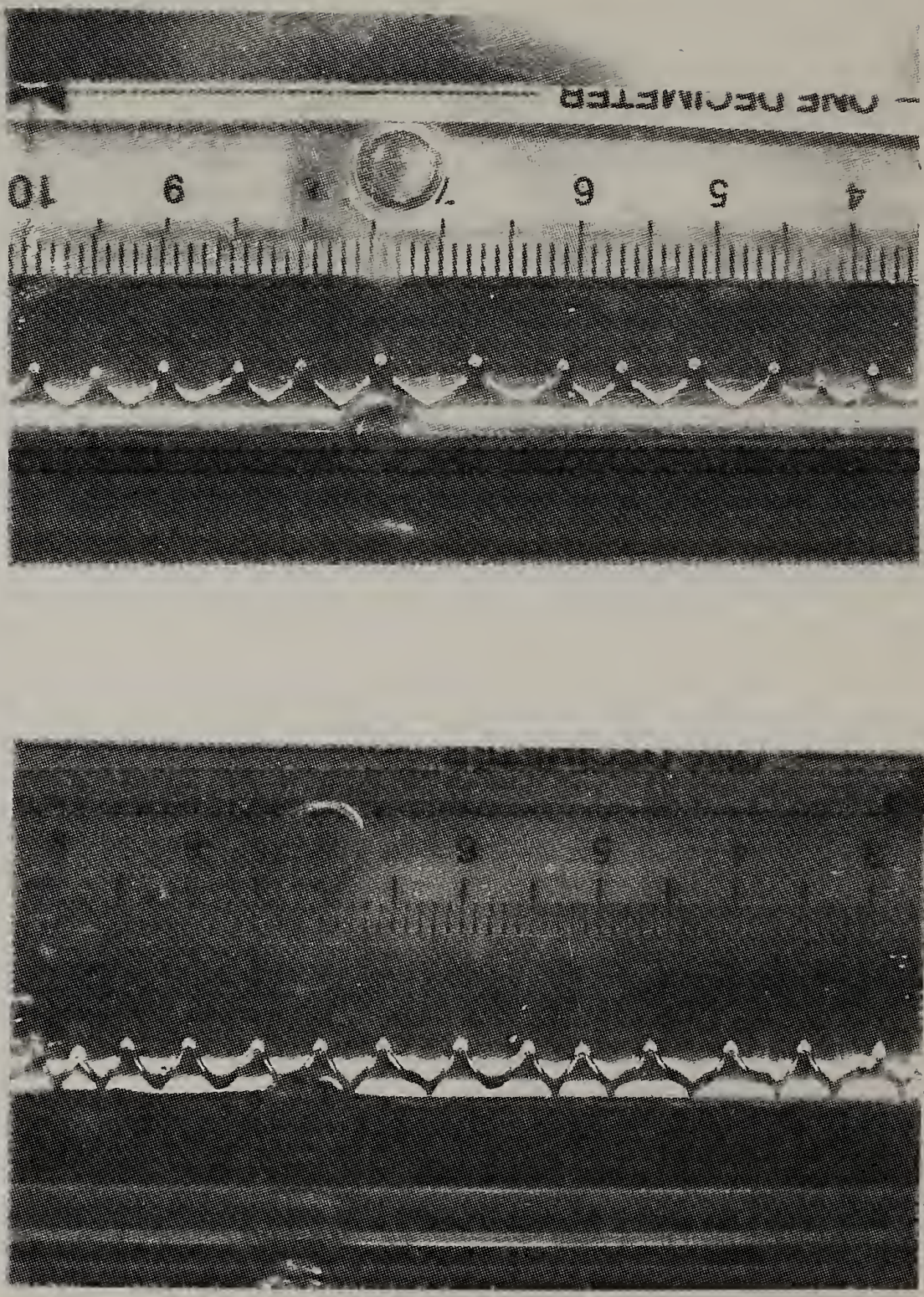

Figure III-12

in Figures III-13 and III-14, as a graph of W/H_0 vs. Ca. Although the data are quite scattered, there appears to be a roller size dependence on the wavelength for these viscoelastic fluids.

III 2.3 Coating Thickness Data. Only limited data on coating thickness were collected for viscoelastic fluids. The final results are tabulated in Appendix B and λ is plotted as a function of the gravity parameter, F, (Figure III-15). As in the case of the Newtonian fluids, the experimental data are in fair agreement with theory at low F values. However, deviation from theory increases as F increases. The average experimental coating thickness is calculated to be 0.7. This value for λ is high compared to the expected range of $0.5<\lambda<0.6$, but a discrepancy between this theory and experiment is expected since the theory was derived assuming the use of Newtonian rather than viscoelastic materials.

Figure III-13. The reduced wavelength, W/H_0, vs. the capillary number, Ca, for viscoelastic fluids using a 1" radius roller. (Key in Table B-11.)

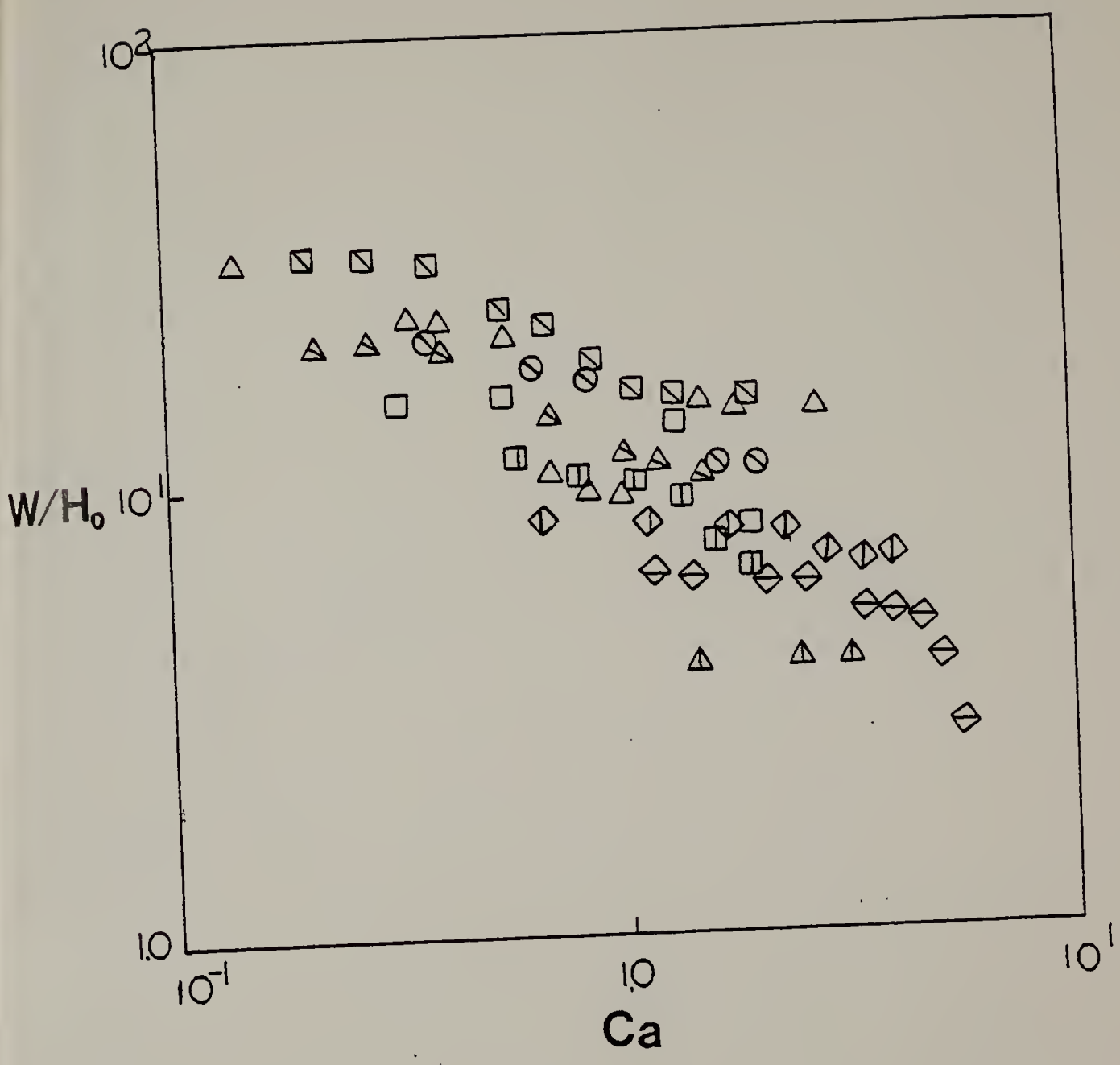

Figure III-13

Figure III-14. The reduced wavelength, W/H_0, vs. the capillary number, Ca, for viscoelastic fluids using a 2" radius roller. (Key in Table B-11.)

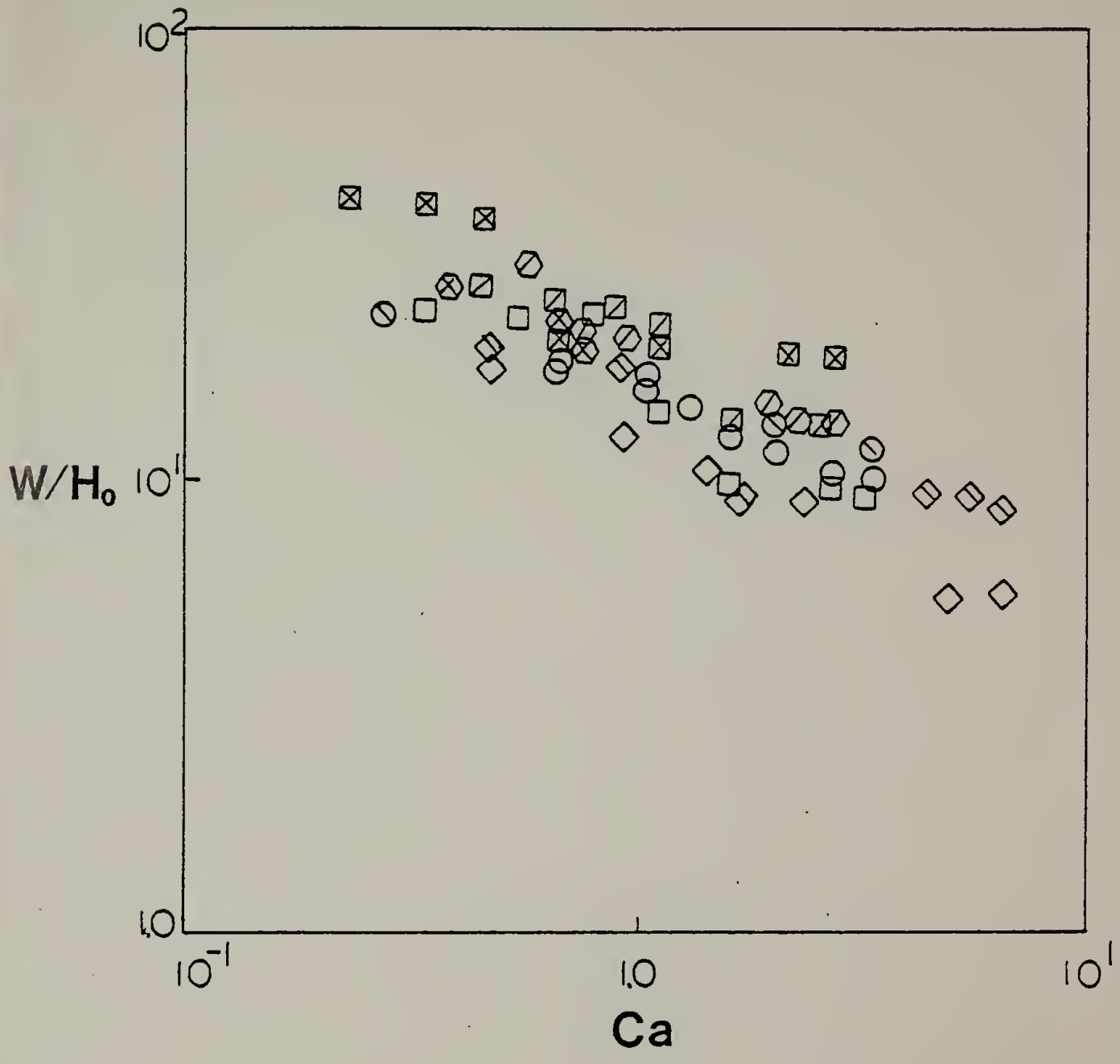

Figure III-14

Figure III-15. The dimensionless coating thickness, λ, vs. the gravity parameter, F, for viscoelastic fluids. (Key in Table B-11.)

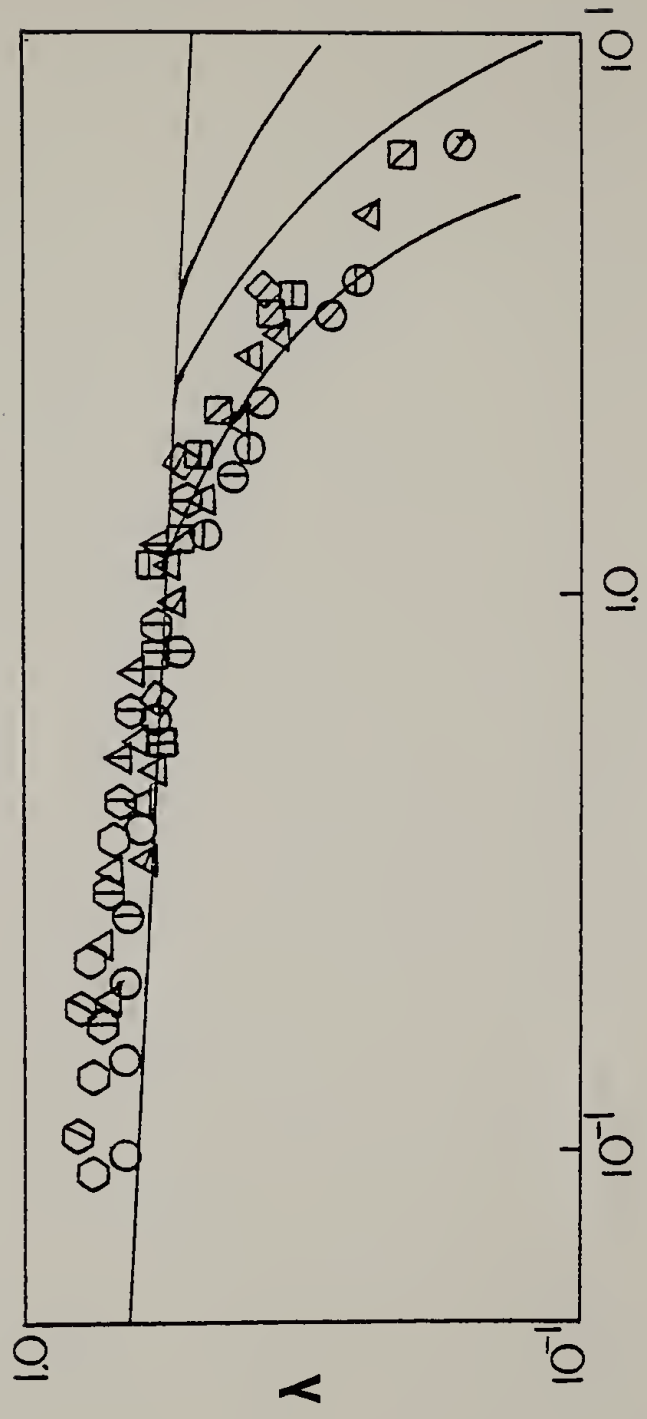

Figure III-15

CHAPTER IV

MISCELLANEOUS EXPERIMENTS

IV.1 Introduction

A number of miscellaneous experiments were performed investigating effects caused by changes in the apparata. Changes were made in the plate surface, its orientation and its shape. In this chapter, the experiments, apparata and procedures will be described and the final results discussed.

IV.2 Experimental Procedures and Results

IV. 2.1 Plate Surface. The effect of different plate surfaces on the onset of ribbing was investigated for four different materials. The materials chosen were Plexiglass^R, metal, Teflon^R and Parafilm^R. The static wetting angle formed by a 90/10 glycerin water solution on the surface of each of these materials was determined from photographs and the results are listed in Table IV-1. A drop of the fluid was placed on the material, a photograph was taken and the wetting angle indicated that there were differences in the surfaces of these materials. Plates of all the materials except Parafilm^R were prepared and fastened to the experimental apparatus as described in Chapter II. The Parafilm^R was fixed to the apparatus with the surface of the Parafilm^R between the plate and roller.

Table IV-1

STATIC CONTACT ANGLE MEASUREMENTS

Material	Contact Angle (degrees)
Plexiglass^{R}	53
Metal	82
Teflon^{R}	79
Parafilm^{R}	88

The experimental procedure for determining the onset of ribbing was the same as that described in Chapter II. The box was filled to the halfway point of the roller with a 90/10 glycerin water solution. While the roller was stationary the desired gap thickness was set using feeler gauges. In this particular case, the range of H_0 was between 7 and 60 mils. The speed of the roller was gradually increased until the onset of ribbing became apparent visually. The procedure for determining the critical speed was repeated three times for each gap thickness and the averaged values are listed in Table IV-2. There was very little deviation in critical speed between materials and the maximum difference was calculated to be 15%. Thus, from these results it was observed that the conditions for ribbing onset were unaffected by varying surface properties of the stationary plate.

IV. 2.2 Plate Orientation. A second set of experiments was taken to determine if the position of the plate affected the critical conditions for ribbing. In these experiments, the plate was oriented in two ways, vertical and horizontal with respect to the roller, as shown in Figure IV-1.

The experimental apparatus and the procedure for setting the gap thickness differed slightly for the two systems. A schematic diagram of the experimental apparatus for the horizontal system is shown in Figure IV-2. In this system, the plate was not directly attached to the apparatus as in the horizontal case, but attached to a load cell. The load cell was attached to a metal stand which

Table IV-2

CRITICAL SPEED DATA FOR SYSTEMS WITH VARIOUS PLATE SURFACES

Roller Size: Radius = 1"

Plate Material	Fluid	H_0(in)	Ω^*(rpm)
Plexiglass^R	Glycerin	0.01	11
		0.02	17
		0.04	20
		0.06	40
Metal	Glycerin	0.01	10
		0.02	16
		0.04	20
		0.06	42
Teflon^R	Glycerin	0.01	10
		0.02	15
		0.04	23
		0.06	41
Parafilm^R	Glycerin	0.01	11
		0.02	18
		0.04	22
		0.06	42

Figure IV-1. Horizontal and vertical plate orientation, respectively.

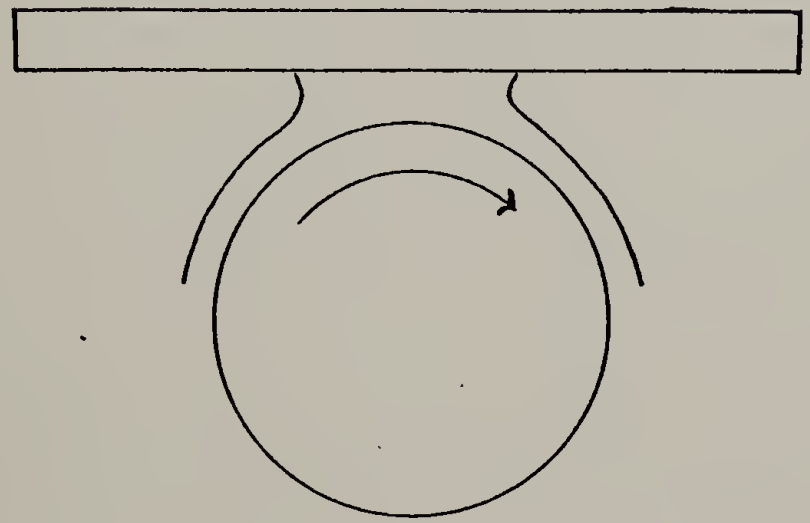

Horizontal System

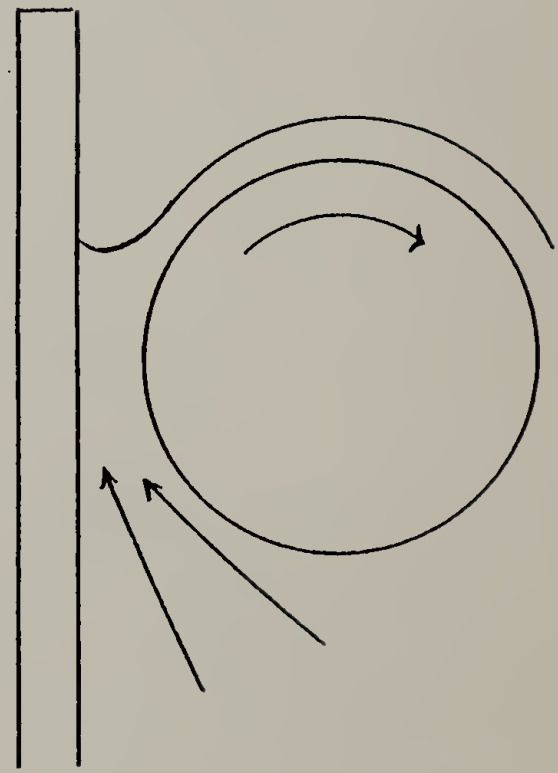

Vertical System

Figure IV-1

Figure IV-2. Schematic diagram of the apparatus with the plate in a horizontal position above the roller. Side view. 1. Box, 2. Roller, 3. Plate, 4. Plate Support, 5. Load Cell, 6. Load Cell Support, 7. Micrometer.

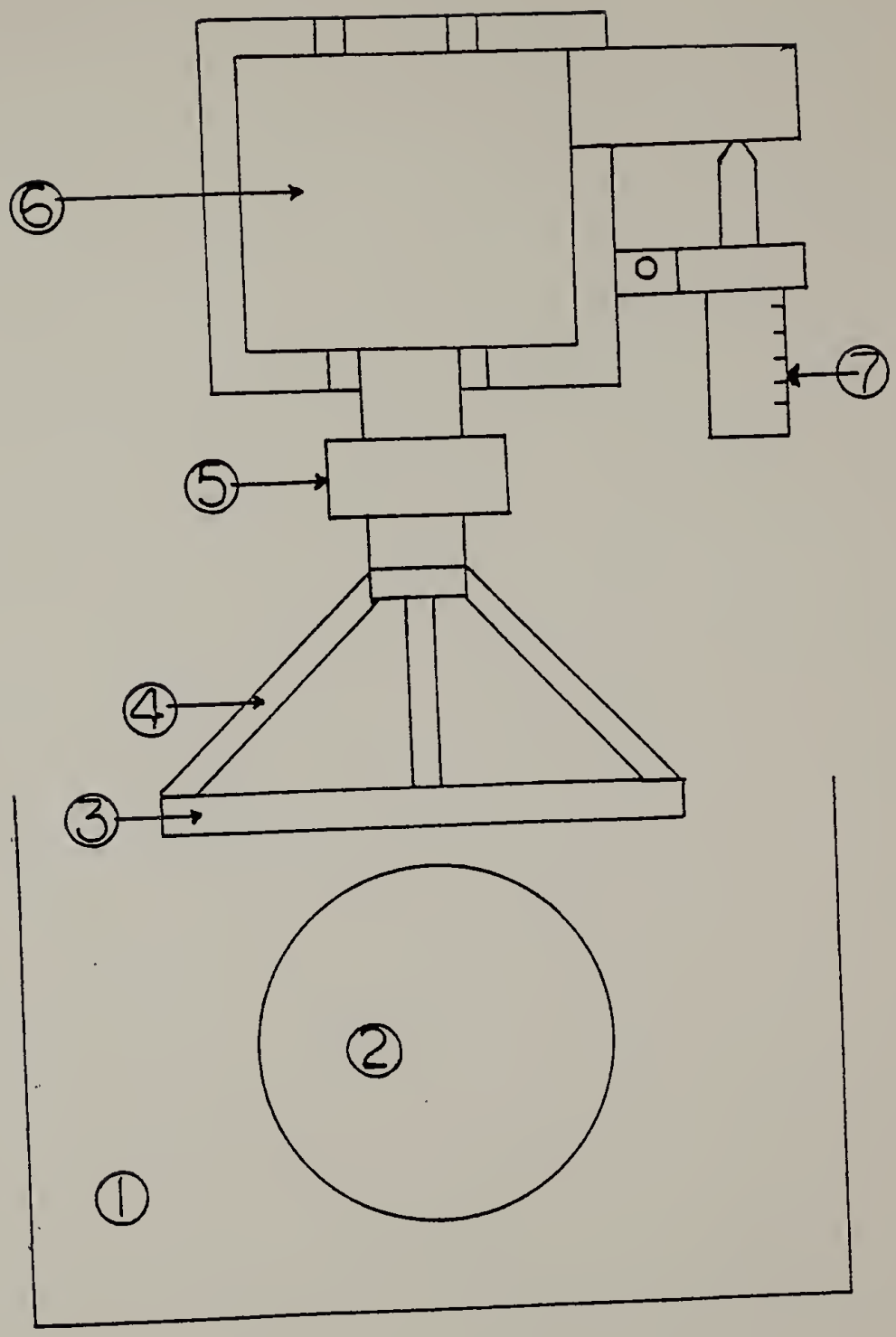

Figure IV-2

supported a micrometer and enabled the plate to be moved vertically with a change in micrometer setting. To set the gap thickness, the plate was lowered to the point where it barely contacted the roller. When the two surfaces touched, the load cell measured the force acting on the plate. The setting of the micrometer was recorded and the desired gap thickness was subtracted from this value. This difference was the micrometer setting which set the plate at the appropriate gap thickness. The micrometer was then reset to the new value. After setting the gap thickness the box was filled halfway with the experimental fluid, 90/10 glycerin water, and the critical speed was then determined in the same fashion as with the vertical plate system. The range of gap thickness was limited to 7 to 40 mils, 40 mils being the maximum H_0 at which the fluid still contacted the plate surface. The experiments were conducted using two different size rollers, a two inch and one inch radius roller.

The data from these experiments are presented in Table IV-3 and graphic comparisons between the final results for the two different plate orientations are shown in Figure IV-3. Although the quantity of data is limited, qualitative differences in the critical conditions are observed between the two different orientations. For both roller sizes, the positioning of the plate system was stable at speeds higher than that of the horizontal systems.

Contact angle data were also collected for the plate horizontally positioned above the roller. These results are listed in Table IV-4. The effect of roller size was also apparent in this

Table IV-3

CRITICAL SPEED DATA FOR THE HORIZONTAL AND VERTICAL PLATE ORIENTATION

Roller Size: Radius = 1"

Plate Orientation	Fluid	H_0(in)	H_0/R	Ca*
Vertical	90/10 Gly-H_2O	0.01	0.01	0.270
		0.02	0.02	0.431
		0.04	0.04	1.29
		0.06	0.06	1.70
Horizontal	90/10 Gly-H_2O	0.007	0.007	0.113
		0.01	0.01	0.141
		0.02	0.02	0.235
		0.03	0.03	0.490

Roller Size: Radius = 2"

Plate Orientation	Fluid	H_0(in)	H_0/R	Ca*
Vertical	90/10 Gly-H_2O	0.01	0.005	0.311
		0.02	0.01	0.528
		0.04	0.02	1.10
Horizontal	90/10 Gly-H_2O	0.02	0.01	0.191
		0.03	0.015	0.402
		0.04	0.02	0.631

Figure IV-3. Comparison between the critical capillary number, Ca^*, as a function of H_0 for the vertical and horizontal plate orientations and for different roller sizes: R=1" and R=2".

Fluid: 90/10 glycerin water

Plate Orientation	Vertical	Horizontal
Roller size: R=1"	□	◫
R=2"	◧	■

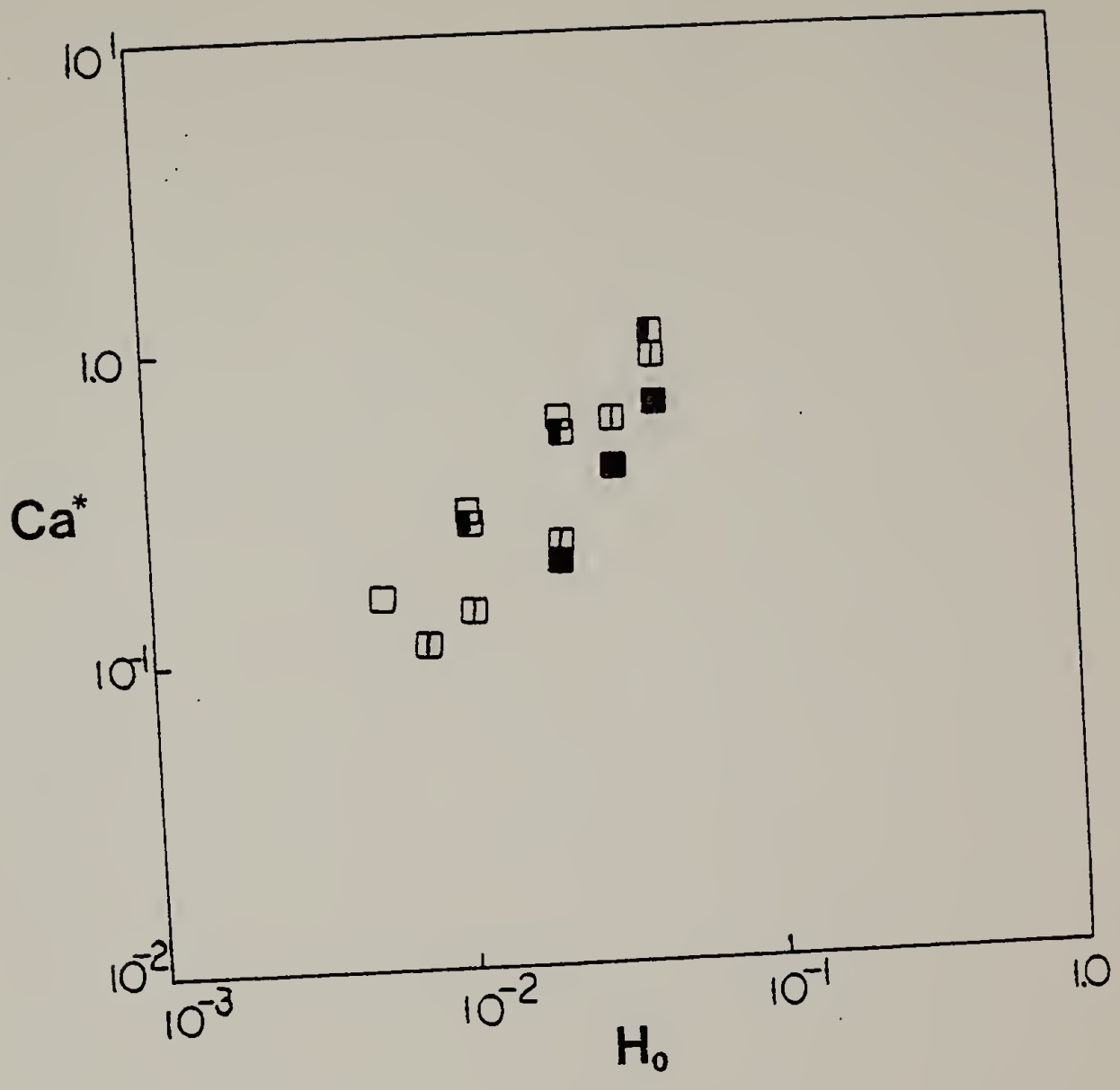

Figure IV-3

Table IV-4

CONTACT ANGLE DATA FOR THE HORIZONTAL PLATE SYSTEM
USING A 90/10 GLYCERIN WATER SOLUTION

Plexiglass^R Plate

Roller Size: R=1"			Roller Size: R=2"		
H_0(in)	H_0/R	θ(degrees)	H_0(in)	H_0/R	θ(degrees)
0.01	0.01	81	0.01	0.005	107
0.015	0.015	100	0.015	0.0075	109
0.02	0.02	90	0.02	0.01	96
0.03	0.030	101	0.03	0.015	107
0.04	0.04	108	0.04	0.02	101

Parafilm^R Plate

Roller Size: R=1"			Roller Size: R=2"		
H_0(in)	H_0/R	θ(degrees)	H_0(in)	H_0/R	θ(degrees)
0.015	0.015	107	0.015	0.0075	119
0.02	0.02	123	0.02	0.01	88
0.03	0.03	95	0.03	0.015	92
0.04	0.04	101	0.04	0.02	94

data. For the same dimensionless gap thickness the contact angle was greater for the larger roller than for the smaller one. This difference in contact angle could account for the apparent difference in stability between the two different sized systems. From comparison of the data in Table III-1 and IV-4 it appeared that contact angle is also dependent on the plate orientation, i.e. the angle for the vertical plate system is less than that of the horizontal system.

One other set of contact angle data was collected using a Parafilm^{R} plate in place of the Plexiglass^{R} plate. From the data, a roller size dependency was also evident. However, in this case the opposite trend was observed. The contact angle was smaller for the larger system as compared to the smaller one. The reason for this discrepancy is unknown, though it may be due to the different surface properties of the two materials. In one last comparison, no apparent trend was present between the Parafilm^{R} and Plexiglass^{R} data for the plate positioned above the roller. This result was unexpected since a trend was observed between the two different plate materials for the vertical system, and since both materials show different wetting characteristics.

Overall, no definite conclusions can be drawn from the entire set of contact angle data. However, one may conclude that contact angle is affected by certain variables, e.g. plate orientation, material, size and cannot be assumed to be a material constant.

IV. 2.3 Plate Shape. The final change in the experimental apparatus was made in the shape of the plate (Figure IV-4). Two curved plates of effective radii 2.2" and 4.3" were placed horizontally above the roller and the critical conditions for ribbing were determined. The curved plates were made from two acrylic pipes of radii 1.73" and 0.91" glued to a flat plate. As described in the previous section, the flat plate was attached to a micrometer driven load cell using the same principle as shown in Figure IV-2. The experiments to determine the critical speed were conducted using two fluids for each system, pure glycerin and 90/10 glycerin water for the system of effective radius 2.2" and oleic acid and 90/10 glycerin water for the effective radius of 4.2". The results of these experiments are listed in Table IV-5. As found in other experiments of this report using similar systems, the correlation of Ca* was a function of H_0, independent of radius. A graph presenting these results is shown in Figure IV-5.

Figure IV-4. Schematic diagram of the curved plate system.

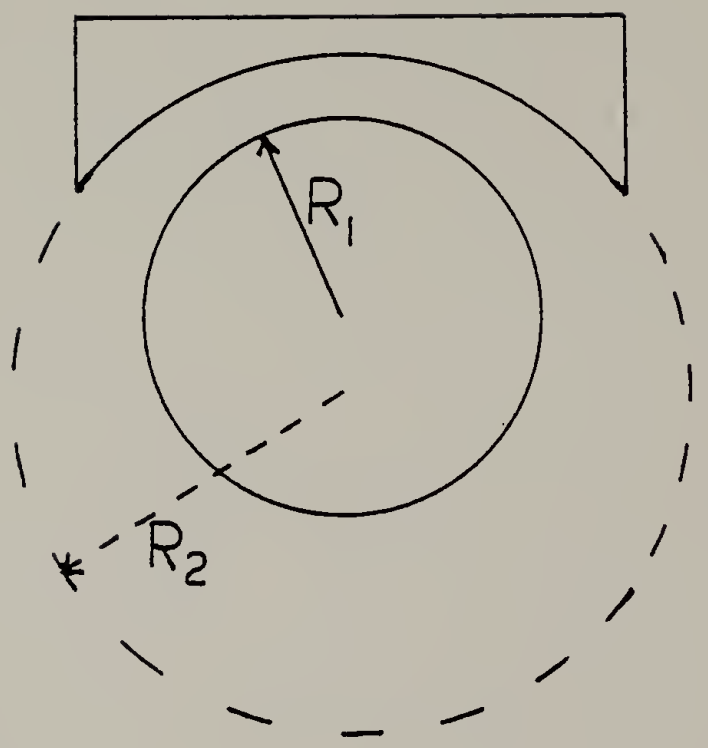

$$R_{eff} = \frac{R_1 R_2}{R_1 + R_2}$$

Figure IV-4

Table IV-5

CRITICAL SPEED DATA FOR THE HORIZONTAL CURVED PLATE SYSTEM

Fluid	R_{eff}(in)	H_0(in)	H_0/R_{eff}	U*	Ca*
Glycerin	2.2	0.01	0.00456	5.82	0.871
		0.02	0.00919	8.73	1.31
		0.03	0.01360	15.7	2.35
90/10 Gly-H_2O	2.2	0.005	0.00228	5.82	0.213
		0.007	0.00318	10.5	0.384
		0.01	0.00456	13.9	0.512
		0.02	0.00919	19.8	0.726
	4.3	0.007	0.00163	12.7	0.465
		0.01	0.00232	18.4	0.676
Oleic Acid	4.3	0.003	0.00070	23.0	0.227
		0.005	0.00116	27.6	0.272

Figure IV-5. The critical capillary number, Ca^*, vs. H_0 for the curved plate system. Roller size: R=2.2" and 4.3".

Fluid	R_{eff} = 2.2"	R_{eff} = 4.3"
Glycerin	◐	●
90/10 Gly-H_2O	◧	■
Oleic Acid	◭	▲

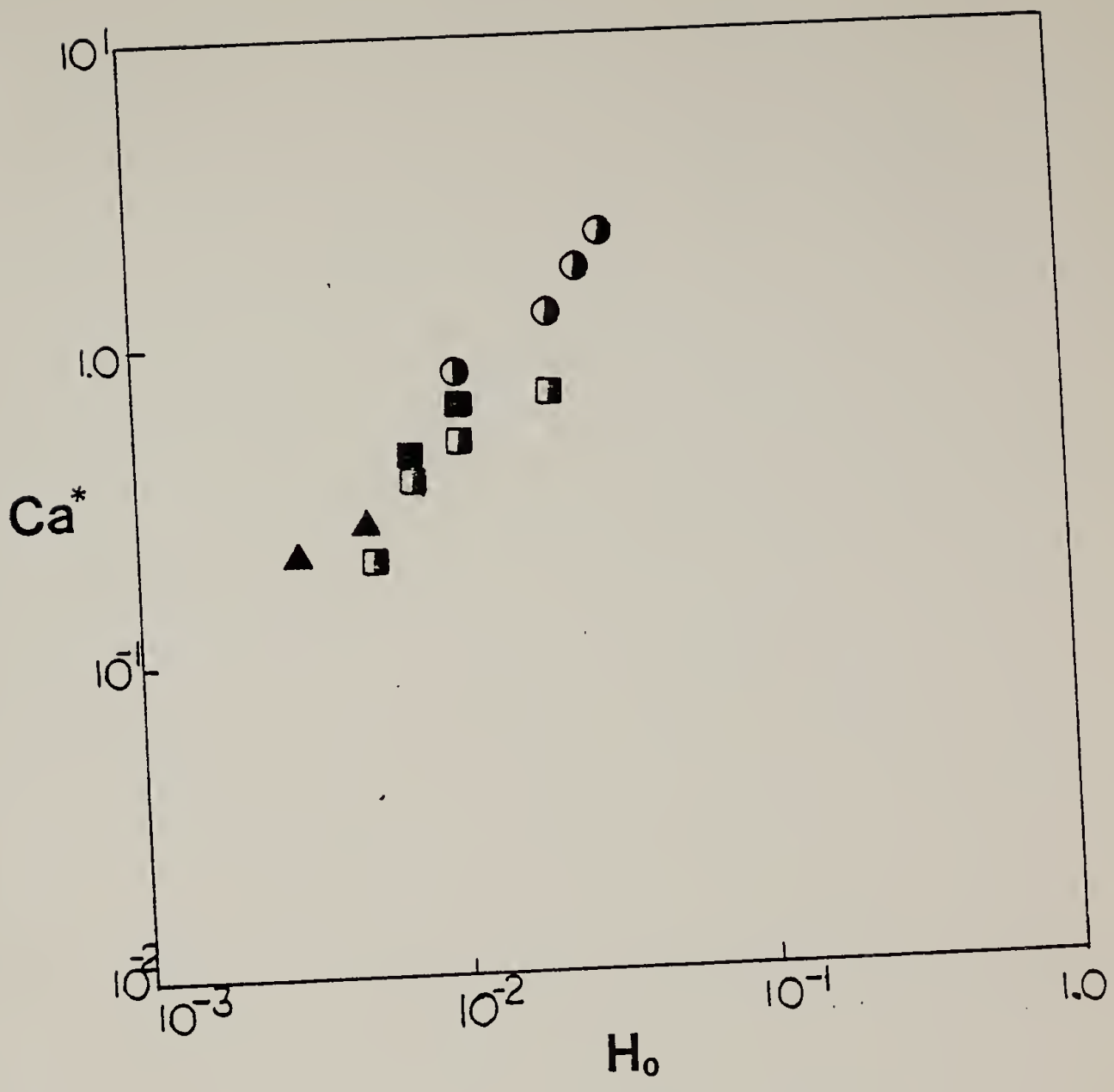

Figure IV-5

CHAPTER V

DISCUSSION

Savage (1976) carried out a linearized perturbation analysis of the ribbing phenomenon and employed the Coyne-Elrod boundary condition. His theory was based on the speculation that the instability is produced by an interaction between the pressure distribution in the region before the meniscus and a pressure caused by surface tension. He proposed the following condition to be necessary for the existence of a stable unribbed cavity-fluid interface

$$\frac{d}{dx}\,(p + \sigma/r) < 0 \qquad \text{(V-1)}$$

Coyne and Elrod proposed another condition to be applicable at the cavity-fluid interface

$$\frac{dp}{dx} = (6\mu U h^2)\,(1 - 2\alpha) \qquad \text{(V-2)}$$

and determined Ca to be a function of α and β where

$$\alpha = H_\infty/h(c) \qquad \beta = r/h(c) \qquad \text{(V-3)}$$

These two equations, V-2 and V-3, transform equation V-1 to

$$\partial h(c)/\partial x > (6\mu U\beta/\sigma)\,(1 - 2\alpha) \qquad \text{(V-4)}$$

From this, Savage predicts ribbing to occur at a critical Ca^*, dependent solely on the geometric parameter, H_0/R. Savage's experimental results appear to be in good agreement with his theory. However, this was not observed to be the case in this research.

The experimental results presented here do not agree with the Savage theory. No correlation between Ca^* and H_0/R was found. A roller size dependency was exhibited in the relationship between the critical Ca^* and H_0/R. The conflict between Savage's data and the data reported here may well be a reflection of the differences in the two apparata. Savage's system consisted of a 5" radius brass cylinder which was 2.5 - 5 times larger than the rollers used in the present experiments. In addition, the plate was positioned horizontally above the wall in the Savage system and in a vertical position in this research.

Indeed, Ca^* appeared to be a function of H_0 for different roller sizes. This suggested that Ca^* should be a function of a dimensionless group involving H_0 and not R. One such dimensionless group is the Bond number, defined as

$$Bo = \rho g H_0^2/\sigma \qquad \text{(V-5)}$$

The Bond number gives some indication of the relative importance of the gravity forces compared to surface tension. From a theoretical standpoint, Greener (1979) argued that a correlation between Ca^* and Bo is reasonable to expect when gravity is important. He presented a stability analysis for Newtonian fluids and included the effect of gravitational forces. He finds the condition for stability to be

$$2 = (Ca_1)^{-1/2}[14(3\lambda - 1)]^{1/2} + 9\frac{Bo}{Ca}\lambda^2 \qquad \text{(V-6)}$$

In the absence of gravity, or for small Bo, $(3\lambda - 1)^{1/2}$ is observed to be independent of Ca^* so equation V-6 reduces to

$$(Ca)\ (\frac{R}{H_0}) = \text{constant} \qquad (V\text{-}7)$$

In the presence of gravity (large Bo number), equation V-6 predicts

$$\frac{Bo}{Ca}\ \lambda^2 = \text{constant} \qquad (V\text{-}8)$$

From the data in Figure III-8, one may assume that λ is nearly constant and independent of gravity over the range of F values used in this research. It follows then that

$$F = Bo/Ca = \text{constant} \qquad (V\text{-}9)$$

where the ratio of Bo to Ca is the gravity number. This qualitative result is not consistent with the experimental results of this report. In Figure Vl, F vs. $Bo^{1/2}$ is plotted. The linear relationship suggests that for the range of parameters studied, neither the Savage theory nor Greener's extension suffice to describe the onset of instability. However, this and the experimental results offer circumstantial evidence that gravity plays an important role in stabilizing the flow. Of the two variables in the Bond number, gap thickness and surface tension, H_0, saw broad variation while σ saw only slight variation in the course of the experiments.

Comparison of the Newtonian and non-Newtonian results offers some indication of the importance of elasticity in this type of roll coating operation. The plots of F vs. $Bo^{1/2}$ for the two types of fluid show no significant variation. The data points for the Newtonian and viscoelastic fluids fall on the same line

Figure V-1. The gravity number, F, vs. $Bo^{1/2}$ for Newtonian fluids. (Key in Table B-10.)

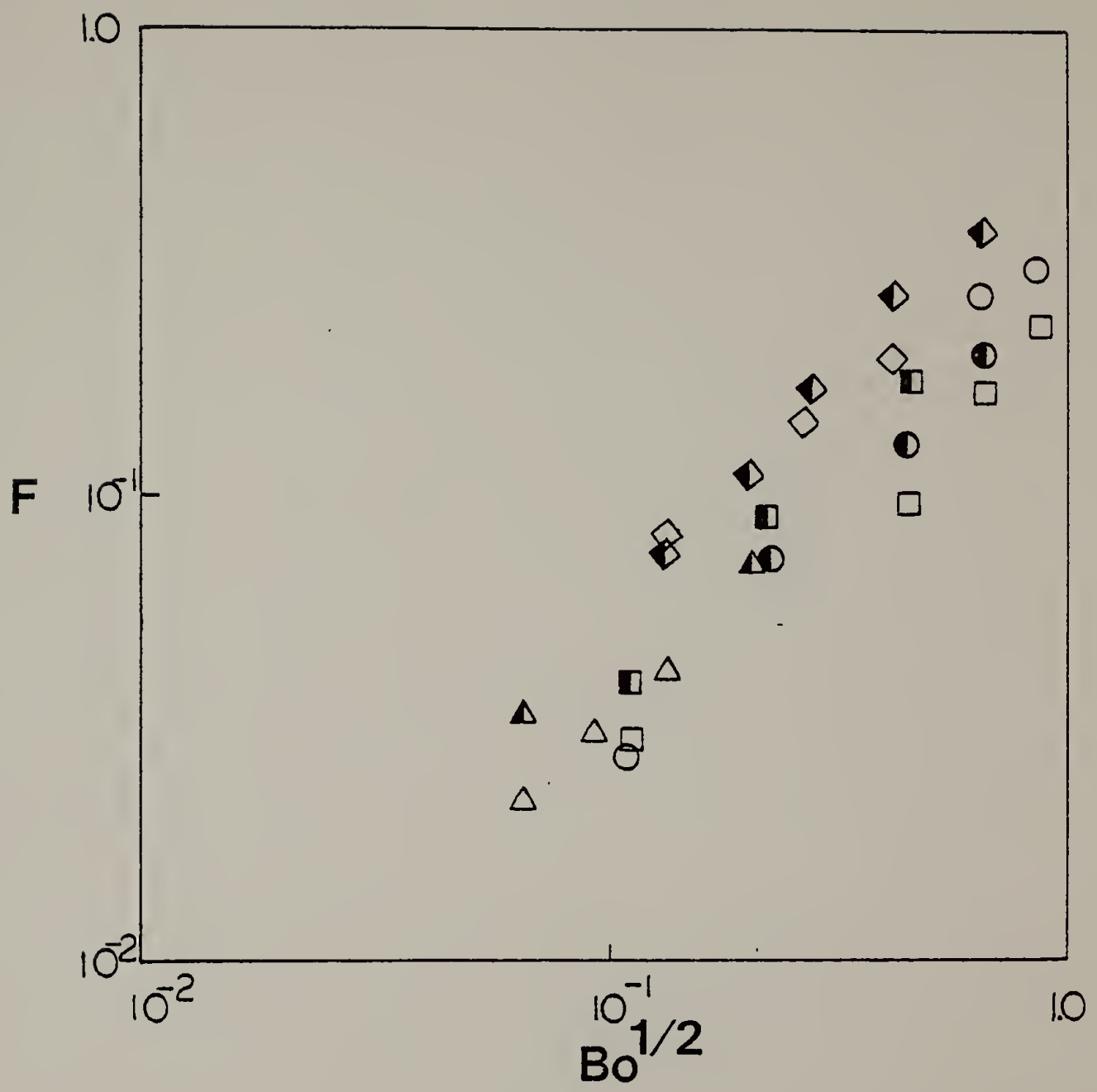

Figure V-1

within the expectation of experimental error as shown in Figure V-2. These results suggest that the effect of elasticity is not significant in the onset of ribbing. The dominant forces controlling the stability are due to viscosity and surface tension forces. Such similarities were not found between Newtonian and non-Newtonian fluids in the counterrotating roll system as reported by Greener (1978). Here the presence of elasticity exerted a strong influence on the conditions for the onset of instability. In effect, the presence of elasticity destabilized the flow, causing the onset of ribbing to occur at lower speeds. Turner and Middleman (1980) have also collected data for the two roll system and have used similar polymer concentrated solutions as used in this research. Like Greener, they too found elasticity to play a major role in the stability of their system. Thus, it is evident that elasticity is important in two roll systems but not in single roll plate coating operations.

Though the same critical conditions prevailed for both Newtonian and viscoelastic fluids, distinct differences were present in the nature of the instability. The effect of elasticity was evident in both the wave pattern and wavelength data. Photographs showing the differences between the type of wave pattern produced for the Newtonian and viscoelastic fluids are presented in Figure V-3. The presence of an instability was manifested in the production of round wavy ribs in the case of Newtonian fluids and sharp pointed ribs for the viscoelastic fluids. The viscoelastic fluids

Figure V-2. The gravity number, F, vs. $Bo^{1/2}$ for Newtonian and viscoelastic fluids.

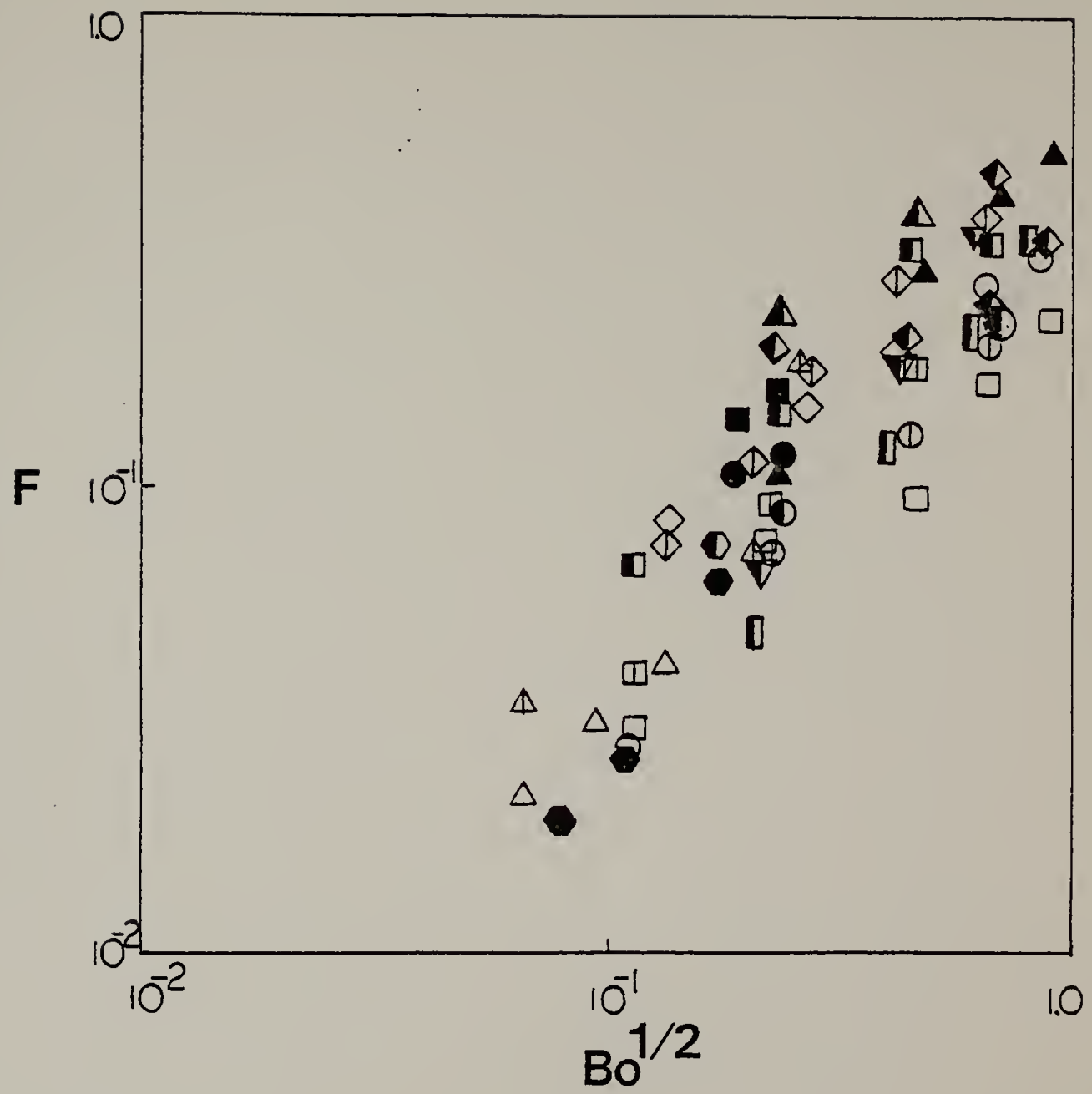

Figure V-2

Figure V-3. Photographs of the wave pattern for the experimental fluids.
a. Mineral Oil, R=2", H_0=0.007", Ω=30 r.p.m.
b. 300 ppm PAA solution, R=2", H_0=0.02", Ω=80 r.p.m.

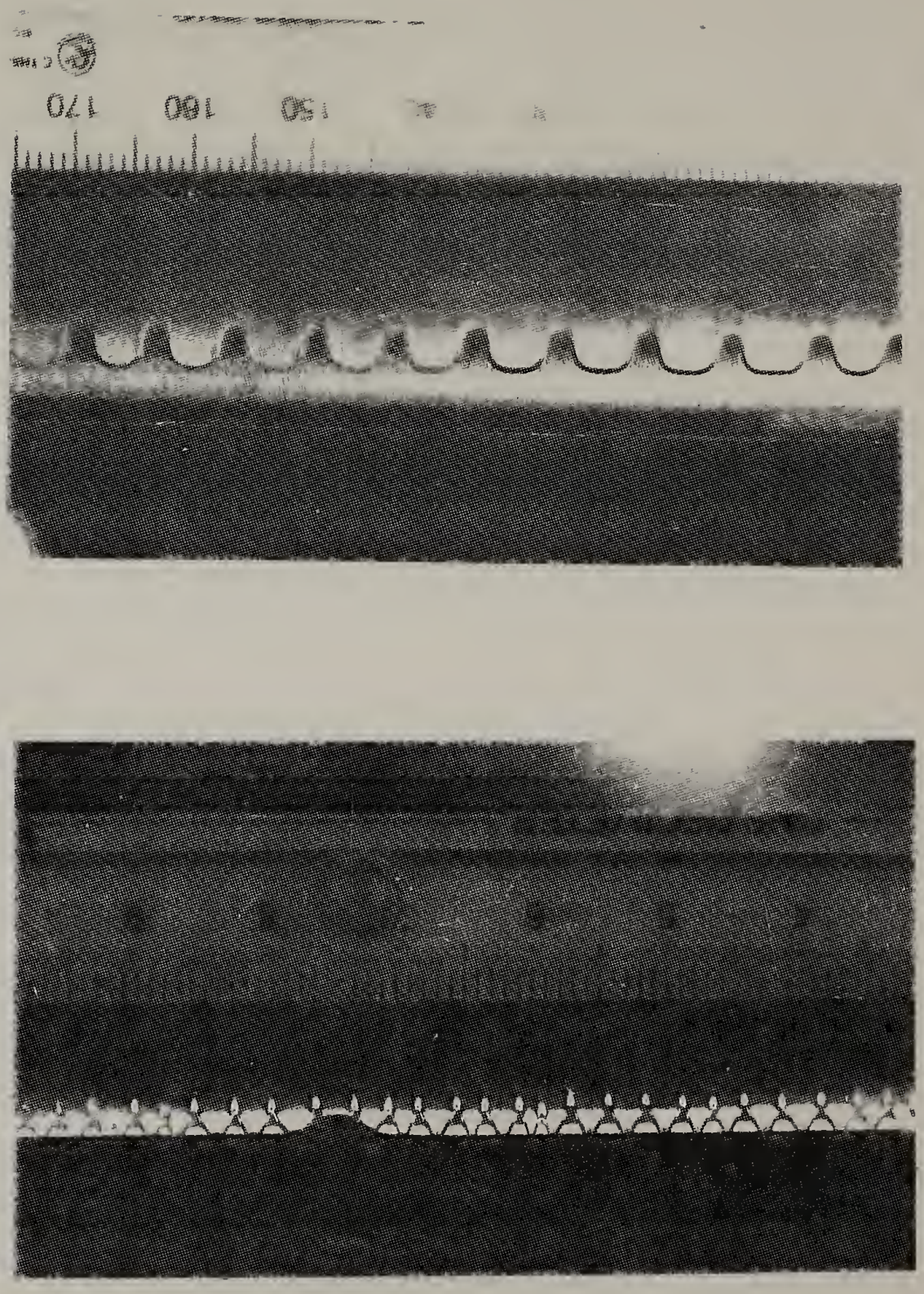

Figure V-3

of higher concentration had a tendency to form two sets of waves at various speeds. One set of large ribs were stationary and had appeared across the length of the roller and a smaller set, superimposed on the larger ones, were approximately six times smaller than the larger ones and travelled from the center to the end of the roll. The limited wavelength data show that, for Newtonian fluids, an asymptotic wavelength was reached at high speeds whereas the viscoelastic wavelength exhibited a continuous decrease in the wavelength value with increasing speed.

Differences between Newtonian and non-Newtonian fluids were also apparent for stable conditions.

Comparisons of Figures III-8 and III-15, which are graphical representations of the dimensionless coating thickness, λ, versus the gravity parameter, F, for Newtonian and viscoelastic fluids respectively, show that the effect of elasticity was to increase the coating thickness. At values of F less than 0.5, the coating thickness was 0.6 for the Newtonian fluids and 0.7 for the viscoelastic fluids. Although quantitative differences in λ were observed for the two sets of fluid, the same general trend of the variations of λ with F was observed for each fluid. That is, the average value of λ was constant at $F<0.5$. At $F>0.5$, λ continually decreased as the gravity parameter increased. It should be noted that for the coating thickness experiments the experimental viscoelastic fluids were not very elastic; $0.4<S_R<0.8$, and that fluids of higher elasticity may have a greater effect on the coating thick-

ness data which would result in a larger deviation from Newtonian fluids.

CHAPTER VI

CONCLUSIONS AND RECOMMENDATIONS

VI.1 Conclusion

A number of different roll coating processes have been developed to satisfy the diversified needs of industry. In this study, attention was focused on the particular coating system of a roller in the presence of a stationary constraint. This system was of interest because of its simple design and because it simulates typical industrial systems.

The objective of this study was to investigate the ribbing phenomenon for this system. It was intended to develop a solid base of experimental findings to aid future efforts in the development of an improved stability analysis. The important results of this work are summarized briefly:

1. The critical capillary number, Ca^*, correlates with the gap thickness, H_0, for a 1" and 2" radius roller, showing no dependence on roller size.
2. All the data for the Newtonian and viscoelastic fluids show a single correlation between $F=Bo/Ca$ and $Bo^{1/2}$.
3. The similarity in data between Newtonian and non-Newtonian fluids suggests that elasticity is insignificant in the onset of ribbing in this geometry.
4. The presence of elasticity is manifested in the wavelength data. Differences are observed in the ribbing pattern.

between the two types of fluids and also in actual wavelengths at high speeds.

5. Elasticity also showed some effects on the performance of coating operations. The coating thickness under similar experimental conditions was greater for viscoelastic fluids as compared to Newtonian fluids.
6. The dimensionless coating thickness was found to be a function solely of the gravity parameter at low F values as the theory of Sullivan and Middleman predicted. Deviations at high F values have been considered by Sullivan and Middleman to be due to surface tension effects.
7. The collection of contact angle data suggests that its variation with certain factors could be important in the stability analysis of the roll and plate system.

VI.2 Recommendations

The basis of the experimental findings suggest that the present theories are inadequate in providing a stability criterion applicable to the roll and stationary plate system. Some recommendations as to what future studies might prove beneficial in understanding the ribbing phenomenon and development of a stability criterion are as follows:

1. In past theories, it has been assumed that the constant angle, θ, is constant and usually given a value of 90°. Experimental results have shown these assumption to be

inaccurate. It appeared that the contact angle is dependent on the roller size and is affected by the material of the plate. These findings suggest that the contact angle and its variation with roller size and shear rate should be given further consideration.

2. Further experiments and theoretical consideration should be given to coating thickness measurements of viscoelastic fluids. Such fluids are commonly used in coating operations and from an industrial standpoint, it is important to be able to determine those operating conditions which will give rise to a coating of a certain thickness. It may prove beneficial in the development of a theory to measure the coating thickness for viscoelastic fluids starting at low speeds in the stable region and proceeding to the point of incipient instability.
3. The effect of varying length may well be significant in changing the conditions for the onset of ribbing. Future experimental studies for both Newtonian and viscoelastic fluids should be conducted on systems changing both roller length and diameter.
4. Theoretical studies of instability
    a. Better correlation
    b. Improved boundary conditions
    c. Improved and less qualitative analysis.

REFERENCES

Beavers, G.S. and D.D. Joseph, "Tall Taylor Cells in Polyacrylamide Solutions", Physics of Fluids, 17, 3, 650 (1974).

Bird, R.B., R.C. Armstrong and O. Hassager, Dynamics of Polymeric Liquids. Vol. 1. Fluid Mechanics. John Wiley & Sons, New York (1977a).

Bird, R.B., O. Hassager, R.C. Armstrong and C.F. Curtis, Dynamics of Polymeric Liquids. Vol. 2. Kinetic Theory. John Wiley & Sons, New York (1977b).

Coyne, J.C. and H.G. Elrod, Dr., "Conditions for the Rupture of a Lubricating Film. Part I: Theoretical Model", ASME Paper No. 60-Lub-3 (1969).

Coyne, J.C. and H.G. Elrod, Jr., "Conditions for the Rupture of a Lubricating Film. Part II: New Boundary Conditions for Reynolds Equations", ASME Paper No. 70-Lub-3 (1970).

Eckert, R.E. and E.J. Novotny, Dr., "Ribbed Flow from a Flat Channel", Nature Phys. Sci., 241, 147 (1973).

Fall, C. "Surface Ribbing of a Thin Viscous Fluid Film Emerging from a Spreader or Roller", Transactions of the ASME, 100, October, 9, 462 (1978).

Gains Jr., G.L., "Surface and Interfacial Tension of Polymer Liquids - A Review", Polym. Eng. Sci., 12, 1, 1 (1972).

Greener, J. and S. Middleman, "A Theory of Roll Coating of Viscous and Viscoelastic Fluids", Polym. Eng. Sci., 15, 1, 1 (1975).

Greener, J. "Bounded Coating Flows of Viscous and Viscoelastic Fluids", Ph.D. Thesis, University of Massachusetts (1978).

Greener, J. and S. Middleman, "Theoretical and Experimental Studies of the Fluid Dynamics of a Two-Roll Coater", I and EC Fundamentals, 18, 35 (1979).

Greener, J., T. Sullivan, B. Turner, S. Middleman, "Ribbing Instability of a Two-Roll Coater: Newtonian Fluids" (In Press).

Hopkins, M.R., "Viscous Flow Between Rotating Cylinders and a Sheet Moving Between Them", Brit. J. Appl. Phys., 8, 443 (1957).

Lin, O.C.C., "Rheology and Surface Coatings", Chemtech, 51 (1975).

Middleman, S., The Flow of High Polymers. Interscience Publishers, New York (1968).

Middleman, S., Fundamentals of Polymer Processing. McGraw-Hill Book Co., New York (1977).

Middleman, S., "Free Coating of Viscous and Viscoelastic Liquids onto a Partially Submerged Rotating Roll", Polym. Eng. Sci., 18, 9 734 (1978).

Mill, C.C. and G.R. South, "Formation of Ribs on Rotating Rollers", J. Fluid Mech., 28, 3 523 (1967).

Pearson, J.R.A., "The Instability of Uniform Viscous Flow Under Rollers and Spreaders", J. Fluid Mech., 7, 4, 481 (1960).

Pitts, E. and J. Greiller, "The Flow of Thin Liquid Films Between Rollers", J. Fluid Mech., 11, 22 (1961).

Roe, R.J., V.L. Bacchetta and P.M.C. Wong, "Refinement of Pendant Drop Technique for the Measurement of Surface Tension of Viscous Fluids", J. Phys. Chem., 71, 4190 (1967).

Savage, M.D., "Cavitation in Lubrication. Part I. On Boundary Conditions and Cavity-Fluid Interfaces", J. Fluid Mech., 80, 4, 743 (1977).

Sone, T. and M. Fukushima, "On the Stripe Pattern During Rolling of Viscous Materials", J. Phys. Soc. Japan, 15, 1708 (1960).

Sullivan, T.M., S. Middleman, "Roll Coating in the Presence of a Fixed Constraining Boundary", Polym. Eng. Sci., 20, 10 (1980).

Taylor, C.M., "Separation Cavitation in Lightly Loaded Fluid Film Bearings with Both Surfaces in Motion", J. Mech. Eng. Sci., 16, 3, 147 (1974a).

Turner, B., Personal Communication (1980).

Wilkinson, M.C., "Extended Use of, and Comments on, the Drop-Weight (Drop-Volume) Technique for the Determination of Surface and Interfacial Tensions", J. Colloid and Inter. Sci., 40, 1, 14 (1972).

NOMENCLATURE

B_o	The bond number
Ca	The capillary number
Ca_1	A modified capillary number
F	Dimensionless gravity parameter
g	Acceleration of gravity
H_0	Gap thickness
H_∞	Coating thickness
h(x)	Separation between roll and plate
p	Pressure
P	Dimensionless pressure
R	Roll radius
S_R	The recoverable shear
u_x	Velocity component in the flow direction
U	Linear roll speed
W	Wavelength of the ribbing instability
x	Primary flow coordinate
z	Neutral axis
$\dot{\gamma}$	Shear rate
η	The shear viscosity function
η'	The dynamic viscosity
η''/ω	Complex viscosity function
θ	Contact angle
λ	Dimensionless coating thickness
μ	Viscosity

ρ	Density
σ	Surface tension
ψ_{12}	Primary normal stress coefficient
ω	Frequency

APPENDIX A

VISCOMETRIC AND VISCOELASTIC DATA

The viscometric and viscoelastic data for the non-Newtonian fluids used in this research are presented in this appendix.

Table A-1

VISCOMETRIC DATA FOR 10 ppm PAA SOLUTION

Temperature: 24.5°C

$\omega(sec^{-1})$	η(Poise)	ψ_{12}*(Poise sec)
25.0	2.00	-
40.0	2.00	-
62.5	2.08	-
100.0	2.00	-
158	1.90	-
250	2.00	-
400	2.00	-
625	2.02	-
1000	2.02	-

*In the present system, ψ_{12} was too small to measure.

Table A-2

VISCOMETRIC DATA FOR 20 ppm PAA SOLUTION

Temperature: 25.5°C

$\omega(sec^{-1})$	η(Poise)	ψ_{12}*(Poise sec)
25.0	3.18	-
40.0	3.20	-
62.5	3.00	-
100	3.04	-
158	3.00	-
250	3.05	-
400	3.04	-
625	3.00	-
1000	3.12	-

*In the present system, ψ_{12} was too small to measure.

Table A-3

VISCOMETRIC DATA FOR 50 ppm PAA SOLUTION

Temperature: 24.5°C

$\omega(sec^{-1})$	η(Poise)	ψ_{12}*(Poise sec)
25.0	2.80	-
40.0	2.75	-
62.5	2.56	-
100	2.60	-
158	3.54	-
250	2.56	-
400	2.50	-
625	2.48	-
1000	2.45	-

*In the present system, ψ_{12} was too small to measure.

Table A-4

VISCOMETRIC DATA FOR 100 ppm PAA SOLUTION

Temperature: 25.5°C

$\omega(sec^{-1})$	η(Poise)	ψ_{12}(Poise sec)
15.8	3.81	0.302
25.0	3.20	0.160
40.0	3.00	0.125
62.5	3.20	0.0768
100	2.90	0.0450
158	2.86	0.0242
250	2.80	0.0118
400	2.75	0.00938
625	2.72	0.00384
1000	2.60	0.00180

Table A-5

VISCOMETRIC DATA FOR 300 ppm PAA SOLUTION

Temperature: 24.5°C

$\omega(sec^{-1})$	η(Poise)	ψ_{12}(Poise sec)
6.25	7.20	1.79
10.0	6.00	0.900
15.8	5.71	0.524
25.0	5.40	0.320
40.0	5.00	0.188
62.5	4.80	0.068
100	4.60	0.044
158	4.76	0.027
250	4.60	0.015
400	4.18	-
625	4.16	-
1000	3.82	-

Table A-6

VISCOMETRIC DATA FOR 1% PAA SOLUTION

Temperature: 24°C

$\omega(sec^{-1})$	η(Poise)	ψ_{12}(Poise sec)
1.00	50	1.60
1.58	34.9	80.6
2.50	32.0	40.0
4.00	22.5	21.9
6.25	19.2	12.8
10.0	13.0	7.00
15.8	9.14	3.20
25.0	6.72	1.60
40.0	5.00	0.800
62.5	3.84	0.430
100	2.72	0.224
158	2.16	0.128
250	1.68	0.0678
400	1.25	0.0363
625	0.928	0.0210

Table A-7

VISCOMETRIC DATA FOR 1.5% PAA SOLUTION

Temperature: 24°C

$\omega(sec^{-1})$	η(Poise)	ψ_{12}(Poise sec)
1.58	76.2	64.1
2.50	56.0	51.2
4.00	45.0	22.5
6.25	32.0	13.3
10.0	22.0	6.80
15.8	15.2	3.36
25.0	12.0	1.73
40.0	8.00	0.850
62.5	6.40	0.471
100	4.40	0.248
158	3.30	0.131
250	2.24	0.0691
400	1.60	0.0350
625	1.22	0.0195

Table A-8

VISCOELASTIC DATA FOR 50 ppm PAA SOLUTION

$\omega(sec^{-1})$	$\eta'(N\ s/m^2)$	$\eta''/\omega(N\ s^2/m^2)$
15.8	1880	40.7
9.96	2130	45.8
6.28	2210	58.9
3.96	2290	80.6
2.50	2340	136
1.57	2320	207
0.996	2460	433
0.628	1780	959

Table A-9

VISCOELASTIC DATA FOR 100 ppm PAA SOLUTION

$\omega(sec^{-1})$	$\eta'(N\ s/m^2)$	$\eta''/\omega(N\ s^2/m^2)$
15.8	846	13.7
9.96	910	18.1
6.28	956	24.2
3.96	985	36.8
2.50	1040	63.7
1.57	1020	104
0.996	1140	198
0.628	1450	467

Table A-10

VISCOELASTIC DATA FOR 300 ppm PAA SOLUTION

$\omega(sec^{-1})$	$\eta'(N\ s/m^2)$	$\eta''/\omega(N\ s^2/m^2)$
15.8	1070	25.2
9.96	1150	37.9
6.28	1240	62.9
3.96	1320	118
2.50	1460	200
1.57	1560	399
0.996	1770	733
0.828	2250	2840

Table A-11

VISCOELASTIC DATA FOR 1% PAA SOLUTION

$\omega(sec^{-1})$	$\eta'(N\ s/m^2)$	$\eta''/\omega(N\ s^2/m^2)$
15.8	49.8	10.4
9.96	98.0	19.1
6.28	13.3	40.1
3.96	189	87.4
2.50	268	187
1.57	371	414
0.496	513	903
0.628	845	1798
0.396	1110	3986
0.250	1660	8240

Table A-12

VISCOELASTIC DATA FOR 1.5% PAA SOLUTION

$\omega(sec^{-1})$	$\eta'(N\ s/m^2)$	$\eta''/\omega(N\ s^2/m^2)$
15.8	9.82	1.72
9.96	15.6	3.44
6.28	22.4	7.51
3.96	32.9	16.4
2.50	47.4	35.2
1.57	67.8	77.9
0.996	99.5	163
0.628	153	340
0.396	207	689
0.250	270	1162
0.157	355	3290

APPENDIX B

EXPERIMENTAL DATA

This appendix contains the experimental data of this research in a tabular form. Both Newtonian and viscoelastic results are listed.

Table B-1

THE RIBBING PHENOMENON:
OBSERVED CRITICAL SPEEDS FOR NEWTONIAN FLUIDS

Roller Size: Radius = 1"

Fluid	H_0(in)	U*(cm/s)	Ca*
Glycerin	0.01	2.84	0.374
	0.02	4.39	0.578
	0.04	5.16	0.680
	0.06	10.3	1.36
	0.08	16.0	2.11
	0.11	24.8	3.26
90/10 Gly-H_2O	0.01	10.8	0.270
	0.02	17.3	0.431
	0.04	51.6	1.29
	0.06	68.4	1.70
	0.08	87.7	2.19
Mineral Oil	0.01	4.39	0.214
	0.02	10.1	0.493
	0.03	18.6	0.909
Oleic Acid	0.005	20.1	0.201
	0.007	28.3	0.282
	0.01	41.8	0.417
	0.016	61.1	0.609
Ivory Liquid	0.007	2.58	0.175
	0.01	4.64	0.315
	0.02	12.4	0.839
	0.04	19.4	1.31

Table B-2

THE RIBBING PHENOMENON:
OBSERVED CRITICAL SPEEDS FOR NEWTONIAN FLUIDS

Roller Size: Radius = 2"

Fluid	H_0(in)	U*(cm/s)	Ca*
Glycerin	0.02	4.26	0.712
	0.04	9.33	1.49
	0.06	13.8	2.20
90/10 Gly-H_2O	0.01	7.86	0.311
	0.02	13.4	0.528
	0.04	27.8	1.10
Mineral Oil	0.01	4.72	0.231
	0.015	7.34	0.358
	0.02	8.38	0.409
	0.031	12.8	0.625
	0.04	21.0	1.02
	0.048	23.3	1.14
Oleic Acid	0.005	12.6	0.125
	0.01	20.4	0.205
	0.02	39.8	0.397
Ivory Liquid	0.01	2.62	0.178
	0.02	8.38	0.568
	0.04	26.7	1.81

Table B-3

WAVELENGTH DATA FOR NEWTOWNIAN FLUIDS

Roller Size: Radius = 1"

Fluid	H_0(in)	H_0/R	Ω(RPM)	U/U*	Ca	W/H_0
Glycerin	0.008	0.008	10	1.25	0.350	25.0
			20	2.50	0.701	22.5
			30	3.75	1.05	22.2
			50	6.25	1.75	17.5
			60	7.50	2.10	14.6
			90	11.2	3.15	12.0
			130	16.2	4.56	11.4
			210	26.2	7.36	11.2
	0.01	0.01	20	1.82	0.701	21.6
			50	4.55	1.75	13.7
			80	7.27	2.80	12.6
			110	10.0	3.86	10.6
			140	12.7	4.91	10.3
			170	15.5	5.96	10.3
	0.02	0.02	20	1.18	0.701	18.0
			50	2.94	1.75	15.0
			80	4.71	2.80	13.2
			110	6.47	3.86	10.0
			140	8.24	4.91	9.50
			170	10.0	5.96	9.08
90/10 Gly-H_2O	0.008	0.008	50	2.38	0.326	29.21
			90	4.29	0.587	26.0
	0.01	0.01	50	1.92	0.326	31.0
			70	2.69	0.457	28.5
			90	3.46	0.587	25.6
	0.02	0.02	110	4.23	0.718	23.0
			140	5.38	0.913	22.3
			170	6.54	1.11	22.2
			110	1.93	0.718	20.0
			230	4.04	1.50	15.0
			300	5.26	1.96	13.6
			350	6.14	2.29	12.9
			400	7.02	2.61	12.2
Mineral Oil	0.01	0.01	35	2.06	0.441	23.0
			50	2.94	0.630	16.1
			65	3.82	0.819	14.3
			75	4.41	0.945	13.4
			100	5.88	1.26	11.5
			125	7.35	1.57	10.8
			175	10.3	2.20	9.92

Table B-4

WAVELENGTH DATA FOR NEWTONIAN FLUIDS

Roller Size: = 2"

Fluid	H_0(in)	H_0/R	U	U/U^*	Ca	W/H_0
90/10 Gly-H_2O	0.007	0.0035	10		0.207	46.2
			20		0.414	25.0
			40		0.828	20.2
			60		1.24	16.8
			100		2.07	17.3
			125		2.59	16.8
	0.01	0.05	25	1.67	0.518	26.2
			35	2.33	0.725	20.8
			75	5.00	1.55	16.0
			100	6.67	2.07	11.8
	0.02	0.01	50	1.96	1.04	16.8
			60	2.35	1.24	16.7
			75	2.94	1.55	13.3
			85	3.33	1.76	12.6
			100	3.92	2.07	12.6
			125	4.90	2.59	12.6
Mineral Oil	0.007	0.0035	10		0.207	38.8
			30		0.621	18.4
			50		1.04	16.5
			75		1.55	15.2
			100		2.07	13.2
			125		2.59	13.2
	0.01	0.005	10	1.11	0.207	39.8
			20	2.22	0.414	20.2
			30	3.33	0.621	16.1
			40	4.44	0.828	14.4
			50	5.55	1.04	14.5
			75	8.33	1.55	12.3
			100	11.1	2.07	11.5
			125	13.9	2.59	11.1
	0.02	0.01	25	15.6	0.518	20.7
			40	2.50	0.828	15.4
			50	3.12	1.04	12.6
			75	4.69	1.55	11.6
			100	6.25	2.07	9.44
			125	7.81	2.59	9.64

Table B-4 (cont.)

Fluid	H_0(in)	H_0/R	U	U/U^*	Ca	W/H_0
Oleic Acid	0.007	0.0035	35	1.13	0.183	36.0
			50	1.61	0.261	23.6
			75	2.42	2.392	19.8
			100	3.23	0.523	16.9
			125	4.03	0.653	16.5
			150	4.84	0.784	14.9
			250	8.06	1.31	14.3
	0.01	0.005	55	1.41	0.287	37.8
			75	1.92	0.392	31.4
			85	2.18	0.444	23.2
			100	2.56	0.523	21.8
			125	3.21	0.653	19.5
			150	3.85	0.784	18.4
			175	4.49	0.914	17.1

Table B-5

COATING THICKNESS DATA FOR NEWTONIAN FLUIDS

Fluid	H_0(in)	H_0/R	F	λ	Ca
Glycerin	0.02	0.02	0.270	0.605	0.173
			0.135	0.685	0.345
			0.090	0.690	0.518
	0.04	0.04	1.19	0.438	0.173
			0.596	0.571	0.345
			0.397	0.617	0.518
	0.06	0.06	2.52	0.336	0.173
			1.26	0.470	0.345
			0.838	0.521	0.518
			0.503	0.598	0.863
	0.08	0.08	2.44	0.351	0.345
			1.22	0.481	0.690
			0.815	0.541	1.03
			0.407	0.588	2.07
90/10 Glycerin-Water	0.02	0.02	0.715	0.56	0.065
			0.357	0.68	0.131
			0.239	0.72	0.197
			0.179	0.70	0.263
	0.04	0.04	3.15	0.30	0.065
			1.05	0.55	0.197
			0.631	0.63	0.328
			0.451	0.67	0.460
			0.287	0.67	0.723
			0.210	0.68	0.986
	0.06	0.06	3.35	0.31	0.131
			1.34	0.52	0.328
			0.837	0.59	0.526
			0.609	0.62	0.723
			0.478	0.63	0.919
			0.394	0.65	1.12
			0.335	0.66	1.31
	0.08	0.08	6.46	0.19	0.131
			2.58	0.36	0.328
			1.62	0.47	0.526
			1.17	0.53	0.723
			0.923	0.57	0.919
			0.760	0.60	1.12
			0.562	0.64	1.49
Motor Oil	0.02	0.02	0.719	0.66	0.078
			0.350	0.70	0.156
			0.240	0.72	0.233
			0.180	0.73	0.311
			0.144	0.71	0.389

Table B-5 (cont.)

Fluid	H_0(in)	H_0/R	F	λ	Ca
Motor Oil	0.04	0.04	1.59	0.44	0.156
			0.794	0.56	0.311
			0.529	0.61	0.467
			0.397	0.61	0.622
			0.317	0.63	0.778
	0.06	0.06	2.61	0.33	0.233
			1.31	0.47	0.467
			0.871	0.52	0.700
			0.653	0.56	0.934
	0.08	0.08	4.97	0.23	0.233
			2.48	0.36	0.467
			1.66	0.44	0.700
			1.24	0.48	0.934
			0.994	0.54	1.17
			0.828	0.55	1.40
			0.710	0.58	1.63
			0.621	0.60	1.87
			0.552	0.62	2.10

Table B-6

THE RIBBING PHENOMENON:
OBSERVED CRITICAL SPEEDS FOR VISCOELASTIC FLUIDS

Roller Size: Radius = 1"

Fluid	H_0(in)	U*(cm/s)	Ca*
10 ppm PAA	0.007	4.13	0.131
	0.01	5.93	0.188
	0.02	11.4	0.360
	0.04	19.4	0.614
20 ppm PAA	0.01	6.54	0.327
	0.02	11.8	0.589
	0.04	23.6	1.18
	0.06	41.9	2.09
50 ppm PAA	0.01	4.45	0.184
	0.02	7.59	0.313
	0.04	14.4	0.594
	0.06	51.3	1.29
100 ppm PAA	0.01	1.83	0.0969
	0.02	4.19	0.222
	0.04	10.2	0.540
	0.06	17.1	0.900
300 ppm PAA	0.02	2.88	0.251
	0.04	6.28	0.548
	0.06	10.5	0.911
	0.08	17.0	1.48
1% PAA	0.02	3.87	0.641
	0.04	5.93	0.934
	0.06	6.97	1.14
	0.08	7.99	1.31
	0.10	9.03	1.44
1.5% PAA	0.02	2.58	0.919
	0.04	5.16	1.48
	0.06	7.22	1.88
	0.08	8.51	2.10
	0.10	9.80	2.48

Table B-7

THE RIBBING PHENOMENON:
OBSERVED CRITICAL SPEEDS FOR VISCOELASTIC FLUIDS

Roller Size: Radius = 2"

Fluid	H_0(in)	U^*(cm/s)	Ca^*
10 ppm PAA	0.007	9.04	0.316
	0.01	13.3	0.464
	0.013	16.0	0.557
	0.016	19.2	0.669
	0.02	23.4	0.817
20 ppm PAA	0.01	6.29	0.262
	0.02	9.43	0.393
	0.04	18.3	0.764
50 ppm PAA	0.01	6.81	0.319
	0.02	11.5	0.540
	0.04	22.5	1.06
	0.06	31.4	1.47
100 ppm PAA	0.02	7.34	0.498
	0.04	10.5	0.711
	0.06	16.8	1.11
300 ppm PAA	0.02	5.24	0.512
	0.04	10.5	0.966
	0.06	21.0	1.83

Table B-8

WAVELENGTH DATA FOR VISCOELASTIC FLUIDS

Fluid	H_0(in)	H_0/R	W/H_0	Ca
10 ppm	0.007	0.0035	28.6	0.464
			23.9	0.650
			21.3	0.743
	0.01	0.005	32.8	0.557
			23.2	0.743
			22.9	0.836
			22.8	0.929
			16.5	1.86
			15.2	2.23
			15.2	2.79
20 ppm	0.01	0.005	24.6	0.266
			19.3	0.665
			17.4	1.06
			17.5	1.59
			15.6	2.00
			14.0	2.66
			13.1	3.32
	0.02	0.01	21.9	0.665
			18.7	1.06
			16.1	1.33
			13.8	1.60
			13.1	2.00
			10.9	2.66
			10.9	3.33
	0.01	0.01	20.8	0.393
			21.2	0.524
			18.2	0.654
			17.0	0.851
			16.1	1.05
			14.9	1.31
			11.7	1.64
			11.9	1.96
50 ppm	0.007	0.0035	45.2	0.219
			44.2	0.329
			40.6	0.437
			22.4	0.656
			21.6	1.09
			21.7	2.16
			21.5	2.69
	0.01	0.005	28.8	0.437
			27.2	0.656
			27.2	0.874
			24.3	1.09
			14.8	1.63

Table B-8 (cont.)

Fluid	H_0(in)	H_0/R	W/H_0	Ca
50 ppm			14.8	2.17
			14.8	2.70
	0.02	0.01	24.9	0.329
			24.9	0.549
			24.9	0.765
			15.3	1.09
			10.6	1.63
			10.3	2.17
			10.8	2.71
			10.1	3.24
	0.01	0.01	32.4	0.205
			3213	0.270
			31.7	0.377
			24.6	.538
			22.6	0.699
			18.1	0.857
			16.1	1.07
			15.8	1.33
			15.7	1.86
	0.02	0.02	15.4	0.324
			15.5	0.534
			15.8	0.807
			15.4	1.07
			13.8	1.34
			8.04	1.87
	0.04	0.04	11.5	0.594
			10.5	0.80
			10.0	1.08
			9.48	1.34
			7.18	1.61
			6.54	1.88
100 ppm	0.01	0.01	30.7	0.138
			20.7	0.208
			20.9	0.277
			19.8	0.399
			14.3	0.690
			11.6	1.03
			11.3	1.23
			10.4	1.51
	0.02	0.02	24.4	0.346
			23.2	0.399
			21.5	0.554
			14.9	1.51
			14.5	1.78
			14.5	2.13

Table B-8 (cont.)

Fluid	H_0(in)	H_0/R	W/H_0	Ca
100 ppm	0.04	0.04	10.3	0.692
			10.1	0.828
			9.70	1.03
			3.98	1.38
			3.98	1.72
300 ppm	0.02	0.01	19.1	0.465
			13.8	0.926
			12.1	1.38
			12.7	1.84
			9.58	2.29
			7.34	4.50
			7.44	6.62
			7.44	7.64
	0.01	0.005	21.9	0.464
			19.7	0.923
			10.2	1.72
			10.2	2.27
			10.8	3.37
			10.8	4.42
			10.8	5.45
			9.88	6.46
	0.04	0.04	8.16	0.685
			8.26	1.14
			8.04	1.70
			8.02	2.25
			6.98	2.80
			6.62	3.35
			6.88	3.89
	0.06	0.06	6.36	1.14
			6.14	1.36
			6.10	1.70
			6.10	2.04
			6.20	2.48
			6.14	2.92
			5.04	3.37
			5.12	3.92
			4.84	4.46
			4.00	5.00
			2.82	5.52

Table B-9

COATING THICKNESS DATA FOR VISCOELASTIC FLUIDS

Fluid	H_0(in)	H_0/R	F	λ	Ca
10 ppm	0.02	0.01	0.177	0.780	0.279
			0.106	0.810	0.464
	0.013	0.0065	0.075	0.808	0.279
			0.045	0.723	0.464
	0.016	0.008	0.113	0.613	0.279
			0.068	0.588	0.464
	0.02	0.02	0.360	0.685	0.137
			0.216	0.755	0.228
			0.135	0.755	0.366
			0.090	0.755	0.549
	0.04	0.04	1.44	0.505	0.137
			0.865	0.585	0.228
			0.618	0.655	0.320
			0.432	0.683	0.457
			0.288	0.710	0.685
			0.216	0.720	0.914
			0.173	0.720	1.14
20 ppm	0.02	0.02	0.396	0.615	0.131
			0.198	0.640	0.262
			0.138	0.640	0.377
			0.099	0.640	0.524
	0.04	0.04	1.59	0.413	0.131
			0.793	0.538	1.262
			0.550	0.610	0.377
			0.396	0.640	0.524
			0.317	0.645	0.654
			0.264	0.643	0.785
	0.06	0.06	3.57	0.250	0.131
			1.78	0.388	0.262
			1.24	0.460	0.377
			0.713	0.543	0.654
			0.509	0.600	0.917
			0.396	0.607	1.18
	0.08	0.08	6.34	0.165	0.131
			3.17	0.284	0.262
			2.20	0.365	0.377
			0.906	0.521	0.917
			0.705	0.554	1.18
			0.577	0.583	1.44
			0.488	0.599	1.70
			0.423	0.613	1.96
			0.373	0.611	2.23
50 ppm	0.02	0.02	0.300	0.720	0.162
			0.225	0.750	0.216

Table B-9 (cont.)

Fluid	H_0(in)	H_0/R	F	λ	Ca
50 ppm			0.180	0.725	0.270
	0.04	0.04	1.20	0.582	0.162
			0.721	0.642	0.270
			0.515	0.665	0.378
			0.400	0.675	0.486
			0.360	0.690	0.540
	0.06	0.06	2.70	0.395	0.162
			1.62	0.510	0.270
			1.16	0.545	0.378
			0.811	0.582	0.540
			0.543	0.602	0.807
			0.407	0.602	1.08
	0.08	0.08	4.80	0.236	0.162
			2.88	0.349	0.270
			2.06	0.409	0.378
			1.44	0.470	0.540
			0.961	0.534	0.807
			0.723	0.550	1.08
			0.579	0.566	1.34
			0.482	0.570	1.61
			0.413	0.579	1.88
			0.363	0.579	2.14
			0.351	0.585	2.41
100 ppm	0.04	0.04	1.52	0.495	0.138
			0.762	0.578	0.277
			0.529	0.610	0.399
	0.06	0.06	3.43	0.333	0.138
			1.71	0.478	0.277
			1.19	0.557	0.399
			0.858	0.595	0.554
	0.08	0.08	6.10	0.216	0.138
			3.05	0.359	0.277
			2.12	0.439	0.399
			1.52	0.486	0.554
			1.22	0.514	0.692
			1.02	0.534	0.831
			0.938	0.544	0.899
300 ppm	0.06	0.06	1.91	0.425	0.229
			0.957	0.550	0.457
			0.637	0.547	0.687
	0.08	0.08	3.40	0.375	0.229
			1.70	0.505	0.457
			1.13	0.552	0.686
			0.853	0.575	0.913
			0.683	0.575	1.14

Table B-10

NEWTONIAN DATA NOTATION

Fluid	Symbol						
	R=1"	R=2"	H_0=0.008"	0.01"	0.02"	0.04"	0.06"
Glycerin	○	◐	⊗	⊘	○	◫	○
90/10 Gly-Water	□	◧	⊠	▨	□	◫	□
Oleic Acid	△	◭	⟑	◭	△	◭	△
Mineral Oil	◇	◆	⊗	⊘	◇	◫	◇
Ivory Liquid	⬡	◐	⊗	⊘	⬡	◫	⬡

Table B-11

VISCOELASTIC DATA NOTATION

Fluid	Symbol						
	R=1"	R=2"	H_0=0.008"	0.01"	0.02"	0.04"	0.06"
10 ppm PAA							
20 ppm PAA							
50 ppm PAA							
100 ppm PAA							
300 ppm PAA							
1% PAA							
1.5% PAA							